UNIVERSITÀ DEGLI STUDI DI NAPOLI
"FEDERICO II"
FACOLTÀ DI SCIENZE MATEMATICHE, FISICHE E NATURALI

TESI DI DOTTORATO IN
SCIENZE CHIMICHE
XXIV CICLO

BIOCHEMICAL AND STRUCTURAL CHARACTERIZATION OF HUMAN CARBONIC ANHYDRASES

Dottoranda
Emanuela Truppo

TUTORE
Prof.ssa Gabriella D'Auria

RELATORE
Prof. Piero Pucci

COTUTORI
Dott.ssa Simona Maria Monti
Dott.ssa Giuseppina De Simone

COORDINATORE DEL XXIV CICLO
Prof. Lucio Previtera

TABLE OF CONTENTS

ABSTRACT

Carbonic anhydrases (CAs. EC 4.2.1.1) are ubiquitous metalloenzymes that catalyze the reversible hydration of carbon dioxide to bicarbonate and proton. In humans, 15 isozymes have been described with different subcellular localization. Indeed, CA I-III, VII, and XIII are cytosolic, CA IV, IX, XII and XIV are membrane-bound, CA VA and CA VB are mitochondrials, and CA VI is secreted. Human CA isozymes are extensively distributed in several tissues and organs where, as modulators of pH and ion transport, they take part in a variety of physiological and pathological processes. As a result, in the last years many of these enzymes have become important therapeutic targets for pharmaceutical research. However, given the high degree of sequence and structure similarity among the different isoforms, to date most of the CA-directed drugs developed lack of selectivity and consequently present many side-effects.

X-Ray crystallography is one of the most useful instruments in the structure-based drug design of selective molecules able to interact with a target enzyme. Indeed, there are several examples in the literature where knowledge of the crystallographic structure of an enzyme allowed the design of molecules able to interact with specific residues, thus regulating enzyme biological activity. This is why in recent years there has been an extensive research effort focusing on the crystal structure resolution of all catalytically active α-CA isoforms, with the result that most of the human CA isoforms have been so far structurally characterized.

As a part of a general research project based on the structure-based drug design of isoform-selective CA inhibitors (CAIs), my Ph.D thesis has been focused on the study of the biochemical and structural features of two cytosolic CA isoforms, namely hCA VII and hCA I, which among the 15 human isoforms have been poorly investigated.

hCA VII was the sole cytosolic isozyme, that at the beginning of this Ph.D thesis was not yet structurally characterized. This enzyme, similarly to hCA II, is a very efficient catalyst for hydration of carbon dioxide, being 10-50 times more active compared to other two cytosolic isoforms, hCA I and hCA XIII. However, in contrast to hCA II which is widely spread in human tissues, CA VII has a more limited distribution, being localized mainly in some brain tissues of humans and rats, in stomach, duodenum, colon, liver and skeletal muscle of mice. In the first part of my Ph.D thesis a complete biochemical characterization of this enzyme was carried out. Interestingly, these studies highlighted the capability of two reactive cysteines to be S-glutathionylated during the purification procedures. Since S-glutathionylation was reported *in vivo* also for another cytosolic CA isozyme, namely CA III, and was associated to a protective response to oxidative stress, this phenomenon was investigated in details also for CA VII. Such studies showed that Cys183 and Cys217 were involved in adduct formation. These reactive cysteines were mutagenized and the corresponding double mutant (C183S/C217S) was expressed. The native enzyme, its double mutant and the S-glutathionylated adduct were fully characterized for their CO_2 hydration, esterase and phosphatase activity. These kinetic studies indicated that the modification of Cys183 and/or Cys217 by glutathione does not have a relevant impact on the active site of the enzyme, causing rather small differences in its specific activity. Moreover, an important observation was that hCA VII was highly effective as esterase and phosphatase, compared to other cytosolic CA isoforms, such as CA I, II, III and XIII. These findings seem to indicate that the observed S-glutathionylation, if present *in vivo*, is not involved in the regulation of the enzyme catalytic activity but rather, as observed for hCA III, can help hCA VII to function as an oxygen radical scavenger to protect cells from oxidative damage. Further *in vivo* studies are currently underway to investigate this issue.

The X-ray crystallographic structure of a hCA VII mutated form in complex with a classical sulfonamide inhibitor, namely acetazolamide, was also solved. A detailed comparison of the obtained structure with those already reported for other CA isozymes provided novel insights into the catalytic properties of this protein family and offered the basis for a mutagenesis approach aimed at determining the contribution of the active site single residues to the enzyme catalytic efficiency. Moreover, on the basis of the structural differences detected within the active site of the various CA isoforms, further prospects for the design of isozyme-specific CA inhibitors have been obtained.

hCA I was one of the first members of the CA family to be identified. Even though the 3D structure of this enzyme was first characterized already in 1975, only few structural studies on complexes formed with different inhibitors have been reported so far. Since these studies are fundamental for the drug design of isoform-selective inhibitors, part of this thesis has been dedicated to the structural characterization of a complex that hCA I forms with topiramate (**TPM**), which is a molecule of pharmacological interest for the treatment of epilepsy. The analysis of the structure of the complex showed that, upon binding of the inhibitor, the active site of hCA I undergoes a profound reorganization, which has never been observed in any other CA/inhibitor complex and might therefore be useful in designing CA inhibitors. Moreover, the comparison with hCA II/**TPM** and hCA VA/**TPM** complex structures, previously investigated, showed that a different H-bond network together with the movement of active site residues to accommodate the inhibitor may account for the difference of inhibition constants of **TPM** towards different CA isozymes. These data may be helpful in the design of CAIs selective for various isozymes.

1. Introduction

1.1 Carbonic Anhydrases

Carbonic Anhydrases (CAs. EC 4.2.1.1) are ubiquitous metallo-enzymes, which were firstly identified in 1933 in red blood cells of cows (Meldrum and Roughton, 1933). Since then, they have been found to be abundant in all mammalian tissues, plants, algae and bacteria. These enzymes are encoded by five distinct evolutionarily unrelated gene families (Maren, 1967), namely the α-, β-, γ-, δ- and ζ-CAs, which appear to have evolved independently from each other, thereby providing an excellent example of convergent evolution. The five CA classes have different distributions in the different organisms; in particular, α-CAs are present in vertebrates, bacteria, algae and chloroplasts, β-CAs have been found predominantly in bacteria, algae and chloroplasts, γ-CAs mainly in archaea and some bacteria while δ-CAs and ζ-CAs have been identified only in some marine diatoms (Hewett-Emmett, 2000; Krungkrai *et al*., 2001; Chirica *et al*., 1997; Smith and Ferry, 2000; Supuran and Scozzafava, 2000; 2002; Supuran *et al*., 2003; Roberts *et al.,* 2008; Soto *et al.,* 2006). The members of these different classes share very little sequence or structural similarity, but they all require a zinc ion in the active site. The only exception is represented by the recently discovered ζ class that can also use a cadmium ion as catalytic metal (Xu *et al.,* 2008; Lane *et al.,* 2005).

Independently on their source, all CAs catalyze the reversible hydration of carbon dioxide to bicarbonate and proton ($CO_2 + H_2O \Leftrightarrow HCO_3^- + H^+$), following a two step catalytic mechanism (see Equations 1.1, 1.2 and Figure 1.1). In the first step the nucleophilic attack of a zinc-bound hydroxide ion on a carbon dioxide molecule leads to the formation of a bicarbonate ion coordinated to Zn(II), which is then displaced by a water molecule (Equation 1.1). In the second step, which is the rate-limiting one, the basic form of the enzyme, which is the catalytically active one, is regenerated by the ionization of the zinc-bound water molecule and the transfer of a proton from the active site to the external medium (Equation 1.2) (Figure

1.1). This process can be assisted either by active-site residues or by buffers present in medium (Supuran *et al*., 2003; Lindskog and Silverman, 2000; Christianson and Fierke, 1996; Bertini *et al*., 1982).

$$EZn^{2+}\text{-}OH^{-} + CO_2 \Leftrightarrow EZn^{2+}\text{-}HCO_3^{-} \Leftrightarrow EZn^{2+}\text{-}OH_2 + HCO_3^{-} \quad (1.1)$$

$$EZn^{2+}\text{-}OH_2 + B \Leftrightarrow EZn^{2+}\text{-}OH^{-} + BH^{+} \quad (1.2)$$

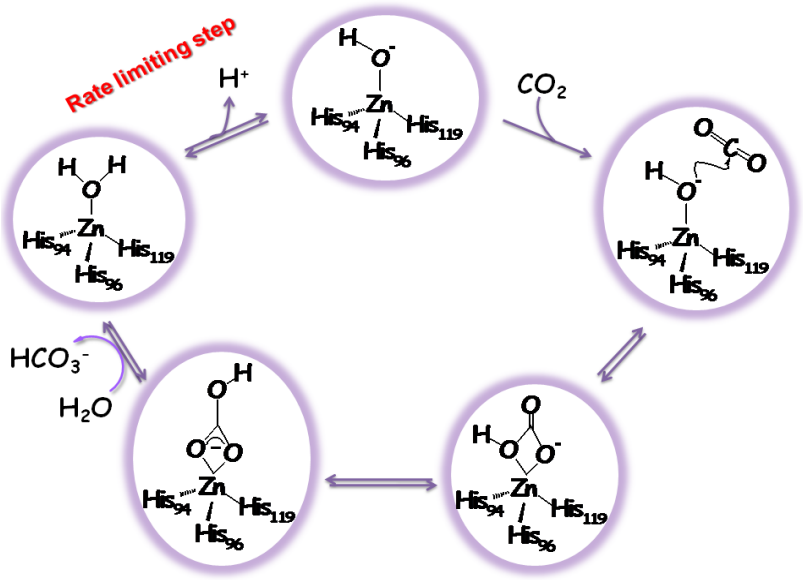

Figure 1.1 *Schematic representation of the catalytic mechanism for the CA-catalyzed CO_2 hydration.*

In addition to the carbon dioxide hydration, CAs catalyze a variety of other reactions, such as hydration of cyanate to carbamic acid or of cyanamide to urea (Equations 1.3 and 1.4); aldehyde hydration to *gem*-diols (Equation 1.5); hydrolysis of carboxylic or sulfonic acid esters (Equations 1.6 and 1.7); as well as other less-investigated hydrolytic processes, such as those described by Equations 1.8 to 1.10, even if it is unclear whether these reactions have physiological significance (Supuran *et al*., 2003).

$$O{=}C{=}NH + H_2O \Leftrightarrow H_2NCOOH \quad (1.3)$$

$$HN{=}C{=}NH + H_2O \Leftrightarrow H_2NCONH_2 \quad (1.4)$$

$$RCHO + H_2O \Leftrightarrow RCH(OH)_2 \quad (1.5)$$

$$RCOOAr + H_2O \Leftrightarrow RCOOH + ArOH \quad (1.6)$$

$$RSO_3Ar + H_2O \Leftrightarrow RSO_3H + ArOH \quad (1.7)$$

$$ArF + H_2O \Leftrightarrow HF + ArOH \quad (1.8)$$

$$PhCH_2OCOCl + H_2O \Leftrightarrow PhCH_2OH + CO_2 + HCl \quad (1.9)$$

$$RSO_2Cl + H_2O \Leftrightarrow RSO_3H + HCl \quad (1.10)$$

1.2 Human isoforms of CA family

All human CAs (hCAs) belong to the α-class; up to now, fifteen different α-CA isozymes have been identified among which twelve are catalytically active, (CAs I-IV, VA, VB, VI-VII, IX and XII-XIV) (Hewett-Emmett, 2000; Supuran and Scozzafava, 2000; 2002; Supuran *et al*., 2003), whereas the remaining three isoforms (CA VIII, X and XI), the so called carbonic anhydrase-related proteins (CARPs), are devoid of any catalytic activity (Tashian *et al.*, 2000), thus their physiological function is still unknown (Table 1.1).

α-CA isozymes widely differ in cellular localization. In particular, among the catalytically active isozymes, four are associated to the cellular membrane (CA IV, CA IX, CA XII and CA XIV), two are located into the mitochondria (CA VA and CA VB), one is secreted in saliva and milk (CA VI) and five are cytosolic (CAs I-III, CA VII and CA XIII) (Supuran, 2008a) (Table 1.1). These enzymes are extensively distributed in several tissues and organs where, as modulators of pH and ion transport, they take part in a variety of physiological and pathological processes. As a result, in the last years they have become important therapeutic targets for pharmaceutical research (Supuran, 2008a). Table 1.2 reports a brief presentation of

the various diseases in which hCAs are involved. Just to give some examples, among the cytosolic isoforms hCA I seems to be involved in retinal and cerebral edema, and its inhibition may be a valuable tool for fighting these conditions (Gao *et al*., 2007). hCA II is involved in several diseases such as glaucoma, edema, epilepsy and probably altitude sickness (Hen *et al*., 2011; Mincione *et al*., 2008; Supuran, 2008b; De Simone *et al*., 2009; Basnyat *et al*. 2003; Swenson and Teppema, 2007). hCA III is involved in the oxidative stress, characterizing a lot of inflammatory diseases. However, it is not yet understood whether the enzymatic activity of hCA III, or to the Cys residues present on its surface are responsible for the antioxidant effects of this protein (Barreiro and Hussain, 2010; Brancaccio *et al*., 2010; Zimmerman *et al*., 2004). hCA VII has been distinguished for its contributions to epileptiform activity together with hCAs II and XIV (Hen *et al*., 2011; De Simone *et al*., 2009; Ruusuvuori *et al.*, 2004), and hCA XIII seems to be involved in the sperm motility processes (Lehtonen *et al.*, 2004) and its inhibition could be used to obtain contraceptive agents.

Table 1.1. *Subcellular localization, organ/tissue distribution and CO_2 hydrase activity of the 15 human α-CA isozymes (Supuran, 2008a).*

	Subcellular localization	**Organ/tissue distribution**	**Catalytic activity (CO_2 hydratation)**
hCA I	Cytosol	Erythrocytes, gastrointestinal tract, eye	Low
hCA II	Cytosol	Erythrocytes, eye, gastrointestinal tract, bone osteoclasts, kidney, lung, testis, brain	High
hCA III	Cytosol	Skeletal muscle, adipocytes	Very Low
hCA IV	Membrane-bound	Kidney, lung, pancreas, brain capillaries, colon, heart muscle, eye	High
hCA VA	Mitochondria	Liver	Moderate
hCA VB	Mitochondria	Heart and skeletal muscle, pancreas, kidney, spinal cord, gastrointestinal tract	High
hCA VI	Secreted into saliva and milk	Salivary and mammary glands	Moderate
hCA VII	Cytosol	Central nervous system	High
hCA VIII	Cytosol	Central nervous system	Acatalytic
hCA IX	Transmembrane	Tumours, gastrointestinal mucosa	High
hCA X	Cytosol	Central nervous system	Acatalytic
hCA XI	Cytosol	Central nervous system	Acatalytic
hCA XII	Transmembrane	Renal, intestinal, reproductive epithelia, eye, tumours	High
hCA XIII	Cytosol	Kidney, brain, lung, gut, reproductive tract	Low
hCA XIV	Transmembrane	Kidney, brain, liver, eye	Medium

Table 1.2. *Diseases in which hCA isoforms are involved.*

CA isoform	Disease in which is involved
hCA I	Retinal/cerebral edema (Gao *et al.*, 2007)
hCA II	Glaucoma (Mincione *et al*., 2008) Edema (Supuran, 2008b) Epilepsy (Hen *et al*., 2011; De Simone *et a*l., 2009) Altitude sickness (Basnyat *et al.*, 2003; Swenson and Teppema, 2007)
hCA III	Oxidative stress (Barreiro and Hussain, 2010; Brancaccio *et al.*, 2010; Zimmerman *et al*., 2004)
hCA IV	Glaucoma (Matsui *et al*., 1996) Retinitis pigmentosa (Datta *et al.*, 2009; Ochrietor *et al*., 2005) Stroke (Tang *et al*., 2006)
hCA VA/VB	Obesity (De Simone *et al*., 2008; De Simone and Supuran, 2007; 2009; Supuran *et al*., 2008)
hCA VI	Cariogenesis (Nishimori *et al*., 2007; Kivelä *et al*., 1999)
hCA VII	Epilepsy (Hen *et al*., 2011; De Simone *et al.*, 2009; Ruusuvuori *et al*., 2004)
hCA VIII	Neurodegeneration (Aspatwar *et al*., 2010) Cancer (Aspatawar *et al*., 2010)
hCA IX	Cancer (Guler *et al*., 2010; De Simone and Supuran, 2010; Pastorekova *et al*., 2006)
hCA X	Unknown
hCA XI	Unknown
hCA XII	Cancer (Guler *et al*., 2010; Pastorekova *et al*., 2006; Battke et al., 2011) Glaucoma (Liao *et al*., 2003)
hCA XIII	Sterility (Lehtonen *et al*., 2004)
hCA XIV	Epilepsy (Hen *et al*., 2011; Shah *et al*., 2005) Retinopathies (Ogilvie *et al*., 2007)

1.3 Structural features of human α-CAs

To date, the three dimensional structures of several human α-CA isoforms have been determined (Kannan *et al.*,1984; Eriksson *et al.*, 1988; Eriksson and Liljas, 1993; Boriack-Sjodin, *et al*., 1995; Stams *et al.*, 1996; Whittington *et al.*, 2001; 2004; Duda *et al.*, 2005; Di Fiore *et al.*, 2008; 2010; Alterio *et al.*, 2009a). The analysis of these structures showed that, as

expected on the basis of their high sequence homology, these enzymes present a similar structure characterized by a central twisted antiparallel β-sheet surrounded by helical connections and additional β-strands. The active site is located at the bottom of a great, conical cavity, roughly wide 12 Å and deep 13 Å, which occurs from the protein surface to the centre of the molecule. The catalytic zinc ion is located on the bottom of this cavity, being tetrahedrally coordinated by three conserved histidine residues (His94, His96 and His119) and a water molecule/hydroxide ion (Figure 1.2) (Lindskog, 1997; Håkansson *et al*., 1992; Stams and Christianson, 2000; Christianson and Fierke, 1996).

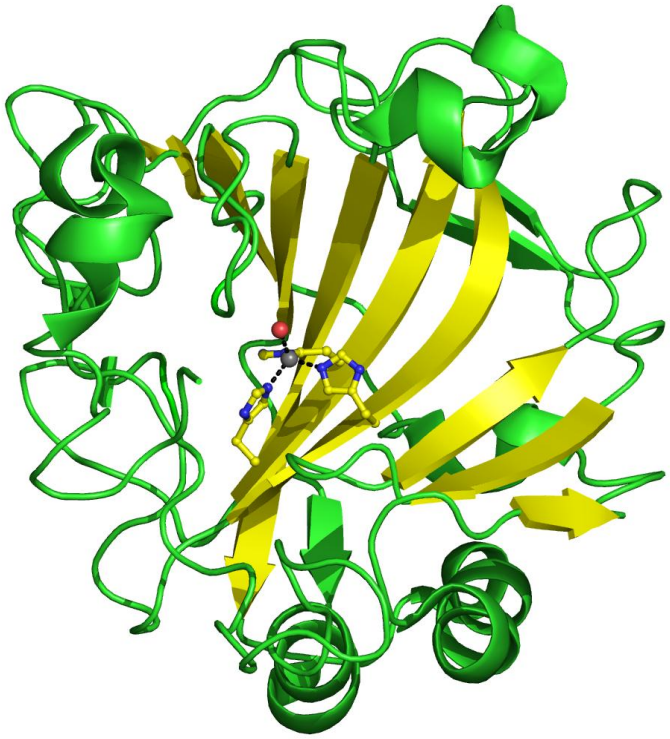

Figure 1.2 *Schematic representation of three-dimensional structure of hCA II, which has been chosen as representative α-CA.* The Zn(II) ion (central gray sphere) and its three histidine ligands (His 94, His 96, His 119) are shown. Helix and β-strand regions are coloured in green and yellow, respectively.

The nucleophilicity of the zinc-bound water molecule, necessary to perform the catalytic reaction, is enhanced by a network of hydrogen bonds of this molecule with the hydroxyl

moiety of Thr199 and with two other water molecules. The first one, also called "deep water", is located in a hydrophobic pocket delimited by the conserved residues Val121, Val143, Leu198 and Trp209 (Christianson and Fierke, 1996), that constitute the substrate-binding site in isozyme II, while the second one is located in a hydrophilic environment toward the entrance of the active site (Figure 1.3) (Supuran *et al*., 2003; Lindskog and Silverman, 2000; Stams and Christianson, 2000).

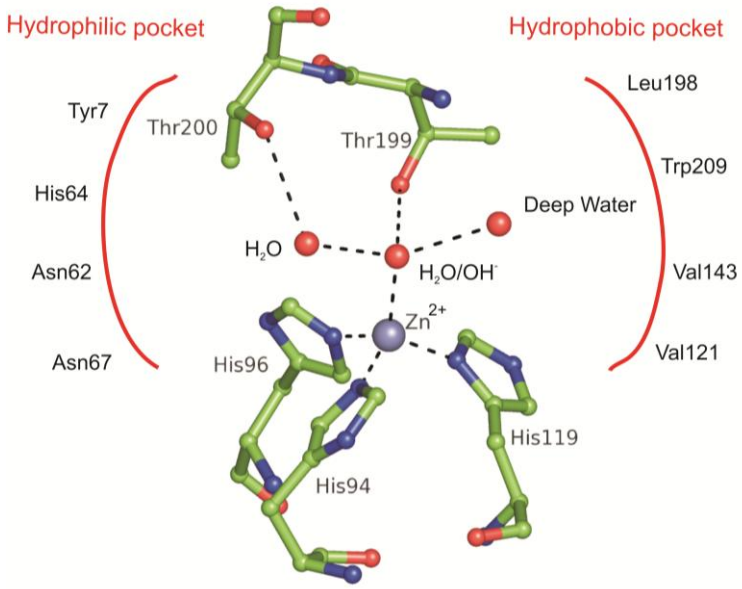

Figure 1.3 *Active site of hCA II.* The zinc ion is tetrahedrally coordinated by the three catalytic histidines and a water molecule/hydroxide ion, which is engaged in well-defined network of hydrogen bonds.

The active site cavity of all the hCA isoforms can be considered as roughly divided into two very different environments: one delimited by a cluster of hydrophobic amino acids, and the other one surrounded with hydrophilic residues (Figure 1.4). These regions have been described as very important in assisting the enzyme to perform the catalytic reaction; indeed the hydrophobic region plays a key role in sequestering the CO_2 substrate, orienting the carbon atom for nucleophilic attack by the zinc-bound hydroxide (Domsic *et al*., 2008; Merz,

1991). On the other hand the hydrophilic region is important to create a well ordered solvent network, which allows the transfer of the proton from the zinc-bound water molecule to the bulk solvent (Figure 1.3), in order to regenerate the active form of the enzyme (Domsic *et al*., 2008; Tu *et al*., 1989; Silverman and McKenna, 2007; Roy and Taraphder, 2007; Fisher *et al*., 2007a).

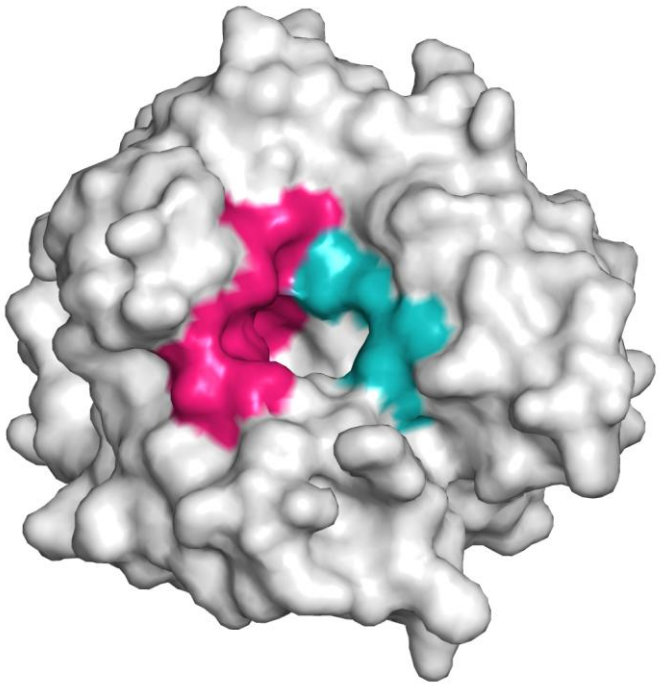

Figure 1.4 *Solvent accessible surface of hCA II.* Residues delimiting the hydrophobic half of the active site cleft are shown in magenta, while residues delimiting the hydrophilic one are shown in cyan.

1.4 Human α-CAs as target for rational drug design

As mentioned in paragraph 1.1, many hCA isozymes represent an attractive goal for the design of inhibitors with biomedical applications. Indeed, while initially CA inhibitors (CAIs) were mainly used as diuretics, antiglaucoma and antiepileptics (Supuran, 2008a), the more recently developed compounds are undergoing clinical investigation as antitumor, antiobesity,

anticonvulsants, and antimicrobials/antifungals agents (De Simone *et al.*, 2008; Thiry *et al.*,2008a; 2008b; Winum *et al.*, 2008; Supuran, 2007).

A careful analysis of the existing literature on CAIs allowed to classify these molecules in two main classes: those that bind the enzyme active site attaching themselves to the catalytic metal, and those that are bound in the active site but do not interact directly with the zinc ion. Inhibitors belonging to the first class have been studied in more detail and are generally characterized by three main structural elements: a zinc-binding group (ZBG), an organic scaffold, and one or more "tails". Several ZBGs have been explored, among which the classical sulfonamide moiety and its bioisosteres, the sulfamate and sulfamide groups, constitute the main players. A large number of organic scaffolds and tails were also examined (Alterio *et al.*, 2009b).

A major problem in this kind of inhibitors resides in the lack of selectivity that they present for the different hCA isoforms. For this reason last years have seen the development of the second class of inhibitors, among which phenols (Nair *et al*., 1994; Davis *et al*., 2011), polyamines (Carta *et al*., 2010), coumarins/thiocoumarins and the antiepileptic drug lacosamide (Maresca *et al.*, 2009; 2010) are the most interesting representatives. These molecules generally bind to the active site but do not interact directly with the catalytic zinc ion. In particular, phenols and polyamines are anchored to the zinc-coordinated water molecule/hydroxide ion, while the coumarins and lacosamide bind at the border of the active cavity partially occluding its entrance. This is a very important feature since the active site regions which are less conserved among the different isoforms are those at the entrance of the cavity. Thus, inhibitors which bind in these regions may have higher probability to show better selectivity.

However, nevertheless a large number of studies performed by several research groups in developing CAIs, none of the currently developed molecules shows a real selectivity for a

specific isozyme (Supuran, 2008a; Supuran *et al*., 2004). Thus, developing isozyme-specific CA inhibitors is currently a very challenging task, that should be highly beneficial in obtaining novel classes of drugs devoid of various undesired side-effects. Some progress in this field has been recently recorded, although a lot of work still has to be performed. As an example, the three-dimensional structure of some hCA isozymes is still unknown at the present. Knowledge of the structural differences between different isozymes should be fundamental to highlight subtle diversities in their active sites to be used in optimized rational drug design of inhibitors selective for one isoform with respect to another one. It is also desirable that interactions of the same inhibitor(s) with all CA isozymes should be characterized by X-ray crystallography, as this will indeed allow us to understand all factors governing selectivity in the drug design of CAIs. This is at the moment possible to some extent only for acetazolamide, a well known CAI, as its crystal structures in complex with CA I, II, VA, VII, IX, XII, XIII and XIV were reported (Di Fiore *et al.*, 2009; 2010; Sippel *et al.*, 2009; Alterio *et al.*, 2009a; Whittington *et al.*, 2004; 2009; Chakravarty and Kannan, 1994; Boriack-Sjodin *et al.*, 1995). However, this is a too simple compound for allowing the use of these structural data for the drug design of isoform-selective compounds. Indeed, compounds with a more sophisticated chemical may afford a deeper insight into phenomena governing these intricate processes.

1.5 Aim of the thesis

On the basis of the above reported considerations, it is clear the interest that several international research groups have shown for studies dedicated to the structure-based drug design of isoform-selective CA inhibitors. In this context my Ph.D thesis is also included, which has been focused on the study of the biochemical and structural features of two cytosolic carbonic anhydrase isoforms, namely hCA VII and hCA I.

1.5.1 hCA VII

hCA VII is one of the least investigated and understood cytosolic hCA isoforms. Similar to hCA II, hCA VII shows very high efficiency as catalyst for hydration of carbon dioxide, being 10-50 times more active compared to other two cytosolic isoforms, hCA I and hCA XIII (Supuran, 2008a; Hilvo *et al*., 2008). However, in contrast to hCA II which is widely spread in human tissues, CA VII has a more limited distribution, being localized mainly in some brain tissues of humans and rats (Hilvo *et al*., 2008; Güzel *et al*., 2009; Ruusuvuori *et al*., 2004), in stomach, duodenum, colon, liver and skeletal muscle of mice (Bootorabi *et al*., 2010). Recently, CA VII has been noted for its contribution in generating neuronal excitation (Thiry *et al*., 2007a), establishing a functionally excitatory GABAergic transmission by supplying bicarbonate anions, which can mediate current through channels coupled to $GABA_A$ receptors (Thiry *et al*., 2008b). The observation that this activity is suppressed by membrane-permeating CA inhibitors corroborates the involvement of CA VII in neuronal excitation and seizures (Ruusuvuori *et al*., 2004; Thiry *et al*., 2007b). More recently, a role of CA VII in the control of neuropathic pain has also been proposed, suggesting that its inhibition may constitute a new pharmacologic mechanism in designing drugs useful for the treatment of this pathological condition (Asiedu *et al*., 2010).

As part of a general research project based on the structure-based drug design of isoform-selective CA inhibitors, the first part of this Ph.D thesis has been focused on a complete characterization of hCA VII. In particular, in chapter 2 an extensive biochemical and catalytic characterization of this enzyme is described, while in chapter 3 its 3D structure together with the preparation of several site directed mutants with improved catalytic efficiency is reported.

1.5.2 hCA I

hCA I is one of the first member of this enzyme family to be identified (Meldrum and Roughton, 1933). It is a cytosolic enzyme mainly localized in erythrocytes, gastrointestinal tract and eyes. The physiological function of this enzyme has been for long time unknown, even if recent studies from Feeener's group (Gao *et al*., 2007) demonstrated its involvement in retinal and cerebral edema, and that its inhibition may be a valuable tool for fighting these diseases. Kinetic characterization of the enzyme showed that hCA I is only a medium catalyst for the CO_2 hydration reaction compared to hCA II and hCA VII (Table 1.1) (Supuran, 2008a). Even though the 3D structure of this enzyme was firstly characterized in 1975 (Kannan et al., 1975), only a few structural studies on the complexes that this enzyme can form with the different inhibitors have been reported so far. As mentioned above these studies are fundamental for the drug design of isoform-selective inhibitors. For these reasons part of this thesis has been dedicated to the structural characterization of a complex which hCA I form with topiramate (**TPM**), a molecule of pharmacological interest for the treatment of epilepsy. The comparative analysis between the structures of the hCA I/**TPM** complex and the hCA II/**TPM** complex allowed to provide useful insights into the molecular bases responsible for the recognition protein-inhibitor, thus providing important hints for the design of new isoform-specific CA inhibitors.

2. Biochemical characterization of hCA VII

2.1 INTRODUCTION

hCA VII is a 263 residues protein which shares 50%, 56%, 49% and 52% sequence identity, respectively, with human CA I, CA II, CA III and CA XIII (Hewett-Emmett and Tashian, 1996; Kivelä *et al.*, 2005; Lehtonen *et al.*, 2004; Pastorekova *et al.*, 2004; Parkkila and Parkkila, 1996; Tashian *et al.*, 1990; Di Fiore *et al*., 2008). Although this protein was firstly identified and characterized by Montgomery and coworkers more than 20 years ago (Montgomery *et al.*,1991), it is still one of the least investigated and understood CA isoforms. It is well established that CA VII is a highly active cytosolic protein with a limited distribution, being localized mainly in brain tissues of humans and rats (Güzel *et al.*, 2009; Ruusuvuori *et al.*, 2004). Only recently, immunohistochemical studies have revealed the presence of CA VII also in the stomach, duodenum, colon, liver and skeletal muscle of mice (Bootorabi *et al.*, 2010), indicating that it represents the major form expressed at the protein level in these tissues. In particular, this protein achieves significant levels of expression in the liver, together with CA VA (Shah *et al.*, 2000) and CA XIV (Parkkila *et al.*, 2002). While it is reported that CA VA regulates the metabolic processes involving hepatic ureagenesis and gluconeogenesis (Shah *et al.*, 2000), the role of hepatic CA VII and CA XIV is still unclear and needs to be further investigated. Thus, in order to deepen our knowledge concerning the functional role of this enzyme, we initiated our studies on hCA VII expressing it in *E.coli* and characterizing it biochemically.

2.2 RESULTS AND DISCUSSION

2.2.1 Cloning, expression and purification of hCA VII

The gene encoding full-length human CA VII (Figure 2.1) was cloned in the pGex-4T-3 expression vector and the recombinant expression of the GST-fused protein was carried out in

E. coli BL21(DE3)pLysS strain, following induction with 0.2 mM IPTG, for 16 h at 22 °C. The total cell recombinant GST-CA VII protein fraction was analyzed by SDS-PAGE, observing a protein band of the expected molecular size (Figure 2.2).

```
atgaccggcc accacggctg gggctacggc caggacgacg gcccctcgca ttggcacaag
ctgtatccca ttgcccaggg agatcgccaa tcacccatca atatcatctc cagccaggct
gtgtactctc ccagcctgca accactggag ctttcctatg aggcctgcat gtccctcagc
atcaccaaca atggccactc tgtccaggta gacttcaatg acagcgatga ccgaaccgtg
gtgactgggg gccccctgga agggccctac cgcctcaagc agtttcactt ccactggggc
aagaagcacg atgtgggttc tgagcacacg gtggacggca agtccttccc cagcgagctg
catctggttc actggaatgc caagaagtac agcacttttg gggaggcggc ctcagcacct
gatggcctgg ctgtggttgg tgttttttg gagacaggag acgagcaccc cagcatgaat
cgtctgacag atgcgctcta catggtccgg ttcaagggca ccaaagccca gttcagctgc
ttcaacccca agtgcctcct gcctgccagc cggcactact ggacctaccc gggctctctg
acgactcccc cactcagtga gagtgtcacc tggattgtgc tccgggagcc catctgcatc
tctgaaaggc agatggggaa gttccggagc ctgcttttta cctcggagga cgatgagagg
atccacatgg tgaacaactt ccggccacca cagccactga agggccgcgt ggtaaaggcc
tccttccggg cc
```

Figure 2.1 *Nucleotidic sequence of the full length human CA 7*

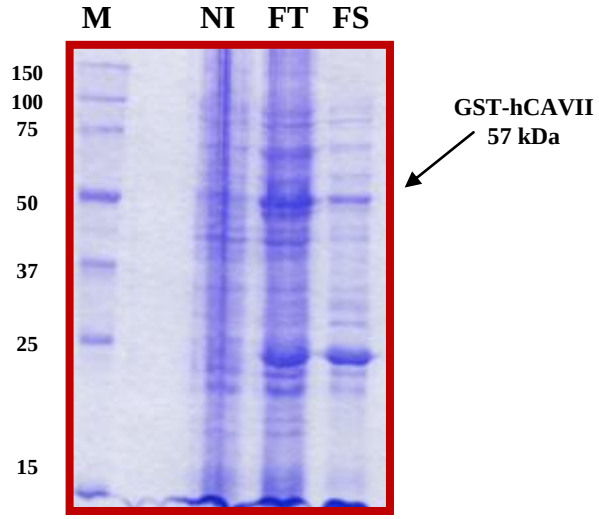

Figure 2.2 *12% SDS-PAGE of GST-CA VII expression in E. Coli.* M, Perfect Protein Markers 15-150 kDa; NI, not- induced cell fraction; FT, total fraction; FS, soluble fraction.

hCA VII-GST from soluble fraction was affinity-purified on GSTrap resin and, following removal of the fused GST-tag by thrombin (GE Healthcare) treatment (Figure 2.3), the resulting digest was purified on NHS-actived Sepharose 4 F resin (Amersham), preactived with 4-Aminomethyl Benzene-Sulfonamide hydrochloride, pAMBS (Sigma). Eluted protein was immediately concentrated and loaded on a Superdex 75 (Figure 2.4) and the

Size Exclusion Chromatography (SEC) purified fractions were analyzed by SDS-PAGE, observing only one protein band of the expected molecular sizes (Figure 2.5).

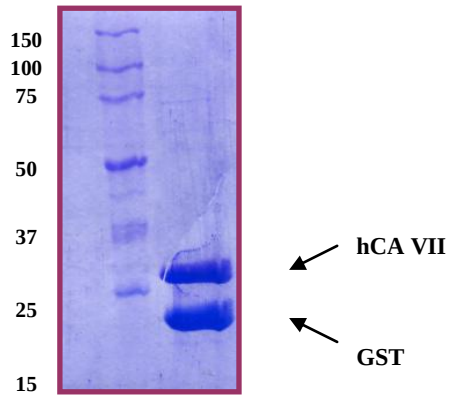

Figure 2.3 *SDS-PAGE analysis of protein upon removal of the fused GST-tag.*

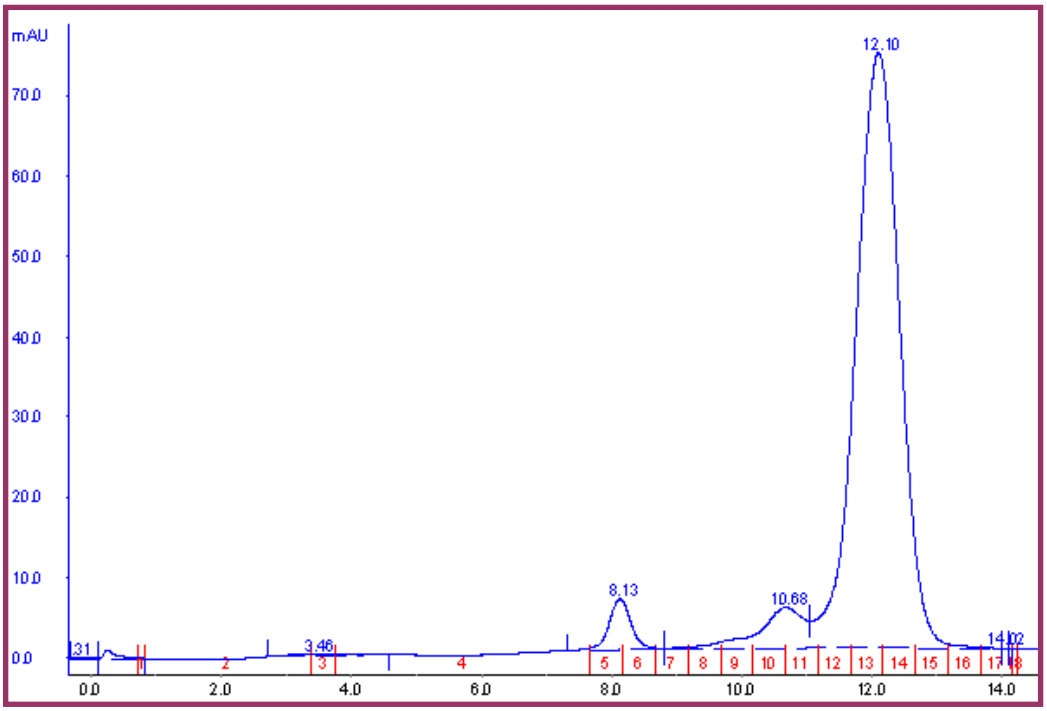

Figure 2.4 *Chromatographic elution profile of hCA VII obtained by SEC on a S75column.*

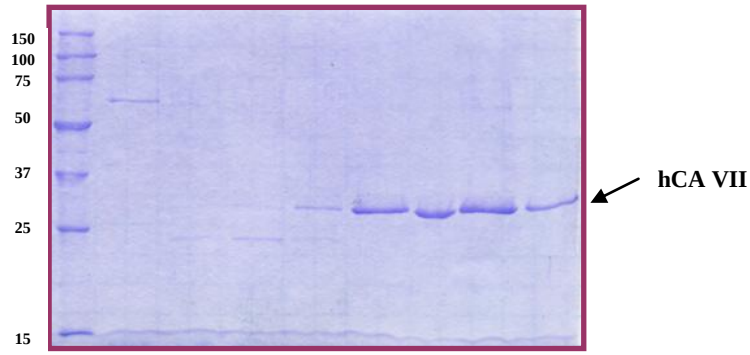

Figure 2.5 *SDS-PAGE of SEC purified fractions.*

2.2.2 Biochemical characterization of hCA VII

Secondary structure of hCAVII was investigated by means of CD in the far-UV region (Figure 2.6). The spectrum clearly demonstrated that the enzyme exhibits a folded structure, showing a large negative band at 214 nm. Estimation of the secondary structure of hCAVII, performed on the basis of the CD spectrum, was carried out according to the Variable Selection Method (CDSSTR) by using DICHROWEB (Lobley *et al.*, 2002; Johnson, 1985) and showing a content of 42% α-helix and 30% β-sheet. hCA VII thermal stability was assessed by following changes of CD signal at 214 nm in the temperature range of 25-85 °C. The Tm value obtained at the midpoint of the thermal denaturation curve was 56.7 °C (Figure 2.7). The process was irreversible under the conditions used, likely due to cross-linking between the free cysteines present within the aminoacidic sequence (Tornatore *et al.*, 2008; Del Vecchio *et al.*, 2006).

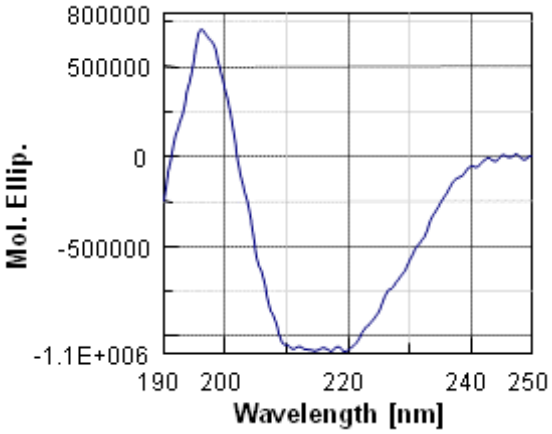

Figure 2.6 *Far-UV CD spectrum of hCA VII.*

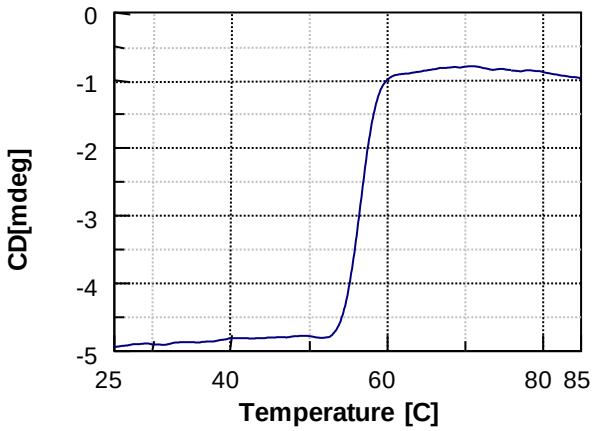

Figure 2.7 *Thermal denaturation of hCA VII.*

hCA VII purity and molecular weight was further characterized by electrospray ionization mass spectrometry. Unexpectedly, the LC-ESI-MS spectrum of purified hCA VII (Figure 2.8 A) showed two major peaks, corresponding to a mass increment of 305 and 610 Da compared to the theoretical molecular weight. When the sample was treated with DTT, a single peak occurred with an experimental mass identical to the expected theoretical molecular weight of 30100.8 Da (Figure 2.8 B). The observed mass increments of 305 and 610 Da were thus ascribed to the incorporation of one or two molecules of glutathione (GSH), that covalently bind to two of the four cysteine residues of hCA VII (Figure 2.9), during elution from the glutathione-Sepharose column with a buffer containing 10 mM GSH. In order to identify

which of the four cysteines were involved in the formation of the covalent adducts with GSH, a protein sample was prepared by digestion with thrombin directly on the column, without the elution with GSH. After elution, it was denaturated with 6 M guanidinium chloride and alkylated with 4-vinylpyridine. The peptide mixture produced by digestion with trypsin was directly analyzed by LC-ESI-MS/MS, with sufficient accuracy to enable unambiguous identification of the triptic peptides (Figure 2.10) (Papa *et al.*, 2007; Tornatore *et al.*, 2008). Fragments containing Cys183 or Cys217 showed that both cysteines were completely modified having incorporated a molecule of 4-vinylpyridine. On the contrary, fragments containing Cys54 and Cys178 were not identified by molecular mass and MS/MS sequencing, but were revealed only after DTT incubation. Altogether these data clearly suggested that of the four cysteines in hCA VII, Cys183 and Cys217 were those involved in S-glutathionylation, whereas Cys54 and Cys178 formed an intramolecular disulfide bridge.

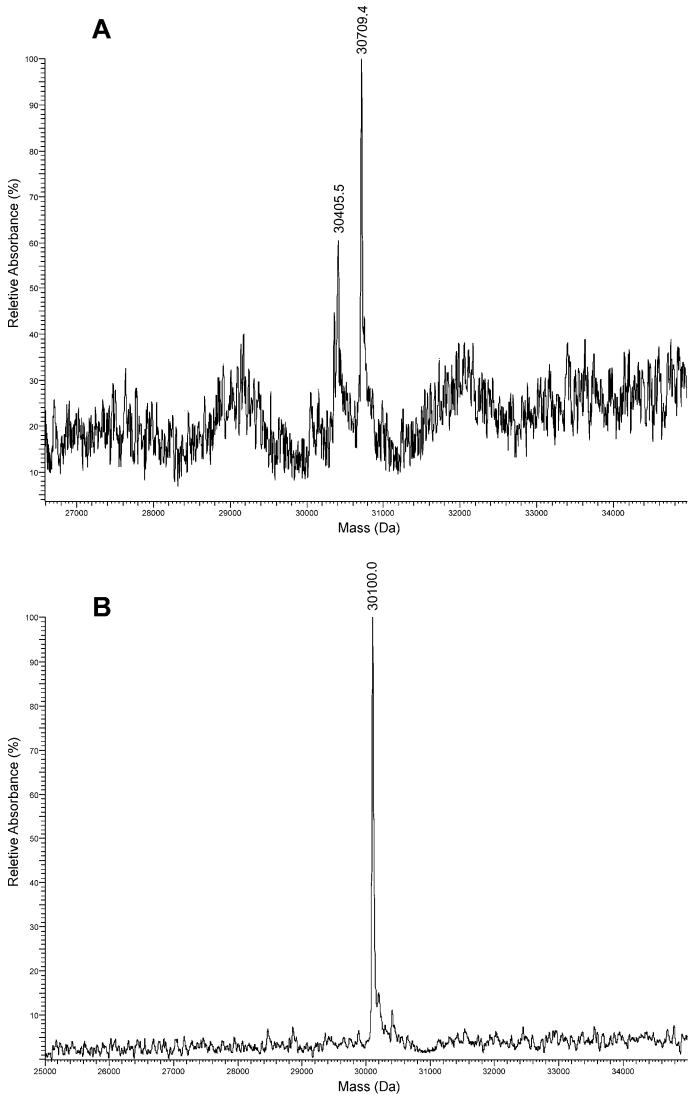

Figure 2.8 *LC-ESI-MS of purified hCA VII*. **(A)** Deconvoluted mass spectrum of purified hCAVII showed the presence of two distinct peaks with a mass greater of 305 and 610 (305*2) compared to the expected one (theorical mw 30100.8 Da). **(B)** After treatment with reducing agent DTT these two peaks disappeared, leading to a unique peak of 30100.0 Da.

GSPNSMTGHHGWGYGQDDGPSHWHKLYPIAQGDRQSPINIISSQAVYSPSLQPLELSYEA**C**MSLSITNNGHSVQV
DFNDSDDRTVVTGGPLEGPYRLKQFHFHWGKKHDVGSEHTVDGKSFPSELHLVHWNAKKYSTFGEAASAPDGLAV
VGVFLETGDEHPSMNRLTDALYMVRFKGTKAQFS**C**FNPK**C**LLPASRHYWTYPGSLTTPPLSESVTWIVLREPI**C**I
SERQMGKFRSLLFTSEDDERIHMVNNFRPPQPLKGRVVKASFRA

Figure 2.9 *Amminoacidic sequence of hCA VII. Cysteines at positions 54, 178, 183, and 217 (numbering refers to hCA I sequence) are highlighted in yellow*. The linker sequence is in red.

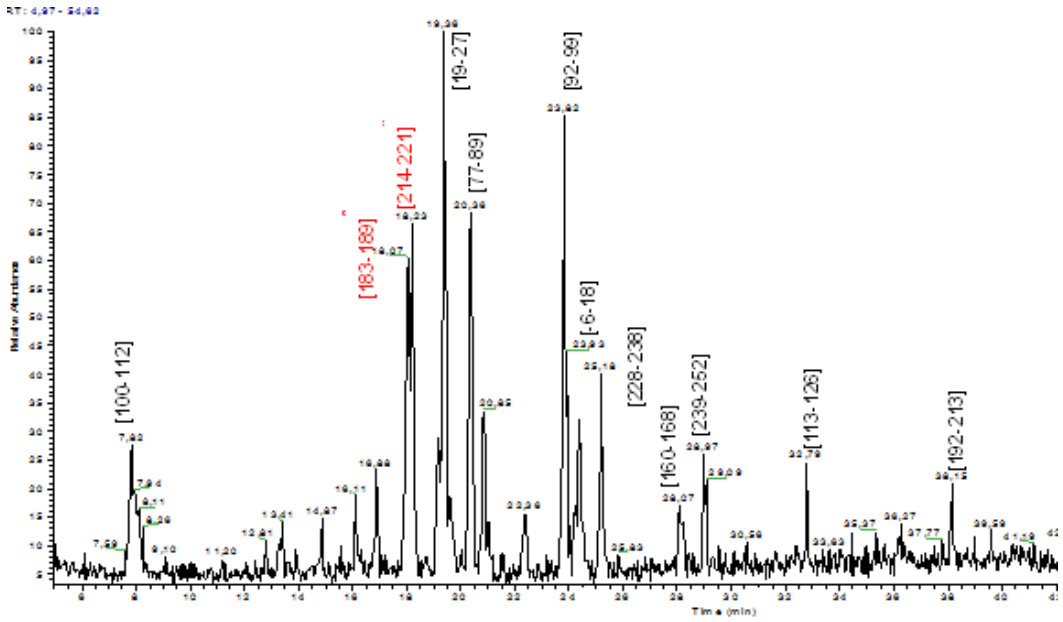

Figure 2.10 *Total Ion Current profile of the peptide mixture of hCA VII produced by digestion with trypsin.*

2.2.3 Role of hCA VII S-gluthationylation

Interesting considerations can be done on the observed *in vitro* S-glutathionylation of Cys183 and Cys217 in hCA VII. This covalent modification can be ascribed to a partial oxidation of cysteines to sulfenic acids or thiol radicals followed by reaction with GSH (Filomeni *et al.*, 2005) used for eluting the protein from GSTrap column. Therefore, both the high reactivity of Cys183 and Cys217 and the high GSH concentration in the experimental conditions were likely the origin of such phenomena.

Interestingly, S-glutathionylation was earlier observed *in vivo* for another member of the CA family, namely rat liver CA III (Chai *et al.*,1991; Lii *et al.*, 1996; Rokutan *et al.*, 1989). This enzyme was shown to be S-glutathionylated at two cysteine residues in positions 183 and 188, likely due to the high concentration of GSH in the liver (Mallis *et al.*, 2000). Moreover, microarray analysis of skeletal muscle of wild type and CA III-deficient knockout mice suggested that CA III, undergoing rapid reversible S-glutathionylation or irreversible oxidation in mildly and exhaustively stressed muscle, has a possible role in the glutathione-

mediated antioxidative system (Zimmerman *et al.*, 2004). These data were also in agreement with a paper of Räisänen and coworkers (Räisänen *et al.*, 1999), where a possible role of CA III as an oxygen radicals scavenger to protect cells from oxidative damage was proposed.

Starting from these observations, a comparative analysis between isozymes VII and III was carried out. hCA VII and hCA III present several analogies: both are cytosolic enzymes and are localized in tissues having a high oxygen consumption rate, such as skeletal muscle, liver and brain. Furthermore, sequence alignment of catalytically active cytosolic α-CAs shows that while hCAs I, II and XIII contain only one cysteine in their sequnce, hCAs III and VII incorporate a higher number of such residues (five and four cysteines for hCA III and VII, respectively). Worth noting is the finding that one of the glutathionylated cysteines of hCA III, namely Cys183, is also conserved in hCA VII (Figure 2.11).

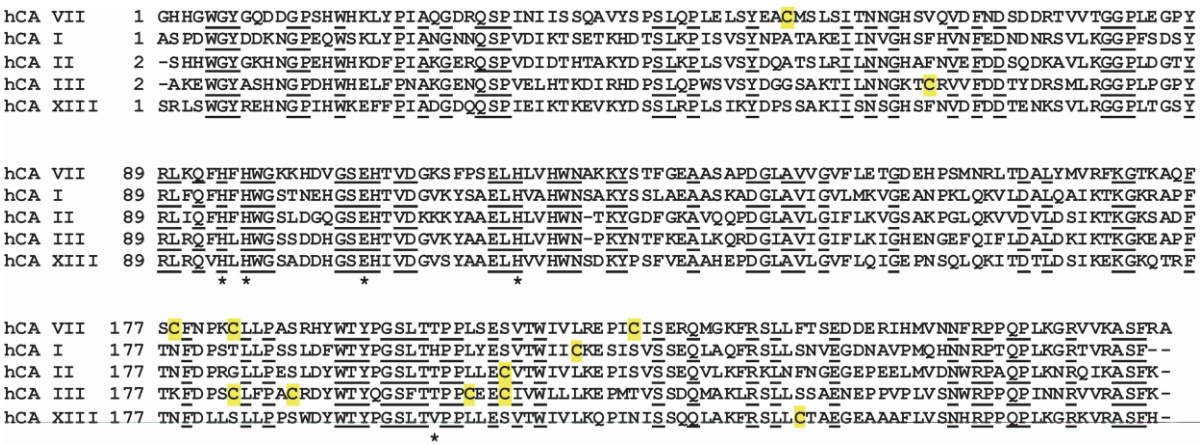

Figure 2.11 *Sequence alignment of catalytically active cytosolic α-CAs.* Conserved residues are underlined, catalytic histidines, and the two residues involved in the orientation of the substrate, Thr199 and Glu106, are indicated with asterisks, whereas the cysteine residues are highlighted in yellow.

All these considerations strongly suggest that the S-gluthathionylation observed *in vitro* for hCA VII could also be present *in vivo*, as observed for isoform III. Thus, to obtain more insight into the role of the covalent modifications of the enzyme, the kinetic parameters for the CO_2 hydration activity were measured (Table 2.1) for the wild type enzyme purified in the absence of GSH (without covalent modifications) and the glutathionylated enzyme (sgCA

VII). Analysis of these data, carried out in collaboration with Supuran's group at the University of Florence, revealed that the kinetic parameters for CO_2 hydration activity of hCA VII and sgCA VII were the same; thus S-glutathionylation of cysteines does not affect the canonical hydrolytic reaction as well as the affinity for acetazolamide (**AZM**), one of the most characterized CA inhibitor.

Table 2.1 *Kinetic parameters for the CO_2 hydration reaction catalysed by cytosolic isozymes I, II, III and VII.*

Isozyme	**k_{cat}/K_M ($M^{-1}s^{-1}$)**	**K_M (mM)**	**K_I (AZM) (nM)**
hCA I	$5.0x10^7$	4.0	250
hCA II	$1.5x10^8$	9.3	12
hCA III	$2.5x10^5$	52	240000
hCA VII	$7.2x10^7$	11.0	2.8
sgCA VII	$8.0x10^7$	10.0	2.7

Measurement of the kinetic parameters was also carried out for non-canonical hydrolytic reactions catalyzed by some CAs, i.e. esterase and phosphatase activities (Tables 2.2 and 2.3), showing that S-glutathionylated enzyme retains the same catalytic activity as the native form. Interestingly, both wild type hCA VII and sgCA VII were shown to act as excellent esterases compared to hCA I, II and III, with 4-nitrophenyl acetate as substrate (Table 2.2). Thus, such data indicate that hCA VII may have another catalytic activity *in vivo*, in addition to the CO_2 hydrase catalytic activity. Finally, wild type hCA VII and sgCA VII were at least one order of magnitude better phosphatases among the cytosolic isoforms reported here (Table 2.3), while hCA III was a better phosphatase compared to hCA II, which instead is the best catalyst for the CO_2 hydration reaction among the cytosolic isozymes. Thus, there is not a clear-cut parallelism between the catalytic activities of these isoforms for the various reactions that they

catalyze. It is tempting to speculate that hCA VII may act as an esterase/phosphatase *in vivo*, but this hypothesis has yet to be verified and eventual alternative substrates of this enzyme determined.

Table 2.2 *Kinetic parameters for the hydrolysis of 4-nitrophenyl acetate catalysed by CA isozymes I ,II,III, VII*

Isozyme	**k_{cat}/K_M ($M^{-1}s^{-1}$)**	**K_M (mM)**	**K_I (AZM) (nM)**
hCA I	753 ± 31	3.025 ± 0.014	1210 ± 76
hCA II	2607 ± 85	30.53 ± 2.10	28 ± 1.1
hCA III	139 ± 12	1.234 ± 0.013	7840 ± 230
hCA VII	(3.27 ± 0.12) x10^6	0.75 ± 0.04	357 ± 12
sgCA VII	(2.39 ± 0.10) x10^6	0.50 ± 0.05	265 ± 9

Table 2.3 *Kinetic parameters for the hydrolysis of 4-nitrophenyl phosphate catalysed by CA isozymes I, II, III, VII.*

Isozyme	**k_{cat}/K_M ($M^{-1}s^{-1}$)**	**K_M (mM)**	**K_I (AZM) (nM)**
hCA I	65.55 ± 5.20	0.935 ± 0.100	330 ± 14
hCA II	14.89 ± 0.54	2.195 ± 0.200	63 ± 5
hCA III	45.32 ± 3.76	1.345 ± 0.160	6500 ± 124
hCA VII	(2.89 ± 0.09) x10^4	1.43 ± 0.09	3440 ± 39
sgCA VII	(3.04 ± 0.11) x10^4	0.97 ± 0.05	2520 ± 49

Altogether these data indicate that the observed S-glutathionylation, if present *in vivo*, is not involved in the regulation of the enzyme catalytic activity but rather, as observed for hCA III, might help hCA VII to function as an oxygen radical scavenger to protect cells from oxidative damage. Indeed, it is worth noticing that *in vivo* glutathione is abundant, reaching millimolar concentration in most cell types, especially in liver (Filomeni *et al.*, 2005; Marì *et al.*, 2009;

2010), which would probably trigger the glutathionylation of CA VII (Filomeni *et al.,* 2005). In order to assess if S-glutathionylation of hCA VII might occur *in vivo* as a result of oxidative stress conditions, Western Blotting analyses were performed on mice liver tissues kindly provided by prof. S. Parkkila of the University of Tampere, Finland. In particular, liver tissues were obtained from mice which had been fed with and without iron since iron can cause oxidative stress conditions in cells according to the Fenton reaction (Rizzello *et al.,* 2007). In fact, the rapid electron transfer between Fe^{3+} and Fe^{2+} allows the generation of two very short-lived and highly aggressive species, such as $OH^{\cdot}$ and O_2 which can lead to cell oxidative stress (Scheme 2.1).

$$Fe^{2+} + H_2O_2 \rightarrow Fe^{3+} + OH^{\cdot} + OH^{-}$$
$$Fe^{3+} + O_2^{-} \rightarrow Fe^{2+} + O_2$$

Scheme 2.1*. Fenton reaction*

For this purpose, two different antibodies were used: anti-CA VII to identify mCA VII, and anti-GSH to verify the S-glutathionylation of cysteines. Preliminary analyses were carried out in order to define minimal antibody sensitivity towards purified recombinant CAVII, and *in vitro* S-gluthationilated recombinant CAVII. Results are reported in figures 2.12A and 2.12B, where it is evident that the two antibodies show different minimal sensitivity, being 100 ng for anti-CAVII (Figure 2.12A), and 500 ng for anti-GSH antibody (Figure 2.12B).

Unfortunately, western blots on liver extracts incubated with anti-CA VII confirmed the presence of the protein in all mice samples (Figure 2.13), but not its S-glutathionylation, likely due to the low concentration of CA VII modified protein in the analysed tissues. All attempts to concentrate CA VII in liver extracts failed thus other experiments are currently

underway to overcome these technical limitations and check the eventual presence and role of CA VII S-glutathionylation *in vivo*.

It is worth to be noticed that apart the formation of mixed disulfide bonds which can protect protein functionality, high cysteine reactivity might have a different biological role not related to S-gluthationylation. This last matter, as well as the detection of an intramolecular disulfide bridge between Cys54 and Cys178 reported by our group and subsequently also by Parkkila's group (Bootorabi *et al*., 2010), taken into account that hCA VII is a protein living in a cytoplasmatic enviroment, is currently under study.

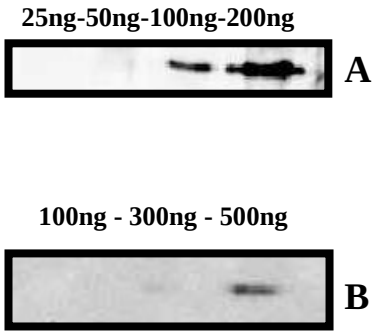

Figure 2.12 A and B *Western blot incubated with anti-CA VII* ***(A)*** *and anti-GSH* ***(B)*** *antibody using different amounts of recombinant CA VII and S-gluthationilated recombinant CA VII.*

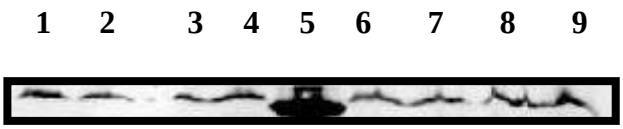

Figure 2.13*Western blot incubated with anti-CA VII* antibody. Lane 1 and 2: male mice liver tissues fed without iron; lane 3 and 4: male mice liver tissues fed with iron; lane 5: 200 ng of hCA VII wild type; lane 6 and 7: female mice liver tissues fed without iron; lane 8 and 9: male mice liver tissues fed with iron.

2.3 MATERIALS AND METHODS

2.3.1 Expression vector

pGeX-4T-3 (GE Healthcare) plasmid was chosen as it represents a powerful host-vector system for cloning and expression of recombinant proteins in *E. Coli.* It contains a strong promoter from T7 bacteriophage for chemical induction by IPTG and overexpression of recombinant proteins, a multiple cloning site (MCS) and a Thrombin protease recognition site for cleaving the fusion protein. In particular, this vector has a GST fusion tag (Figure 2.14).

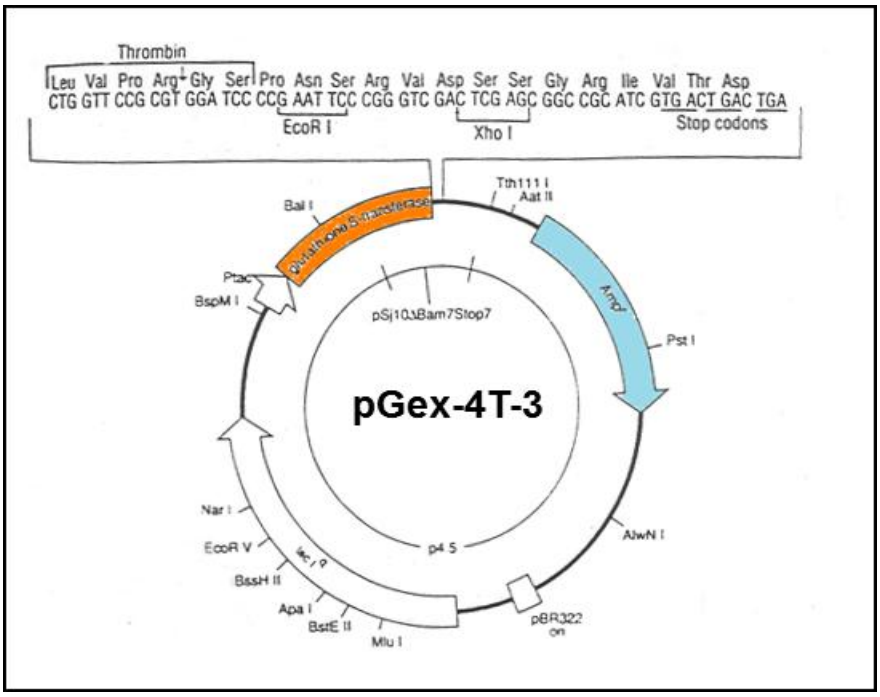

Figure 2.14. *Map of expression vector pGex-4T-3.*

2.3.2 Chemicals

Reagents used for preparation of buffers were supplied by Sigma Aldrich and the reagents for the growth media of *E. coli* were from Becton-Dickenson. The reagents for polyacrylamide gel electrophoresis were supplied by GE Healthcare. Protein molecular weight markers were from Novagen. Phusion DNA polymerase was from Finnzymes and Pfu DNA polymerase is a

Stratagene product. Restriction enzymes and T4 DNA ligase were from New England Biolabs. All molecular biology kits were from Qiagen. Oligonucleotides were synthesized at Primm s.r.l. (Milano, Italy); pGex *E. coli* expression plasmids were from GE Healthcare. cDNA of the hCA VII were kindly provided by Prof. Kai Kaila (University of Helsinki, Finland). *E. coli* TOPF'10 strain, used for cloning, was supplied by Invitrogen; *E. coli* BL21(DE3)pLysS cells, used for overexpression, were supplied by Novagen. PMSF was supplied by Sigma-Aldrich.

2.3.3 Cloning of *hCA 7* in pGex-4T-3

The *CA7* gene was amplified by PCR from cDNA using Phusion DNA polymerase and the following primers:

Forward 5'- CGCGCG**GAATTC**CATGACCGGCCACCACGGCTGG – 3'

EcoRI

Reverse 5'-CGCGCG**CTCGAG**TCATCAGGCCCGGAAGGAGGCCTTTAC – 3'

XhoI

The forward primer contained the *EcoRI* restriction site, while the reverse primer was designed with the *Xho* I restriction site plus two stop codons. The amplification reactions were performed in a final volume of 50 μL, using 10 ng of template DNA. The reaction mixture contained the specific primers (100 pmol each), dNTPs (25 mM each) and the *Phusion* DNA polymerase (2.5 U). PCR was performed using a *Biorad* apparatus, following the procedure indicated below:

* Initial denaturation (step 1) 1 min at 98 °C

* Denaturation (step 2) 10 sec at 98 °C

* Annealing (step 3) 30 sec at 63° C

* Elongation (step 4) 30 sec at 72 °C

for 30 cycles, from step 2.

* Elongation (step 5) 10 min at 72 °C

All amplification products were analyzed by 0.8% agarose (Euroclone) gel electrophoresis performed in 0.5X TBE buffer (1 mM EDTA, 45 mM Tris base, 45 mM boric acid pH 8.3). PCR products were purified by using the *QIAquick PCR Purification Kit* (Qiagen), and digested with *Eco RI* (20 U/μL) and *Xho* I (20 U/μL) restriction enzymes. The amplified fragment (1μg) was digested with 5 U restriction enzymes for 1 h at 37 ºC in a buffer containing 50 mM NaCl, 10 mM Tris-HCl, 10 mM $MgCl_2$, 1 mM DTT pH 7.9 supplemented with BSA 100 μg/mL. Following digestion, the fragment was cloned into the corresponding sites of the pGex-4T-3 expression vector, downstream from the GST-tag sequence. For this purpose, the expression vector was previously digested with the same restriction enzymes (5 U/μg), and treated with alkaline phosphatase (CIP, 1 U) (NEB) for 15 min at 37 ºC, then for 45 min at 50 °C. Following digestion, PCR amplifications were purified by *QIAquick PCR Purification Kit* (Qiagen), while the *EcoRI*/*XhoI* pGex-4T-3 was purified by *QIAquick Gel Extraction Kit* (Qiagen). For ligation reactions a 1:3 molar ratio (vector/insert DNA) was used. Reactions were performed using 20 U/μg DNA of the T4 DNA Ligase (400 U/μL), in a final volume of 20 μL, for 3 h at RT. *E. coli* TOPF'10 strain was used for cloning. Minipreps were performed with Qiaquick miniprep (Qiagen). The identity of the inserts in the resulting recombinant plasmids was confirmed by digestion and DNA sequencing (SBM-Zoological Station, Napoli).

2.3.4 *E. coli* cell transformation techniques

2.3.4.1 Preparation of *E. coli* TOPF'10 cells and transformation by electroporation

2.5 mL of an overnight culture of *E. coli* TOPF'10 cells was inoculated into 250 mL of LB medium. The cells were grown up to mid-log phase (0.5 OD at 600 nm) at 37 °C, stored on ice for 30 min then harvested by centrifugation (4000 rpm, 15 min, 4 °C). The pellet was washed in 125 mL 10% glycerol and recentrifuged. The wash was repeated before resuspending in 750 μL 10% glycerol, 0.125% yeast extract, 0.24% tryptone.

Aliquots of 50 μL cells were mixed with 2 μL of the DNA ligase reaction, incubated for 1 min on ice and transferred into chilled plastic cuvettes with an electrode gap of 0.1 cm (BioRad). High voltage electroporation (1.8 V) was performed with a Micropulser^{TM} (BioRad) at 50 Hz. A shock pulse was applied to competent cells producing pulse length of ~4.0 ms. Immediately after electroporation cell mixtures were diluted to 1 mL with LB medium and incubated for ~1 h shaking at 37 °C. The cells were then plated onto selective solid medium supplemented with 100 μg/mL ampicillin and grown 16 h at 37 °C, to isolate the recombinant clones. Single clones were inoculated in 5 mL LB medium with the same antibiotic and grown over night shaking at 37 °C. Finally, the cells were harvested by centrifugation (13000 rpm, 5 min, 4 °C) and processed to extract plasmidic DNA by using the *QIAprep Spin Miniprep Kit* (Qiagen).

2.3.4.2 Preparation of *E. coli* BL21(DE3)pLysS competent cells and transformation by heat shock

Single clones of *E. coli* strains, grown at 37 °C in LB agar, were inoculated into 5 mL LB medium and incubated overnight shaking at 37 °C. The cells were inoculated into 400 mL LB medium, the culture was grown up to mid-log phase (0.5 OD at 600 nm) at 37 °C, stored on ice for 15 min then harvested by centrifugation (4000 rpm, 10 min, 4 °C). The pellet was resuspended in 100 mL of 50 mM $CaCl_2$, 10 mM Tris HCl, pH 7.5, stored on ice for 30 min

and harvested by centrifugation (4000 rpm, 10 min, 4 °C). The pellet was resuspended in 10 mL of 50 mM $CaCl_2$, 10 mM Tris HCl, pH 7.5 and 15% glycerol. Aliquots of 200 μL were frozen on dry ice and stored at -80 °C.

Aliquots of 200 μL of competent cells were mixed with 20 ng of plasmidic DNA and stored on ice for 30 min. The cell mixtures were transferred at 37 °C for 2 min, on ice for 2 min (heat shock) and then diluted to 1 mL with LB medium. An incubation of 1 h shaking at 37 °C was performed before plating the cells onto selective solid medium supplemented with the appropriate antibiotics (ampicillin, chloramphenicol).

2.3.5 Large-scale expression

After an initial screening of small-scale expression cultures, performed using different strains, temperatures, IPTG concentrations and induction lengths, recombinant constructs were transferred into *E. coli* BL21(DE3)pLysS that assured the best expression level in soluble phase. Single clones of *E. coli* strain, previously transformed with the recombinant expression vector and grown at 37 ºC on LB agar containing the appropriate antibiotic, were inoculated into 2 mL of LB medium, containing the same antibiotic, and after 2 h were inoculated in 20 mL prewarmed LB medium. Once at mid-log phase this was in turn inoculated into 400 mL of pre-warmed LB medium. Cultures were grown at 37 °C under shaking until they reached the mid-log phase (0.7/0.8 OD at 600 nm); then, were induced with 0.2 mM IPTG and growth proceeded at 22° over night. The cells were harvested by centrifugation (4000 rpm, 20 min, 4 °C) and cell pellets were resuspended in a lysis buffer containing PBS 1x, PMSF 1 mM, Lysozyme 1 mg/mL, Benzamidine 5 mM and protease inhibitors (Leupeptin 1 μg/μL, Pepstatin 1 μg/μL, Aprotinin 1 μg/μL). The suspension was left for 30 min at room temperature then sonicated for 12 min, using a Misonix Sonicator 3000 apparatus with a micro tip probe and an impulse output of 9/12 Watt. Bacterial lysate was then centrifuged

(15000 rpm, 40 min, 4 °C) and the supernatant (soluble fraction) collected and analyzed by SDS-PAGE to assess the presence of recombinant products of interest.

2.3.6 Purification of GST-hCA VII

Lysate containing tagged recombinant protein was purified by affinity chromatography on 1 mL GSTrap column connected to an AKTA-FPLC system. Before loading the lysate, the resin was extensively washed with water then equilibrated in PBS 1x. The lysate was loaded into a 10 mL loop at a flow of 0.5 mL/min. Flow-through containing all unbound proteins was collected and the resin was washed with PBS 1x; finally GST-tagged protein was eluted with 10 mL of a solution containing Tris-HCl 30 mM, GSH 10 mM, pH 8.0. All collected pools (flow-through, washes and elutions) were analyzed on SDS–PAGE gel and stained with Coomassie Brilliant Blue R-250.

2.3.7 Digestion of GST-hCA VII

2.3.7.1 Thrombin digestion of tagged protein by dialysis

After purification by affinity chromatography, the GST-tagged protein was dialyzed overnight against Thrombin (GE Healthcare) buffer (20 mM Tris-HCl, 150 mM NaCl, pH 8.0) at 4 °C. 1 U of Thrombin was added to 200 μg of protein substrate. Cleavage product was analyzed by polyacrylamide gel electrophoresis.

2.3.7.2 On column thrombin digestion

1 mL of buffer containing 20 mM Tris-HCl, 150 mM NaCl, pH 8 and thrombin 1 U/200 μg of protein and the column was sealed and incubated for 16 h at 4 °C. The protein was eluted and the cleavage product was analyzed by SDS-PAGE gel.

2.3.8 Affinity chromatography on pAMBS actived resin

NHS-actived Sepharose 4 Fast Flow (GE Healthcare) was applied to an empty econocolumn (BioRad) and washed with 10 c.v. cold 1 mM HCl. The resin was incubated with 1 mL cold sodium phosphate 100 mM, pH 7.5 containing 20 mg of 4-Aminomethyl Benzene-Sulfonamide hydrochloride, pAMBS (Sigma), for 2 h at RT. The resin was repeatedly washed with 100 mM sodium acetate solution, pH 4.0 and 0.5 M Tris-HCl, pH 8.0. Finally, the resin was equilibrated in 20 mM Tris-HCl, 150 mM NaCl, pH 8.0.

The thrombin cleaved recombinant protein was loaded on pAMBS resin actived and incubated for 30 min at R.T. Flow-through containing all unbound proteins was collected, the resin was extensively washed with 20 mM Tris-HCl pH 8.0 and the protein linked to the resin was eluted with 500 mM $NaClO_4$, 100 mM NaAc, pH 5.2. Fractions were analyzed by SDS-PAGE gel and concentrated on Amicon Ultra membranes (Millipore), changing the buffer with a solution containing 50 mM Tris-SO_4, 150 mM NaCl, pH 8.0.

2.3.9 Size Exclusion Chromatography

Size exclusion chromatography was performed to purify all recombinant proteins by removing aggregates and contaminants. Runs were performed at 0.5 mL/min on a Superdex-75 10/300 GL (GE Healthcare) column connected to an AKTA Purifier system, in 30 mM Tris-HCl pH 8.0, 150 mM NaCl. Molecular weight standards from GE-Healthcare were used to calibrate the column. Pools of interest were analyzed by SDS-PAGE gel.

2.3.10 Proteins analysis

2.3.10.1 Determination of protein concentration

Protein concentration was determined according to the Bradford's method (Bradford, 1976). The Coomassie Brilliant (Bio-Rad) reagent was added to the samples and the absorbance at 595 nm was monitored. A solution of bovine serum albumin (BSA) was used as standard. Protein concentration was also measured by UV spectroscopy, reading the tryptophan absorbance at 280 nm, using a Jasco V-550 UV-VIS spectrophotometer, in a 1 cm quartz cell.

2.3.10.2 Electrophoretic analysis of proteins (SDS-PAGE)

The electrophoresis on 12% polyacrylamide gel in denaturing conditions was performed according to Laemmli's protocol (Laemmli, 1970). Samples were denatured at 100 °C for 2 min in 1% SDS (Applichem), 5% β-mercaptoethanol (Sigma), 0.001% bromophenol blue (ICN Biomedicals) and 10% glycerol (Applichem) before loading on a polyacrylamide gel. Electrophoresis was performed in 0.025 M Tris-HCl, 0.2 M glycine pH 8.3 and 0.1% SDS, at 30 mA for ~1 h and proteins were revealed by Coomassie Brilliant-Blue (Applichem) staining; the gel was submerged in the staining solution (0.1% Coomassie Brilliant-Blue R250, 25% isopropilic alcohol and 10% acetic acid) for 30 min with gentle agitation. The gel was washed in a solution containing 30% ethanol and 10% acetic acid to remove the excess of Coomassie before drying.

2.3.10.3 Western Blot analysis

After gel electrophoresis, proteins were transferred to a nitrocellulose membrane (Hybond, Amersham Biosciences) in Blotting Buffer (19 mM Tris-HCl pH 8.0, 140 mM Glycine and 20% methanol) for 90 min, at 100 V, the gel and nitrocellulose membrane being initially equilibrated in Blotting Buffer for 15 min. After electro-blotting, the membrane was stained

with Ponceau Red to verify protein transfer and incubated in blocking solution (0.5% Milk (BioRad) in TBST 1x buffer, containing 500 mM NaCl, 20 mM Tris-HCl pH 7.5, 0.3% Tween 20) at room temperature for 1 h.

To verify the presence of CA VII in mice liver tissues, the membrane was washed with TBST 1x buffer and then incubated with an anti-CA VII antibody (dilution 1:1000) at 4 °C over night (anti-CA VII antibody and mice liver tissues were kindly provided by prof. Seppo Parkkila of University of Tampere, Finland). Successively, the membrane was washed with TBST 1x buffer and shaked for 1 h at room temperature in 1:5000 diluted horseradish peroxidase-conjugated anti-rabbit antibody (BioRad), as the secondary antibody. The membrane was finally washed with TBST 1x buffer. In order to verify S-gluthationylation of CA VII in mice liver tissues, the membrane was incubated in an anti-GSH antibody (ViroGen, Watertown, MA) 1:500 diluition, at 4 °C over night and successively washed with TBST 1x buffer and shaked for 1 h at room temperature in 1:5000 diluted horseradish peroxidase-conjugated anti-mouse antibody (BioRad), as the secondary antibody.

The detection of immunopositive species by enzyme-linked chemi-luminescence (enhanced chemi-luminescence, ECL) was performed according to the manufacturer's instructions (Super Signal®West Pico Chemiluminescent Substrate, Pierce), using a ChemiDoc XRS apparatus (Bio-Rad).

2.3.11 Protein characterization by LC-ESI-MS

To estimate hCA VII purity and assess its molecular weight, protein analyses were performed on a LC-MS system comprising a LCQ DECA XP ion trap mass spectrometer (ThermoElectron, Milan, Italy) equipped with an OPTON ESI source (operating at a needle voltage of 4.2 kV and 320 °C temperature) and a complete Surveyor HPLC system (including MS pump, autosampler and photo diode array [PDA]). For this analysis, 0.5 μg of hCA VII

was loaded on a Phenomenex Jupiter C4 column (2.0x 250 mm, 300Å) and a linear gradient of buffer B (0.05% TFA in CH_3CN) in buffer A (0.08% TFA in H_2O) from 30% to 70% in 40 min was used. Mass spectra were recorded continuously in the mass interval 400-2000 amu, in 27 positive mode (LC-MS, condition 1). Multicharge spectra were then deconvoluted using the BioMass program implemented in the Bioworks 3.1 package provided by the manufacturer's instruction. Mass calibration was performed automatically by means of selected multiple charged ions, in the presence of a calibrant agent (UltraMark; ThermoElectron, Milan). All mass values are reported as average.

2.3.12 Redox-state study of hCA VII

In order to estimate the redox-state of hCA VII, 50 μg of purified protein was denatured in 50 μL of a solution containing 250 mM Tris-HCl, 1 mM EDTA, and 6 M guanidine chloride pH 8.5, for 30 min at 45 °C without reducing agents. The protein was then alkylated by incubating the sample mix in the presence of 0.12 M 4-vinyl-pyridine (4-VP) at 25°C for 60 min. The reaction was stopped by cooling the sample at 4 °C. As a control, the protein also was reduced, before alkylation by 4-VP.

Trypsin digestion of wild type hCA VII and its alkylated form, both previously heated at 50 °C for 30 min, was performed in 50 mM Tris-HCl pH 7.5, choosing a molar ratio trypsin:hCA VII of 1:100. The reaction was allowed to proceed at 37 °C for 16 h and the mixture of peptides was analyzed by LC-MS, using a BioBasic C18 column (30x2.00 mm ID, ThermoElectron) and a method developed with a linear gradient of buffer B in buffer A from 5% to 70% in 65 min. Mass spectra were recorded continuously at mass intervals of 400-2000 amu, in positive mode and Data-Dependent Analysis (DDA) in order to fragment the eluted peptides and obtain sequence information.

2.3.13 CD analysis

Far-UV circular dichroism spectra of hCA VII were obtained by using a Jasco J-715 spectropolarimeter, equipped with a PTC-423S/15 Peltier temperature controller, in a 0.1 mm quartz cell. Spectra were acquired according the following parameters: far UV range of 190-260 nm, band width of 2 nm, response of 4 sec, data pitch of 0.1 nm and scanning speed of 20 nm/min. Spectra were performed at 20 °C, at a protein concentration of $5.5x10^{-5}$ M in 10 mM phosphate buffer pH 8.0. Molar ellipticity per mean residue, [θ] in deg cm^2 $dmol^{-1}$, was calculated from the equation: $[\theta]=[\theta]_{obs}\cdot mrw/10\cdot l\cdot C$, where $[\theta]_{obs}$ is the ellipticity measured in degrees, mrw is the mean residue molecular mass, 114 Da, C is the protein concentration in gxL^{-1} and l is the optical path length of the cell in cm. Spectra processing was obtained by using the Spectra Manager software.

Thermal denaturation of hCA VII was monitored by using CD spectroscopy. The spectrum was recorded using the same Jasco apparatus with a protein sample at the concentration of $5.5x10^{-5}$ M in 10 mM phosphate buffer pH 8.0. Specifically, the minimum centered around 214 nm was monitored as the temperature of the solution was increased from 25 °C to 85 °C with a scan rate of 1.0 °C/min. Data were fitted to a two-state transition model, and the resulting curve was used to calculate the value of Tm, which corresponds to the temperature at the midpoint of the thermal denaturation.

2.3.14 Catalytic activity assays

All investigations concerning the catalytic activity of wild type hCA VII and sgCA VII were carried out in collaboration with Supuran's group of the University of Florence, Italy.

2.3.14.1 CO_2 hydrase activity

Initial velocities were determined by following the change in absorbance using a stopped-flow spectrophotometer (Applied Photophysics Model SX.18MV). CO_2 solutions were made by bubbling carbon dioxide into water or D_2O for the solvent hydrogen isotope effect studies. Dilutions were made through two syringes with a gastight connection. The CO_2 concentrations for the substrates ranged from 1.7 to 17 mM in H_2O. Maximum absorbance was observed at 557 nm, using as buffer-indicator pair 10 mM Hepes, pH 7.4, 0.1 M Na_2SO_4 and 0.2 mM phenol red.

In order to determine the K_I, different concentrations of the inhibitor and the enzyme were preincubated for 10 min at RT. The kinetic constants were carried out by PRISM 3 software (Khalifah, 1971).

2.3.14.2 Esterase activity assays

Measurement of the esterase function of wild type hCA VII and sgCA VII was performed following the hydrolysis of 4-nitrophenyl acetate and the absorbance change at 405 nm, using UV-VIS spectrophotometer (Perkin Elmer Lambda Bio20). The substrate was dissolved in acetonitrile and diluted in 10 mM Hepes, 10 mM Tris, pH 7.4, adding 0.1 M Na_2SO_4. Initial velocities were determined at 25 °C and the kinetic constants were carried out by Michaelis-Menten model at substrate concentrations in the range 0.3-5.0 mM. The uncatalyzed rates were subtracted from the observed rates and the values of k_{cat}/K_M were determined by PRISM software.

2.3.14.3 Phosphatase activity assays

This assay was performed following the hydrolysis of 4-nitrophenyl phosphate at 405 nm, using UV-VIS spectrophotometer (Perkin Elmer Lambda Bio20) at 25 °C. Substrate concentrations varied in the range 0.08-5 mM and the kinetic constants were carried out by Michaelis-Menten model, using PRISM software.

3. Insights into structural determinants responsible of the different catalytic efficiency of cytosolic CAs

3.1 INTRODUCTION

Although important advances have recently been reported concerning the catalysis and inhibition of human CAs, an important and still unresolved issue in this research field is the complete understanding of the structural determinants of the various isozymes contributing to the different catalytic efficiency and response to inhibitors. Indeed, kinetic studies on human CA isozymes show significant differences in catalytic efficiency. For example among the cytosolic isoforms hCA II and hCA VII act as very efficient catalysts, hCA I and hCA XIII with medium efficiency, and finally hCA III as a very poor catalyst (Supuran, 2008a; Hilvo *et al.,* 2008). Even greater differences have been observed between isozymes when comparing the K_I values measured for certain clinically used inhibitors. These data are rather surprising considering that most of the CA active site residues are highly conserved among the different isoforms (Alterio *et al.,* 2009b).

Much insight regarding the role of different residues on the catalytic mechanism has been obtained by mutating residues within the CA active site (Genis *et al.,* 2009; Domsic *et al.,* 2008; Fisher *et al.,* 2007b; Elder *et al.,* 2004; Elleby *et al.,* 1999; Liang *et al.,* 1993; Fierke *et al.,* 1991; Hunt and Fierke, 1997; Taoka *et al.,* 1992; Tu *et al.,* 1989; Almstedt *et al.,* 2009). However, most of these mutations have been performed on the ubiquitous, physiologically dominant isoform hCA II and to a lesser extent on the slower isoform hCA I. During my Ph.D thesis I have continued such studies, focusing my attention on two cytosolic isoforms, hCA VII and hCA XIII. In particular, at the beginning of my Ph.D I solved the X-ray structure of isoform VII, thus completing the structural characterization of cytosolic human CAs. Subsequently, having all the 3D structures of the cytosolic isoforms available, I performed a rational design of several hCA VII and hCA XIII mutants, by a detailed structural comparison of the active sites of all cytosolic isoforms. The aim of this was to obtain mutated hCA

isoforms with improved catalytic efficiency in order to clarify the contribution to the catalytic activity of each single residue within the enzyme active site.

3.2 RESULTS AND DISCUSSION

3.2.1 Structural characterization of hCA VII

3.2.1.1 Crystallization experiments on native hCA VII

Several crystallization trials on native hCA VII, produced as described in Chapter 2, were carried out using the hanging-drop vapour-diffusion method (Ducruix and Giegè, 1999). The search for initial crystallization conditions was performed using Hampton Research Crystal Screens I and II (Jancarik & Kim, 1991; Cudney *et al.*, 1994). In particular, an aliquot of hCA VII was concentrated to 10 mg/mL in 20 mM Tris-HCl pH 9.0, containing 100 mM NaCl. Drops were prepared by mixing 1.0 µL of protein with 1.0 µL of precipitant solution and equilibrated against 500 µL of precipitant solution at 20 °C. Analysis of all drops showed the formation of several microcrystalline precipitates that, in general, could represent a good starting point for searching for the optimal precipitating agent. Several parameters such as buffer composition, pH and protein concentration were thus varied to optimize crystallization conditions. However, all trials failed since no suitable crystals for X-ray diffraction data grew. In order to assess the enzyme stability and homogeneity at the high concentration used for the crystallization experiments, the protein sample was analyzed by SDS-PAGE under reducing and non-reducing conditions after three days storage at 4 °C. The results of the gel-electrophoresis showed the presence of covalent oligomers due to the formation of an intermolecular disulfide bridge (Figure 3.1).

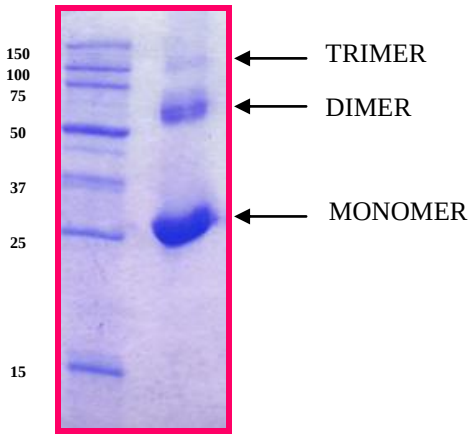

Figure 3.1 12*% SDS-Page of hCA VII under non reducing conditions.*

Thus, to avoid the crystallization problems caused by the mixture of structurally different reduced and oxidized enzyme forms, we expressed a hCA VII mutant, hereafter called hCA VII C183S/C217S, where cysteine residues in position 183 and 217, which in the previous chapter were demonstrated to be particularly reactive, were mutated into serines (Figure 3.2).

GSPNSMTGHHGWGYGQDDGPSHWHKLYPIAQGDRQSPINIISSQAVYSPSLQPLELS
YEACMSLSITNNGHSVQDFNDSDDRTVVTGGPLEGPYRLKQFHFHWGKKHDVGSEHT
VDGKSFPSELHLVHWNAKKYSTFGEAASAPDGLAVVGVFLETGDEHPSMNRLTDALY
MVRFKGTKAQFSCFNPK**S**LLPASRHYWTYPGSLTTPPLSESVTWIVLREPI**S**ISERQ
MGKFRSLLFTSEDDERIHMVNNFRPPQPLKGRVVKASFRA

Figure 3.2 *Amminoacidic sequence of hCA VII C183S/C217S (pI 7.0, MW 30068.2 Da).* Cysteines 54 and 178 are shown in red; cysteines 183 and 217 mutated in serines in blue; the linker sequence in brown.

3.2.1.2 Production of the hCA VII C183S/C217S mutant

hCA VII mutations were performed using the QuikChange Site-Directed Mutagenesis Kit (Stratagene) and expression of the positive clone was performed in *E. Coli* BL21(DE3)pLysS, following induction with 0.2 mM IPTG, for 16 h at 22 °C. The cell recombinant GST-hCA

VII C183S/C217S protein fraction was analyzed by SDS-PAGE, observing a protein band of the expected size (Figure 3.3).

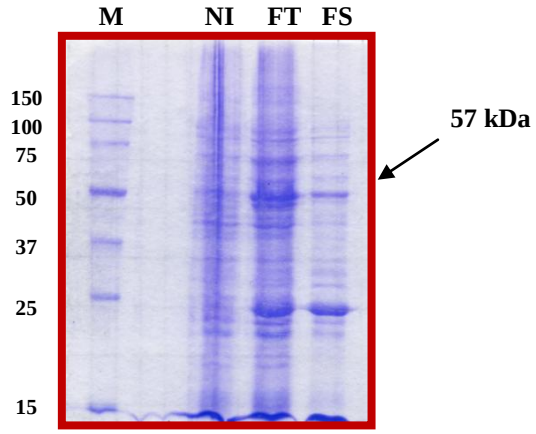

Figure 3.3 *12% SDS-PAGE of the expression of GST-CA VII C183S/C217S protein in E. Coli.* M, Perfect Protein Markers 15-150 kDa; NI, non-induced cell fraction; FT, total fraction; FS, soluble fraction.

The soluble fraction of GST-hCA VII C183S/C217S was affinity-purified on GSTrap resin and, following removal of the fused GST-tag by thrombin (GE Healthcare), the resulting digest was purified on NHS-actived Sepharose 4 F resin (Amersham) preactived with pAMBS (Sigma). Eluted protein was concentrated and loaded on a Superdex 75 (Figure 3.4A) and the SEC purified fractions were analyzed by SDS-PAGE, observing a protein band of the expected size (Figure 3.4B).

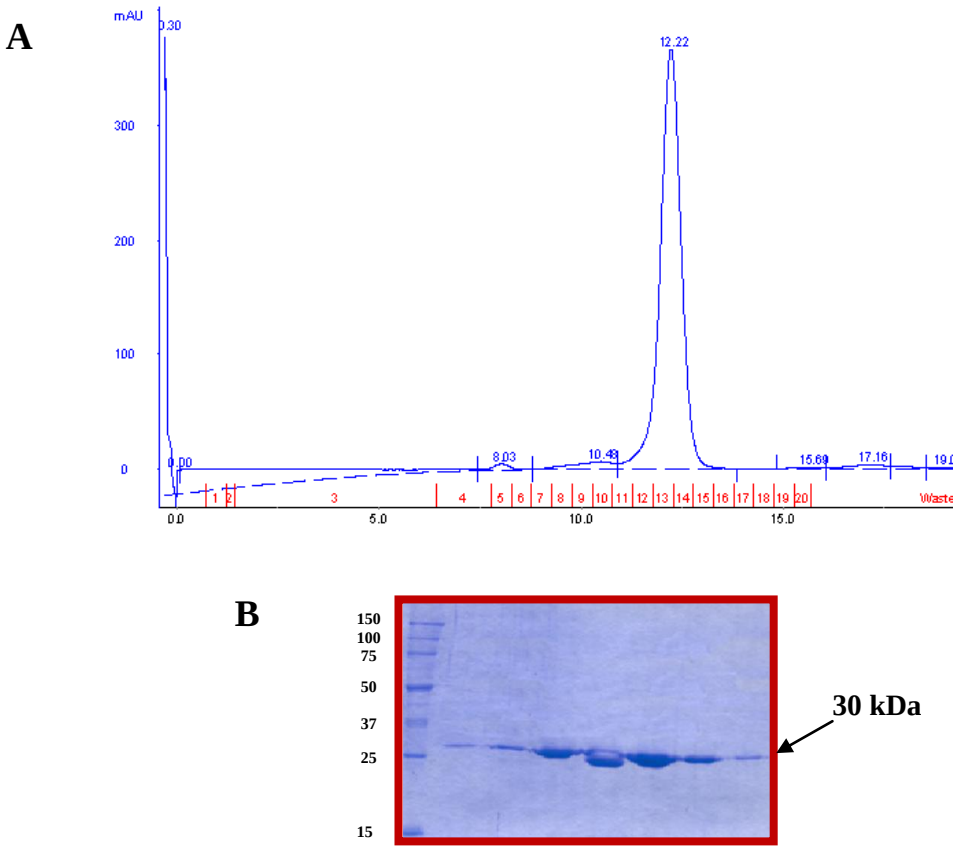

Figure 3.4 ***A)*** *Chromatographic elution profile of hCA VII C183S/C217S obtained by S75 SEC column.* ***B)*** *SDS-PAGE of SEC purified fractions.*

hCA VII C183S/C217S purity and molecular weight were further characterized by electrospray ionization mass spectrometry. The LC-ESI-MS spectrum of the purified enzyme showed a single peak with an experimental mass identical to the expected theoretical molecular weight of 30068.2 Da (Figure 3.5).

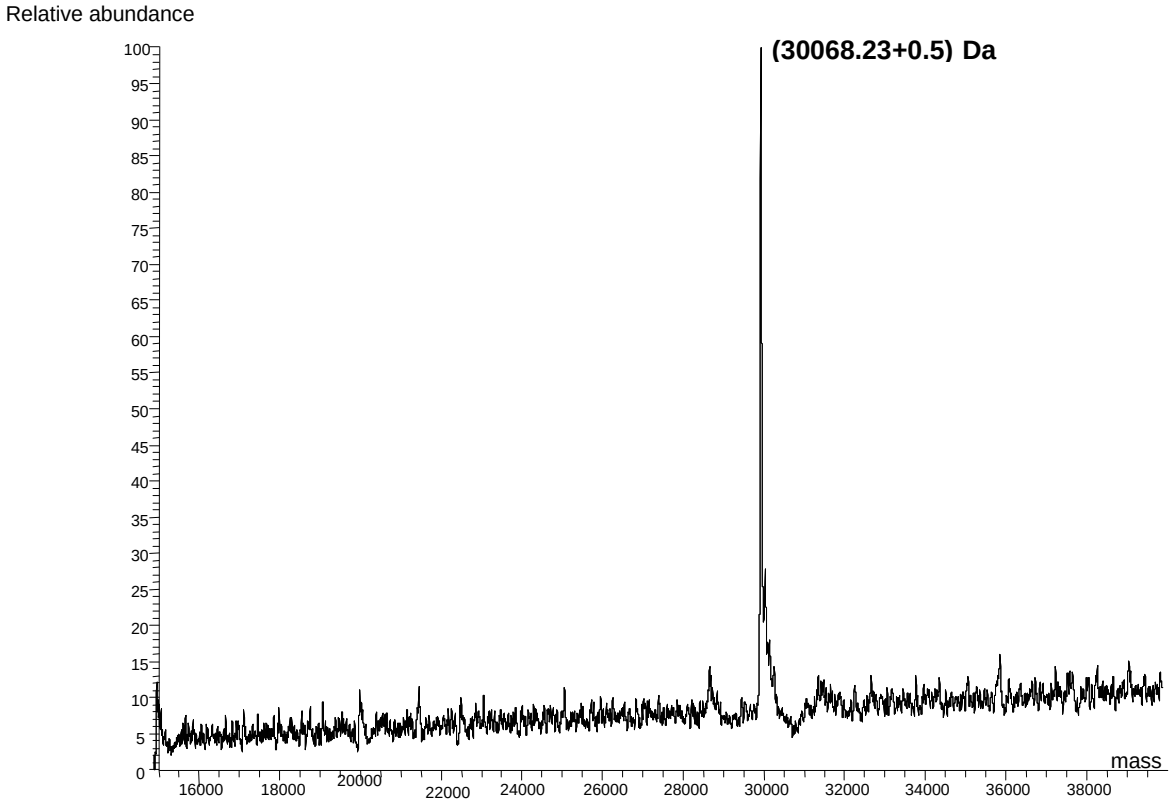

Figure 3.5 *LC-ESI-MS of purified hCA VII C183S/C217S.*
Deconvoluted mass spectrum showed the presence of a unique peak of 30068.23 Da.

A preliminary characterization of hCA VII C183S/C217S structure was carried out by far-UV CD spectroscopy. CD spectra, recorded in the 200-250 nm region, clearly showed that the mutated protein exhibited a folded structure. In particular, overlap of the spectra of wild type hCA VII and hCA VII C183S/C217S indicated that the mutations cysteine/serine did not affect the enzyme secondary structure (Figure 3.6). Thermal stability of the protein was investigated by following the CD signal at 214 nm in the temperature range 25-85 °C. The Tm value, obtained at the midpoint of the thermal denaturation curve, was 57.0 °C indicating that this enzyme had the same stability as the native one (see paragraph 2.2.2).

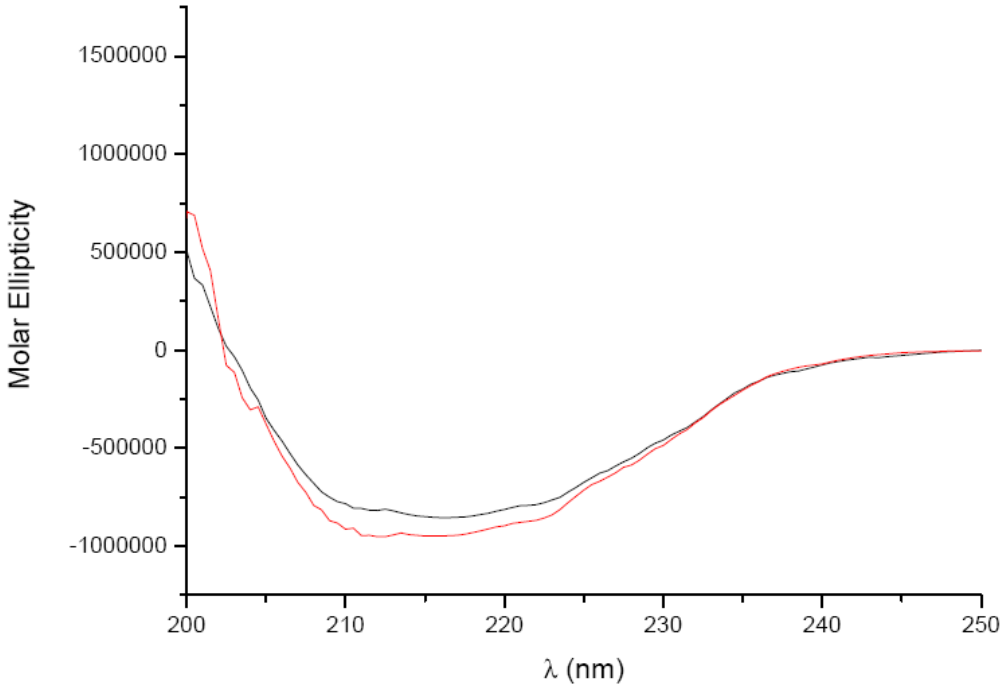

Figure 3.6 *Overlap of wild type hCA VII (red line) and hCA VII C183S/C217S (black line) CD spectra.*

The kinetic parameters for the CO_2 hydration activity of hCA VII C183S/C217S were measured in collaboration with Supuran's group. Data in Table 3.1 show that the mutation of the two cysteines to serines does not significantly affect the CO_2 hydration activity and affinity for acetazolamide (**AZM**), a strong inhibitor of CA isozymes (Supuran, 2008a). Indeed, the kinetic parameters of hCA VII C183S/C217S were almost identical to those of the native enzyme as were their inhibition constants for the inhibitor. Also the ability of hCA VII C183S/C217S to act as an esterase and phosphatase was tested and the results compared to hCA VII wild type. As is evident from Tables 3.2 and 3.3, the native enzyme and its double mutated form show very similar kinetic parameters using 4-nitrophenyl acetate and 4-nitrophenyl phosphate as substrates.

Table 3.1 *Kinetic parameters for the CO_2 hydration reaction*

Isozyme	k_{cat}/K_M ($M^{-1}s^{-1}$)	K_M (mM)	K_I (AZM)(nM)
hCA VII	$7.2x10^7$	11.0	2.8
hCA VII C183S/C217S	$6.5x10^7$	10.8	3.0

Table 3.2 *Kinetic parameters for the hydrolysis of 4-nitrophenyl acetate*

Isozyme	k_{cat}/K_M ($M^{-1}s^{-1}$)	K_M (mM)	K_I (AZM) (nM)
hCA VII	$(3.27 \pm 0.12)\ x10^6$	0.75 ± 0.04	357 ± 12
hCA VII C183S/C217S	$(4.20 \pm 0.18)\ x10^6$	1.06 ± 0.08	170 ± 14

Table 3.3 *Kinetic parameters for the hydrolysis of 4-nitrophenyl phosphate*

Isozyme	k_{cat}/K_M ($M^{-1}s^{-1}$)	K_M (mM)	K_I (AZM) (nM)
hCA VII	$(2.89 \pm 0.09)\ x10^4$	1.43 ± 0.09	3440 ± 39
hCA VII C183S/C217S	$(3.03 \pm 0.11)\ x10^4$	2.21 ± 0.13	2910 ± 45

3.2.1.3 Crystal structure of hCA VII C183S/C217S

Crystallization experiments were performed on hCA VII C183S/C217S in its unbound and inhibitor-bound form. **AZM** was used for this purpose. Crystals were only obtained in the case of the hCA VII C183S/C217S/**AZM** complex, using the hanging drop vapour diffusion method and PEG 4000 as precipitant. They belonged to the space group $P2_1$ with one molecule per asymmetric unit, according to a solvent content of 41%. Upon diffraction with synchrotron radiation, data were collected to 2.05 Å resolution. The structure was solved by molecular replacement using the hCA II structure (Eriksson *et al.,* 1988) as starting model and refined with the CNS (Brunger *et al.,* 1998) program. There were no outliers in the Ramachandran plot (Laskowski *et al.,* 1993), and all residues were well defined in the electron density maps except the for first five N-terminal residues, whose large conformational flexibility was also confirmed by high B-factor values. The final model of the complex was refined to Rfactor/Rfree values of 0.166/0.207. A full list of refinement statistics is reported in Table 3.4.

Table 3.4 *Summary of refinement statistics*

Refinement Statistics	
Resolution limits (Å)	20.00-2.05
Number of reflections used in the refinement	15099
No. of reflections in working set	14352
No. of reflections in test set	747
Rfactor/Rfree[a]	0.166/0.207
No. of protein atoms	2099
No. of inhibitor atoms	13
No. of water molecules	261
RMSD from ideal values	
Bond lengths (Å)	0.008
Bond angles (°)	1.5
Average B-factors (Å^2)	
Protein, overall	13.9
Main chains	11.6
Side chains	14.1
Solvent and inhibitor atoms	22.3/11.5
Ramachandran plot statistics	
Residues in the most favored regions (%)	88.2
Residues in the additionally allowed regions (%)	11.8

[a] *Rfactor= $\Sigma_{hkl}\,\Sigma_i\,||F_0(hkl)|-|F_C(hkl)||/\Sigma_{hkl}\,|F_0(hkl)$, Rfree calculated with 5% of data withheld from refinement.*

hCA VII C183S/C217S is a monomeric compact globular protein, whose roughly ovoidal shape is approximately 40 x 44 x 40 Å^3 in size. As already observed for other α-CAs (Alterio et al., 2009b), its structure consists of a central 10-stranded β-sheet surrounded by four α-, four 3_{10}-helices and five additional β-strands (Figure 3.7).

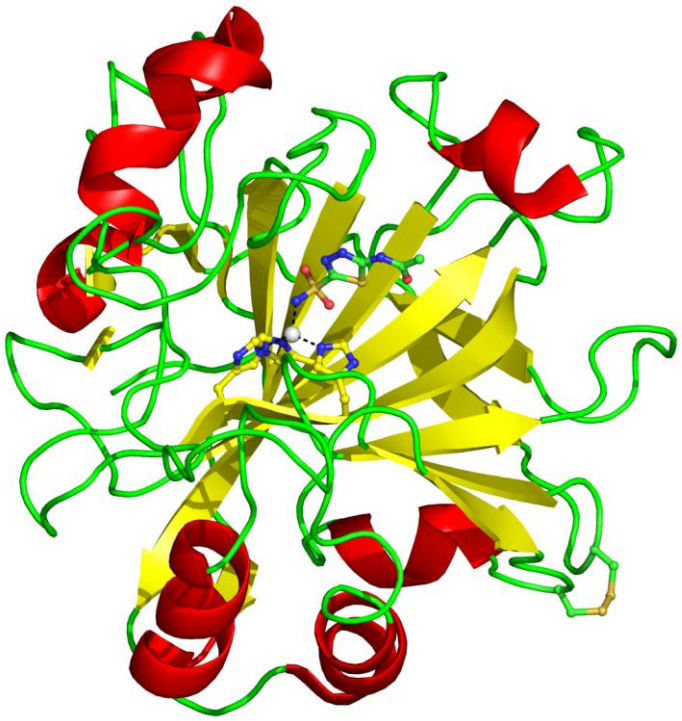

Figure 3.7 *hCA VII C183S/C217S overall fold.* β-Strands are reported in yellow and helices in red. Disulfide bond, zinc ion, catalytic histidine and inhibitor molecule are also shown.

An intramolecular disulfide bond is present in the structure between Cys54 and Cys178. However, the observation that these two cysteines are not conserved within the α-CA family (Alterio *et al.*, 2009b) and that disulfide bonds are extremely rare in cytosolic proteins (Kadokura *et al.*, 2003) suggests that this disulfide bond is not present in hCA VII under physiological conditions, but instead is an artefact generated by the oxidizing conditions that arise during protein handling. Intriguingly, the same intramolecular disulfide bridge was recently reported by Parkkila's group (Bootorabi *et al*, 2010) making it appealing to deepen our knowledge on the role and function of this protein in its cytosolic environment. Further studies are currently under way to clarify this point.

As observed for other α-CA isozymes, the active site is located in a conical cavity about 15 Å wide and 15 Å deep, which extends from the surface of the protein to the centre of the molecule. The catalytic zinc ion is located at the bottom of this cavity, coordinated by three

histidine residues (Figure 3.7). The fourth coordination position is occupied by the deprotonated sulfonamide NH^- group of the **AZM** inhibitor which co-crystallized with the enzyme (Figure 3.7). Figure 3.8 shows the main protein–inhibitor interactions. According to this figure, the NH^- group of the inhibitor is coordinated with the Zn^{2+} ion and is hydrogen bonded to the Thr199OG atom (2.80 Å). One oxygen from the sulfonamide moiety accepts a hydrogen bond from the Thr199N atom (2.93 Å), while the other one is located 3.07 Å away from the catalytic zinc ion. Additional hydrogen bond contacts are established between the two N atoms of the 1,3,4,-thiadiazole ring and the hydroxyl group of Thr200, and the O atom of the acetamide moiety with the Gln92NE2 atom. A further water-mediated H-bond is observed between the N atom of the acetamide group and carbonyl group of Pro201. Several other hydrophobic interactions stabilize the inhibitor within the active site cavity. In particular, the 1,3,4-thiadiazole ring establishes a number of strong van der Waals interactions (distance < 4.5 Å) with residues Gln92, Val121, Leu198 and Val200, while the acetamido moiety is stabilized by van der Waals contacts with Gln92, Val121, Phe131 and Leu198.

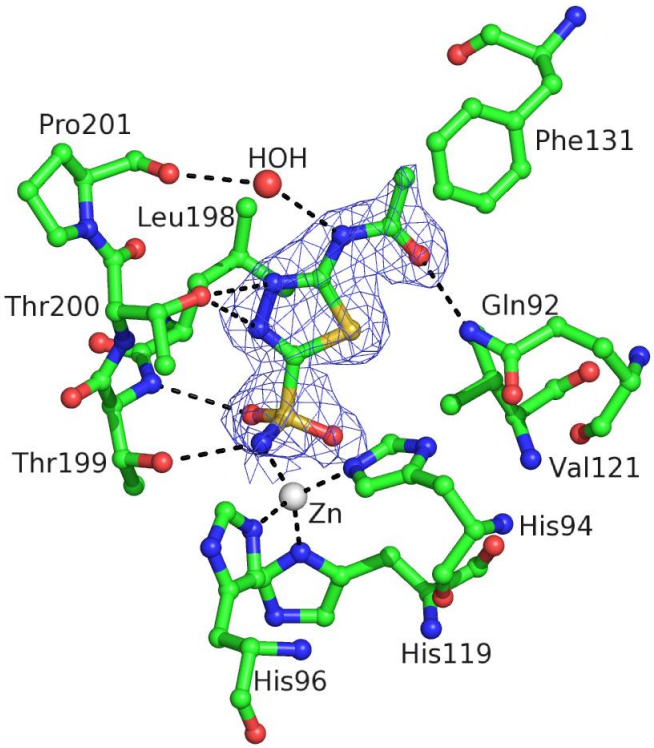

Figure 3.8 *The active site of the hCA VII C183S/C217S/**AZM** complex.* Hydrogen bonds, Zn^{2+} coordination and residues establishing strong van der Waals interactions with the inhibitor are shown. The simulated annealing omit |2Fo-Fc| electron density map, relative to the inhibitor molecule, is reported.

Similarly to that observed for other CA isozymes, the hCA VII C183S/C217S active site is a conical cavity consisting of two distinct portions, one delimited by hydrophobic residues (Val121, Phe131, Ala135, Leu141, Val143, Leu198 and Val207) and another delimited by hydrophilic ones (Asn62, His64, Gln67, Lys91 and Gln92). Very well defined electron density maps were observed for all these residues with the exception of His64, which on the contrary was disordered. The high conformational mobility of this residue is likely associated with its role as a proton shuttle in catalysis, as already observed for the same residue in other α-CA isozymes (Fisher *et al.*, 2005).

3.2.1.4 Structural comparison with other cytosolic α-CAs

As previously described, all cytosolic hCAs are characterized by very different kinetic features (Supuran, 2008a). Indeed, hCA II and hCA VII are very efficient as catalysts (for hCA II k_{cat}/K_M = 1.5 x 10^8 M^{-1} s^{-1} and for hCA VII k_{cat}/K_M =8.3 x 10^7 M^{-1} s^{-1}), hCA I and hCA XIII are 10–50 times less efficient (for hCA I k_{cat}/K_M = 5.0 x 10^7 M^{-1} s^{-1} and for hCA XIII k_{cat}/K_M =1.1 x 10^7 M^{-1} s^{-1}), while hCA III is a very poor catalyst (k_{cat}/K_M =3.0 x 10^5 M^{-1} s^{-1}) (Supuran, 2008a; Di Fiore *et al.*, 2008).

In order to investigate the reasons of the higher catalytic activity of hCA VII and hCA II compared to the others cytosolic hCAs, a structural comparison analysis was performed. Figure 3.9 shows the structural superposition of all cytosolic isozymes. Analysis of this figure reveals that hCA VII has a substantial degree of 3D similarity with all other cytosolic hCAs, as expected on the basis of the high sequence identity (hCA VII/hCA I = 50%, hCA VII/hCA II = 55%, hCA VII/hCA III = 49% and hCA VII/hCA XIII = 52%). Indeed, the RMSD for the superposition of the Cα atoms of hCA VII C183S/C217S with the corresponding atoms of hCA I (Kannan *et al.*, 1984), hCA II (Eriksson *et al.*, 1988), hCA III (Duda *et al.*, 2005) and hCA XIII (Di Fiore *et al.*, 2008) was 0.91, 0.55, 0.72 and 0.69 Å, respectively.

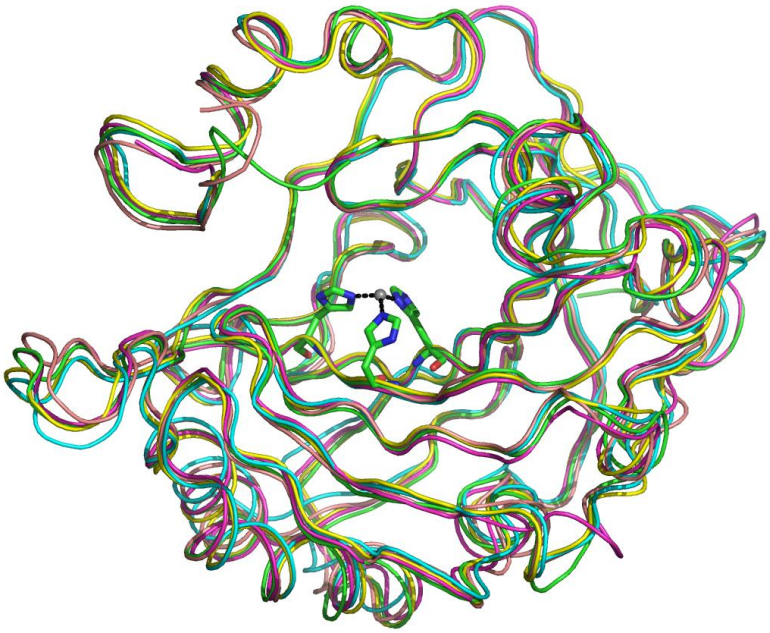

Figure 3.9 *Structural superposition of cytosolic hCAs.* hCA I is showed in cyan, hCA II in magenta, hCA III in yellow, hCA VII in green and hCA XIII in salmon.

The main differences among these proteins were observed in the loops connecting βb and βB, βC and βc, βE and αD, αD and βF, and in the C-terminal region. Since these regions are located distant to the active site, the observed differences should not have effect on either catalytic activity or substrate binding.

Limiting the comparison to the active site regions, it is possible to observe that most of the residues which delimit this cavity are generally conserved either by nature or conformation (Figure 3.10). This finding is particularly true when comparing hCA VII to hCA II. Indeed, in this case only six substitutions, namely S65A, Q67N, D69E, K91I, A135V, and S204L, are observed among the 23 residues which delimit the cavity (Figure 3.11).

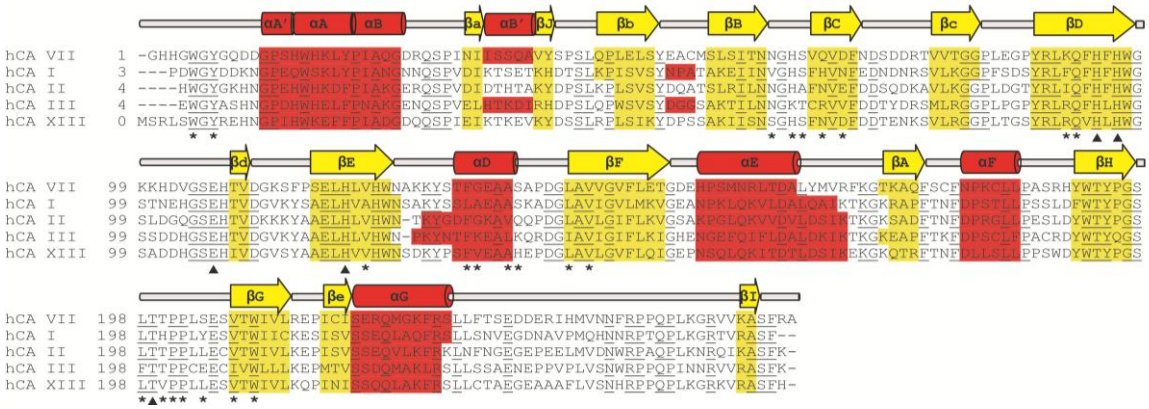

Figure 3.10 *Sequence alignment of all cytosolic α-CAs.* hCA VII secondary structure elements are shown schematically: helices are represented by solid cylinders and β-strands as arrows. These regions are named as reported by Eriksson et al. (1988), for hCA II. Secondary structure elements not present in the hCA II structure are primed. α- and 3_{10}-helices and β–strands for hCA I (Kannan *et al.*, 1984), hCA II (Eriksson *et al.*, 1988), hCA III (Duda *et al.*, 2005) and hCA XIII (Di Fiore *et al.*, 2005) are highlighted in red and yellow, respectively. Conserved residues are underlined, catalytic triad, Thr199 and Glu106 are indicated with black triangles, while residues delimiting the active site cavity are marked with asterisks.

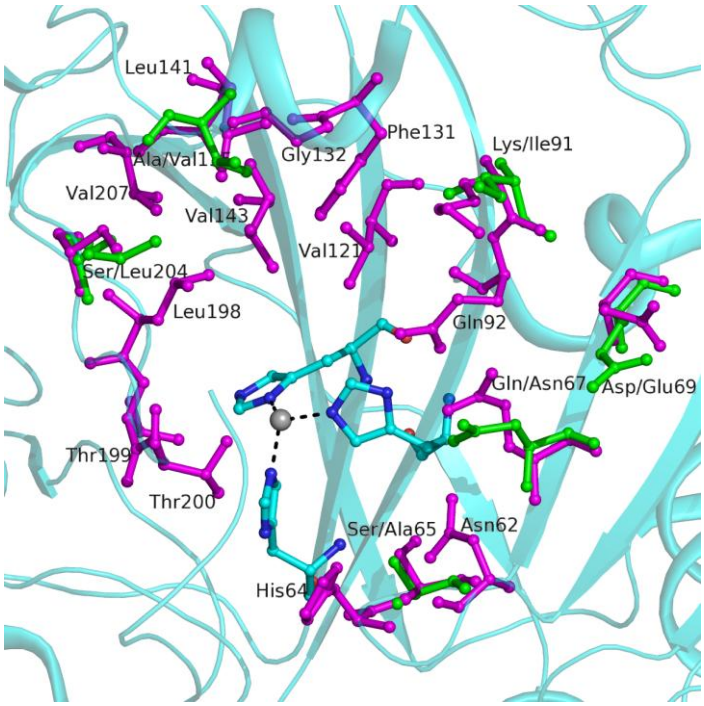

Figure 3.11 *Active site region of hCA VII with residues which delimit the cavity highlighted in magenta. The residues of hCA II active site, which are not conserved in hCA VII, are shown in green.*

3.2.2 Mutagenesis studies on hCA VII: design and preparation of mutants with improved catalytic efficiency

As mentioned above hCA II was the most efficient catalyst of the CA family with a k_{cat}/K_M = 1.5 x 10^8 M^{-1} s^{-1}. hCA VII, even though being a very active enzyme, presented a catalytic efficiency nearly half of that of hCA II, with a k_{cat}/K_M value of =8.3 x 10^7 M^{-1} s^{-1}. Structural comparison between the two enzymes highlighted six amino acid substitutions between their active sites (S65A, Q67N, D69E, K91I, A135V and S204L). Among these residues, four (A65, N67, I91 and L204) were previously reported to be important for the catalytic efficiency of isoform II. On the basis of these considerations, to clarify the role of different residues on the hCA VII catalytic efficiency, four hCA VII mutants, namely S65A, Q67N, K91I and S204L, were designed and produced. In each of these mutants, a single amino acid of hCA VII was mutated in the corresponding residue present in hCA II.

Previously reported studies suggested also that the highest catalytic efficiency of hCA II was associated with a unique histidine cluster within the enzyme active site, comprised of His3, His4, His10, His15, His17 and His64 (Briganti *et al.*, 1997). This cluster extends from the interior of the active site to its entrance and, finally, to the surface of the protein (Figure 3.12A). It has been suggested that this structural motif could be an appropriate ‘‘channel’’ for efficiently assisting proton transfer from the enzyme active site to the reaction medium (Briganti *et al.*, 1997). The importance of this cluster for catalytic efficiency is supported by other kinetic/structural studies on hCA I (Lindskog *et al.*, 1991). In this case, the reduced catalytic efficiency of hCA I well paralleled with a cluster that was not well defined in the enzyme structure, as a result of some histidine substitutions between isozymes I and II and a number of additional residues within the active site, namely His67, His200 and His243, placed at bifurcating positions and buried enough to only partially assist proton transfer (Figure 3.12B). The crystallographic structure of hCA XIII was in line with these

observations. Indeed, the lower catalytic efficiency measured for hCA XIII, with respect to hCA II and hCA I, corresponded to an isozyme structure where the histidine cluster was not present (Figure 3.12C). In fact, apart from His64, no other histidine residue was present in the channel connecting the active site to the protein surface. The external residues His10 and His15 were placed too distant to ensure a proper proton transfer. Finally the poorest activity measured for hCA III was again in agreement with these observations. For this isoform, His64, present in all isozymes and acting as the initial proton transfer moiety, was replaced by a Lys residue. Also in this case, His10, His15 and His17, confined on the protein surface, were non-influent for a proper proton transfer (Figure 3.12D). Structural data here reported on hCA VII seems to further confirm the role of the histidine cluster. In fact hCA VII, the most active cytosolic hCA after hCA II, presents a well defined histidine cluster, consisting of His2, His3 and His64 which connect the interior of the active site to its entrance. However, the connection with the protein surface is not well established as in hCA II, as a consequence of the lack of His4 and this absence could explain the lower activity with respect to hCA II (Figure 3.12E).

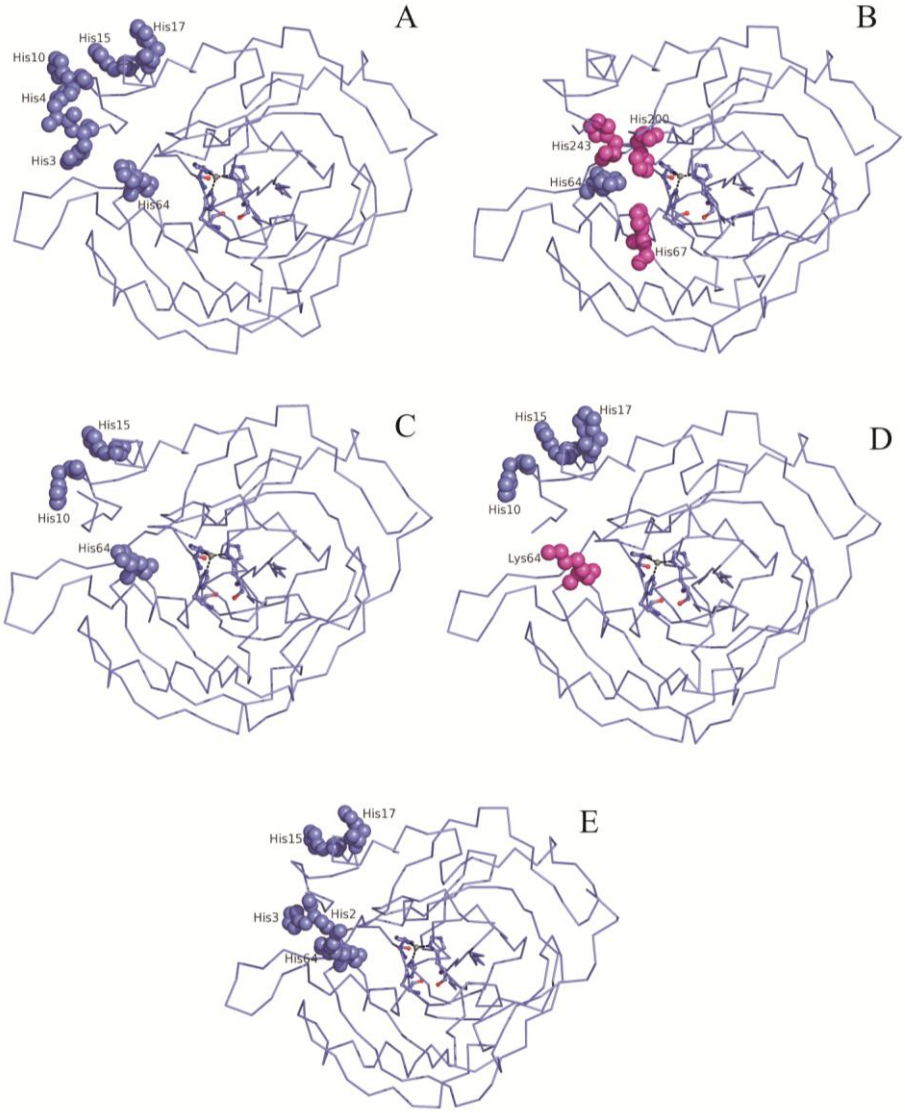

Figure 3.12 *Schematic view of the hCA II (**A**), hCA I (**B**), hCA XIII (**C**), hCA III (**D**) and hCA VII (**E**) structures.* The zinc ion and its three histidine ligands (**H94**, **H96,** and **H119**) are shown. For each isozyme, the histidine residues participating to the proton-transfer reaction are also reported as spheres.

In order to prove this hypothesis the hCA VII double mutant H2S/G4H was also designed and produced. So in total five hCA VII mutants were produced. All mutations were carried out on the hCA VII C183S/C217S construct; this choice was made because the hCA VII C183S/C217S form showed the same biochemical and kinetic parameters as native hCA VII being, however, much more stable and homogeneous. The five hCA VII mutants were

expressed and purified applying the same protocol as the native enzyme. Correctness of sequences was confirmed by DNA sequencing, whereas LC-ESI-MS experiments on purified proteins confirmed their integrity and purity. Figures 3.13A and 3.13B report the deconvoluted spectra of two out of five purified mutants.

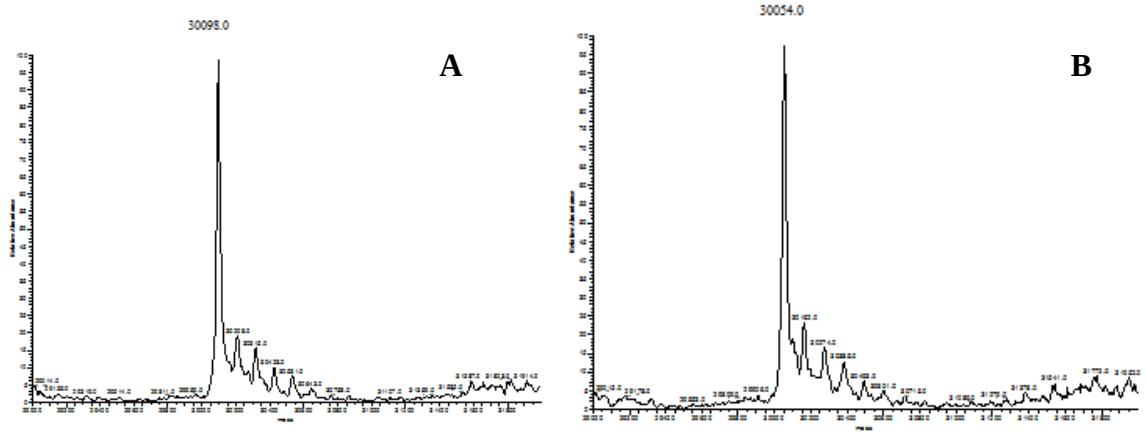

Figure 3.13 *LC-ESI-MS of (**A**) purified hCA VII H2S/G4H (theorical MW 30098.75 Da) and (**B**) hCA VII Q67N (theorical MW 30054.70 Da).*

Kinetic parameters of CO_2 hydration activity of the five purified mutants were determined in collaboration with Supuran's group and data obtained are reported in Table 3.5. Results show that improvements of the catalytic activity of the mutants were achieved compared to the native enzyme, though they did not reach the values of hCA II, whose mutation studies were referred to. These results suggest that improvement of the catalytic efficiency of an already very active enzyme, such as hCA VII, is probably most evident when only one mutant comprehensive of all the mutations identified above is produced. Work is in progress to achieve this new construct and verify this hypothesis.

Table 3.5 *Kinetic parameters of hCA VII mutants.*

Enzyme	Mutation	k_{cat} (s^{-1})	K_M (mM)	k_{cat}/K_M ($M^{-1}s^{-1}$)	KI (AZM) (nM)
hCA VII	**wt**	9.5×10^5	11.4	8.33×10^7	2.5
hCA VII	**H2S/G4H**	10.8×10^5	11.3	9.55×10^7	2.0
hCA VII	**S65A**	10.5×10^5	11.3	9.29×10^7	2.5
hCA VII	**Q67N**	9.7×10^5	11.4	8.50×10^7	2.3
hCA VII	**K91I**	8.4×10^5	11.5	7.30×10^7	2.4
hCA VII	**S204L**	10.3×10^5	11.4	9.03×10^7	2.0
hCA II	**wt**	1.4×10^6	9.3	1.50×10^8	12
hCA I	**wt**	2.0×10^5	4.0	5.00×10^7	250

3.2.3 Mutagenesis studies on hCA XIII: design and preparation of mutants with improved catalytic efficiency

The same approach used to design hCA VII mutants was also applied to hCA XIII. In detail, by a structural comparison of hCA XIII and hCA II active sites, five differences among 23 aminoacids were highlighted in the area close to the substrate binding pocket and to the hydrogen-bond network involved into proton transfer, namely: S62N, S65A, R91I, A135V and V200T (Figure 3.14). In particular, data reported for hCA II gave evidence of the main role that Thr200 and Asn62 have for the proton transfer capacity, as well as Ile91 and Ala65 due to their vicinity to the substrate binding pocket and their contribution to the hydrogen-bond network which also facilitates proton transfer (Scolnick and Christianson, 1996; Kockar *et al.,* 2010; Mikulski and Silverman, 2010). Thus, four mutants were prepared: hCA XIII S62N, hCA XIII S65A, hCA XIII R91I and hCA XIII V200T. In addition, in order to verify the hypothesis of the role of the histidine cluster on enzyme efficiency (Briganti *et al.,* 1997), we prepared a fifth hCA XIII mutant where Leu3 and Ser4 were mutated into His, obtaining the hCA XIII L3H/S4H mutant, where the histidine cluster present in hCA II was reproduced. So in total five mutants were designed. In this case site-directed mutagenesis was performed

and the mutants of hCA XIII were expressed and purified applying the same protocol as described for hCA VII (see paragraphs 2.3.4-2.3.9). Correctness of sequences was confirmed by DNA sequencing, whereas LC-ESI-MS experiments on purified proteins confirmed their integrity and purity. In figure 3.15 the deconvoluted spectra of four out of five purified mutants are shown.

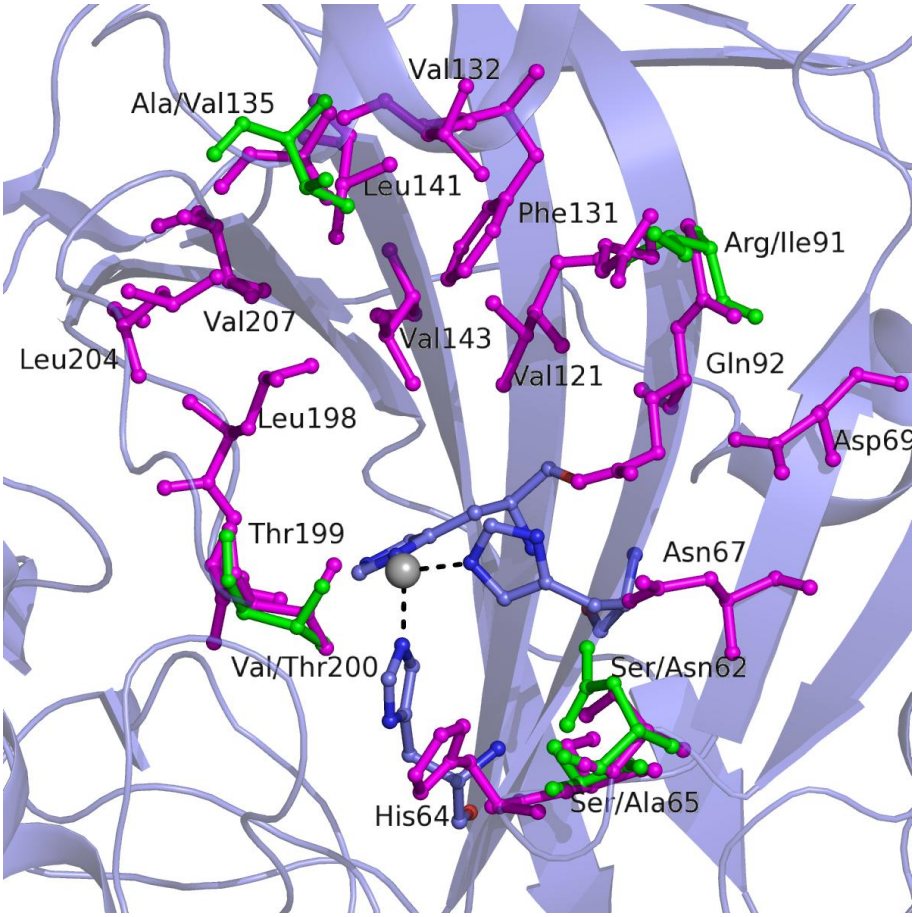

Figure 3.14 *Active site region of hCA XIII with residues which delimit the cavity highlighted in magenta. Residues of hCA II active site, which are not conserved in hCA VII, are shown in green.*

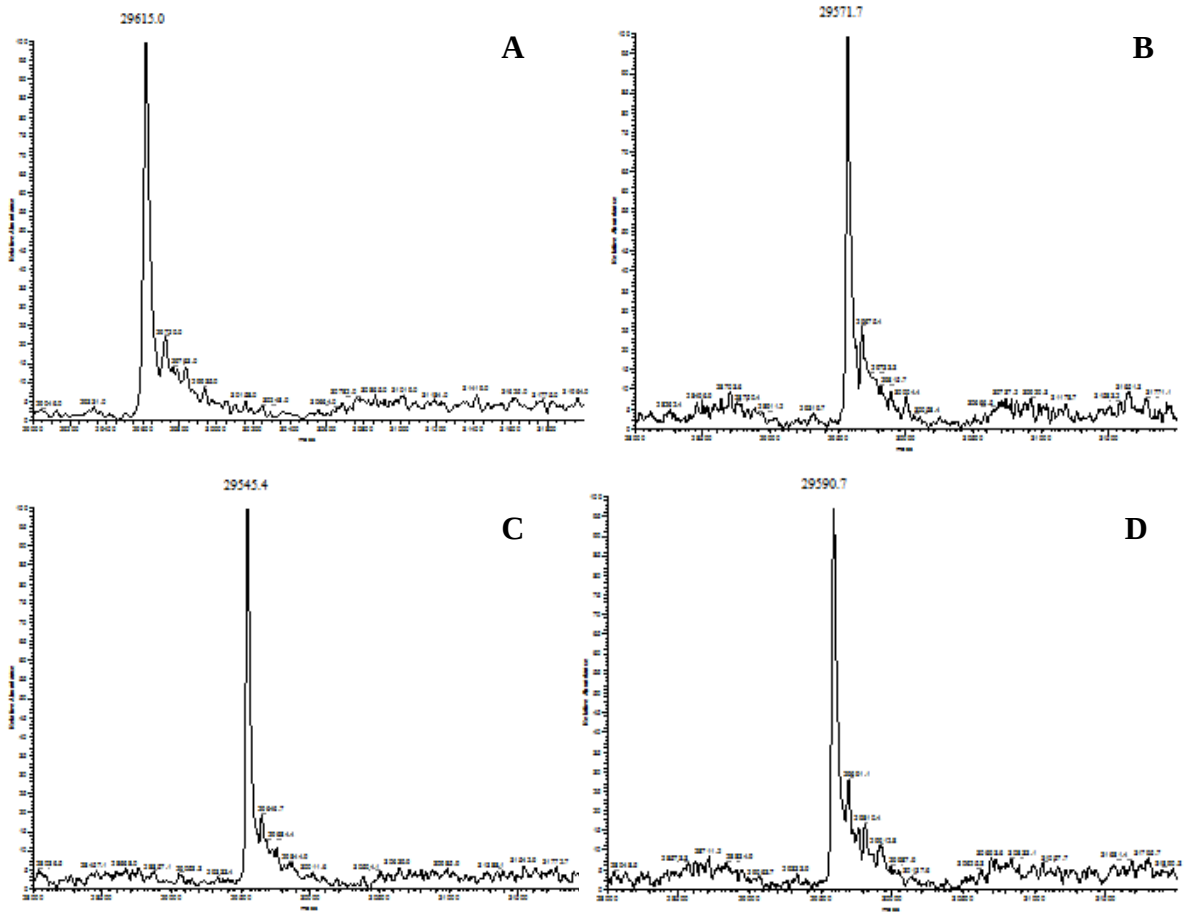

Figure 3.15 *Deconvoluted mass spectra of:* ***A****) hCA XIII S62N (theorical MW 29614.30 Da);* ***B****) hCA XIII S65A (theorical MW 29571.28 Da);* ***C****) hCA XIII R91I (theorical MW 29544.25 Da);* ***D****) hCA XIII V200T (theorical MW 29589.25 Da).*

Kinetic parameters of CO_2 hydration activity of the five purified hCA XIII mutants were determined and the data obtained reported in Table 3.6. In this case, improvements of the catalytic activity of the hCA XIII mutants were more significant; as an example the V200T variant showed a catalytic efficiency double than that of wild type isoenzyme. However, also in this case none of the designed mutants was able to reproduce the hCA II catalytic efficiency. Again mutants containing more than one aminoacidic substitution should be prepared and tested to verify a cumulative effect of these single mutations.

Table 3.6 *Kinetic parameters of hCA XIII mutants*

Isozyme	Mutation	k_{cat} (s^{-1})	K_M (mM)	k_{cat}/K_M ($M^{-1}s^{-1}$)	KI (AZM) (nM)
hCA XIII	**wt**	1.5×10^5	13.8	1.08×10^7	16
hCA XIII	**L3H/S4H**	1.8×10^5	13.6	1.32×10^7	11
hCA XIII	**S62N**	1.4×10^5	10.1	1.40×10^7	105
hCA XIII	**S65A**	1.6×10^5	10.0	1.60×10^7	23
hCA XIII	**R91I**	1.6×10^5	14.5	1.10×10^7	108
hCA XIII	**V200T**	1.7×10^5	9.4	1.80×10^7	13
hCA II	**wt**	1.4×10^6	9.3	1.5×10^8	12
hCA I	**wt**	2.0×10^5	4.0	5.0×10^7	250

3.3 MATERIALS AND METHODS

3.3.1 *hCA7* gene mutagenesis

Cys183 and Cys217 residues were mutated in serine using the QuikChange Site Directed Mutagenesis Kit (Stratagene), for the production of hCA VII C183S/C217S. His2, Gly4, Ser65, Gln67, Lys91 and Ser204 residues were also mutated in order to produce the following variants of hCA VII: H2S/G4H; S65A; Q67N; K91I and S204L. The primers employed for mutagenesis PCR reaction are reported below.

For **C183S:**

FOR 5'-CTTCAACCCCAAGAGCCTCCTGCCTGCC-3'

REV 5'-GCAGGCAGGAGGCTCTTGGGGTTGAAG-3'

For **C217S**:

FOR 5'-GAGCCCATCAGCATCTCTGAAAG-3'

REV 5'-CTTTCAGAGATGCTGATGGGCTC-3'

For **H2S:**

FOR 5'-G ACC GGC TCG CAC GGC TGG GGC -3'

REV 5'-GCC CCA GCC GTG CGA GCC GGT C-3'

For **G4H**:

FOR 5'-C GGC CAC CAC CAC TGG GGC TAC GGC-3'

REV 5'- GCC GTA GCC CCA GTG GTG GTG GCC G-3'

For **S65A**:

FOR 5'-C AAT GGC CAC GCC GTC CAG GTA G-3'

REV 5'-C TAC CTG GAC GGC GTG GCC ATT G-3'

For **Q67N**:

FOR 5'-GGC CAC TCT GTC AAT GTA GAC TTC-3'

REV 5'-GAA GTC TAC ATT GAC AGA GTG GCC-3'

For **K91I:**

FOR 5'-CC TAC CGC CTC ATT CAG TTT CAC TTC-3'

REV 5'-GAA GTG AAA CTG AAT GAG GCG GTA GG-3'

For **S204L**:
FOR 5'-CT CCC CCA CTC CTG GAG AGT GTC ACC-3'
REV 5'-GGT GAC ACT CTC CAG GAG TGG GGG AG-3'

The recombinant construct pGex-4T-3/*hCA 7* with two reactive cysteines mutated into serines was used as template. PCR was performed using Pfu Turbo DNA polymerase enzyme following the procedure indicated below:

* Initial denaturation step (step 1) 30 sec at 95 °C

* Denaturation (step 2) 30 sec at 95 °C

* Annealing (step 3) 60 sec at 55 °C

* Elongation (step 4) 6 min at 68 °C
for 16 cycles from step 2.

Degradation of the methylated, non mutated, parental DNA was carried out by adding Dpn I (10 units) to the PCR reaction and incubating for 2 hrs at 37 °C. *E. Coli* TOPF'10 was transformed with circular nicked obtained dsDNA. The correct insertion of desired mutations was confirmed by DNA sequencing.

3.3.2 *hCA13* gene mutagenesis

Lys3, Ser4, Ser62, Ser65, Arg91 and V200 residues were mutated in order to produce the variants L3H/S4H, S62N, S65A, R91I and V200T of hCA XIII, and study their catalytic activity in comparison with that of hCA II.

The sequences of hCA XIII mutants were synthesized by Blue Heron Biotechnology into the vector pUCminusMCS, all in frame for cloning in pGex-4T-3 and all containing 5' BamHI site and 2 STOP codons + XhoI site at 3' end. The mutated codons are reported below:

Leu3/His ⇨ (CTG/CAT)

Ser4/His ⇨ (AGC/CAT)

Ser62/Asn ⇨ (AGC/AAC)

Ser65/Ala ⇨ (AGC/GCG)

Arg91/Ile ⇨ (CGC/ATT)

Val200/Thr ⇨ (GTG/ACC)

The vectors were digested with BamHI (10U/μl) and XhoI (20U/μl) restriction enzymes and cloned in pGex-4T-3 vector as described in paragraph 2.3.3.

3.3.3 Large-scale expression and purification of hCA VII and hCA XIII variants

The expression and purification of hCA VII C183S/C217S, hCA VII and hCA XIII mutants were performed using the same protocols described in paragraphs 2.3.4 to 2.3.9, whereas the LC-ESI-MS characterization was carried out as described in paragraph 2.3.11.

3.3.4 hCA VII C183S/C217S/AZM crystallization

Initial crystallization trials of hCA VII C183S/C217S bound and unbound forms were performed at 20 °C using the sparse-matrix sampling method. Screening was carried out using commercially available kits (Crystal Screen kits I and II from Hampton Research) and performing the trials both by hand and using a Nanodispersion Robotic System, "Microlab Starlet Nanojet 8+1" by Hamilton Life Science Robotics. In particular, the hCA VII C183S/C217S/**AZM** complex was prepared by adding a 5-molar excess of inhibitor to a 7 mg/mL protein solution in 20 mM Tris-HCl, pH 9.0, 100 mM sodium chloride. Thin crystals

were only obtained in the presence of the inhibitor from a crystallization conditions containing PEG 4000 as precipitant.

In order to obtain crystals suitable for diffraction data collection a minute optimization of the crystallization conditions was performed varying the concentration of precipitant, pH values and nature of the buffer. Good results were obtained using a precipitant solution containing 30% (w/v) PEG 4000, 0.2 M magnesium chloride and 0.1 M Tris-HCl, pH 8.5. Crystals appeared in the drops within 2–3 days and grew to a maximum dimension of 0.2x0.15x0.2 mm^3 in about 2 weeks (Figure 3.16). The protein-to-reservoir solution ratio was 1:1 in 1 μL drops.

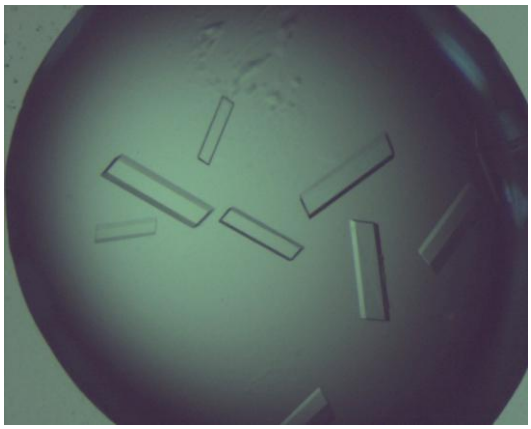

Figure 3.16. *Crystals of hCA VII C183S/C217S/**AZM** complex*.

3.3.5 Data collection

X-ray data collection was performed at the ELETTRA synchrotron source (Trieste, Italy) using a MAR CCD detector. Prior to data collection, crystals were transferred into a cryo-protectant solution containing 20% (v/v) glycerol as cryogenic agent, and frozen at 100 K under a nitrogen stream produced by an Oxford Cryosystem and maintained at 100 K during the data collection. Data were indexed, processed, and scaled with HKL-2000 package (Otwinowski and Minor, 1997). Crystal parameters and data collection statistics are reported

in Table 3.7. The crystals belong to the space group $P2_1$ with one molecule per asymmetric unit, according to a solvent content of 41%.

Table 3.7. *X-Ray data collection statistics for hCA VII C183S/C217S/**AZM** complex.*

Space group	$P2_1$
Unit cell parameters	
a (Å)	43.78
b (Å)	66.28
c (Å)	46.46
β (°)	113.84
Resolution limits (Å)	20.00-2.05
No. of observations	55467
No. of unique reflections	15321
Completeness (%)	99.9 (99.1)
I/σ(I)	26.5 (10.4)
Average multiplicity	3.6
R-sym (%)[a]	0.046 (0.094)
Mosaicity	0.44
V_M ($Å^3Da^{-1}$)	2.05
Solvent content (%)	39.9

[a] R-sym=Σhkl Σi|Ii (hkl)-<I(hkl)>|/Σhkl ΣiIi (hkl), where Ii(hkl) is the ith measurement and <I(hkl)> is the weighted mean of all measurements of I(hkl).
Values in parentheses refer to the highest resolution shell (2.12–2.05 Å).

3.3.6 Structure determination and refinement

The hCA VII C183S/C217S/**AZM** crystal structure was solved by molecular replacement using the program AMoRe (Navaza, 1994) and the crystallographic structure of hCA II (PDB code 1CA2) (Eriksson *et al.*, 1988) as starting model. To avoid bias, water molecules were removed from the model. The rotation and translation functions were calculated using data between 15.0 and 3.5 Å resolution. The one body translation search, using centred-overlap function (c-o), on the first 50 rotation solutions led to a single solution with a correlation coefficient of 0.499 and a Rfactor of 0.406.

Refinement of the structure was performed with CNS (Brunger *et al.*, 1998), and model building was performed with O (Jones *et al.*, 1991). Cycles of rigid-body refinement were

performed on the model using data between 20.0 and 3.5 Å resolution. At this stage, the resulting Rfactor and Rfree were 0.391 and 0.386 respectively. Clear electron density for the inhibitor was observed in the difference map after this single round of refinement. Introduction of the **AZM** molecule was followed by several cycles of addition of water molecules, manual rebuilding, energy minimization and thermal B-factor refinement, reducing the Rfree and Rfactor values to 0.207 and 0.166, respectively. Refinement statistics are summarized in Table 3.4. Coordinates and structure factors have been deposited in the Brookhaven Protein Data Bank (Accession code 3ML5).

3.3.7 Catalytic activity assays

All investigations concerning the catalytic activity of the hCA VII C183S/C217S, hCA VII and hCA XIII mutants were carried out in collaboration with Supuran's group of the University of Florence, Italy, as described in paragraph 2.3.14.

4. The carbonic anhydrase I-topiramate complex

4.1 INTRODUCTION

Obesity is the most frequent metabolic disease in industrialized countries (Friedman, 2003; Hill *et al.*, 2003; Ioannides-Demos *et al.*, 2006; Campfield *et al.*,1998), with more than one billion overweight adults worldwide, of which at least 300 million are clinically obese (Cooke and Bloom, 2006). Despite its recognition as a healthcare issue, obesity remains largely an unsolved medical problem, being a major contributor to the global burden of chronic disease and disability. Indeed, obesity is a risk factor for a variety of other diseases such as type 2 diabetes, cardiovascular diseases and various types of cancer (Van Gaal and Mertens, 1998), and like obesity the prevalence of such obesity-related diseases continues to increase. Thus, the development of strategies to reduce the worldwide obesity epidemic has recently become an important research goal (Van Gaal and Mertens, 1998; Avenell *et al.*, 2004). Although an healthy diet and balanced lifestyle should theoretically help to control the body weight, unluckily weight losses achieved with such approaches are quite modest and limited by high rates of recidivism and a compensatory slowing of the metabolism (Lau, 2007; Leibel *et al.*, 1995). Thus, pharmacological interventions for the treatment of obesity are essential to deal this problem. Paradoxically, there are very few drugs currently available for the treatment of this disease, their mechanism of action is poorly understood and their side effects are rather important (Ioannides-Demos *et al.*, 2006). Consequently, the development of new anti-obesity agents possessing different mechanisms of action is strongly needed. Fortunately, in last years the increased understanding of the physiological mechanisms of body weight regulation has allowed to identify new molecular targets, and a wealth of new agents are under active development (De Simone *et al.*, 2008). Among the recently suggested approaches to treating obesity, it should be mentioned that based on the inhibition of CAs involved in *de novo* lipogenesis, namely hCA VA or/and hCA VB within the mitochondria as well as hCA II

within the cytosol (Supuran *et al.*, 2008; De Simone and Supuran, 2007; 2009; De Simone *et al.*, 2008).

Topiramate (**TPM**, Figure 4.1) (Shank *et al.*, 1994; Edmonds *et al.*, 1996; Stringer, 2000; Sabers and Gram, 2000; Bourgeois, 2000; Bialer, 2001) is a sugar sulfamate derivative marketed worldwide for the treatment of epilepsy (Lyseng-Williamson and Yang, 2007) and prophylaxis of migraine (Ramadan and Buchanan, 2006). However, a growing number of other applications (Mirza *et al.*, 2009) of this compound have been recently identified, some of which are the treatment of bipolar disorder (Vasudev *et al.*, 2006) and post traumatic stress disorder (Berlin, 2007). **TPM** is also under investigation for the treatment of several other pathologies such as bulimia nervosa (McElroy *et al.*, 2009), obsessive/compulsive disorder (Hollander and Dell'Osso, 2006), idiopathic intracranial hypertension (Celebisoy *et al.*, 2007), neuropathic pain (Bendaly *et al.*, 2007) and infantile spasms (Zou *et al.*, 2008). Obesity is among the pathologies that have been recently explored for treatment with **TPM** (Astrup and Toubro, 2004). In fact, data from studies on **TPM** performed on several animal models have demonstrated that this drug is able to induce weight loss (Richard *et al.*, 2002) and have led to clinical trials of **TPM** for treatment of obesity (Astrup and Toubro, 2004). Recently, it was also demonstrated that **TPM** is a potent *in vitro* inhibitor of several hCA isozymes (Casini *et al.*, 2003) (see Figure 4.1), suggesting that the anti-obesity effects of this drug could be ascribed to the inhibition of hCAs VA, VB and II (Supuran *et al.*, 2008; De Simone *et al.*, 2008; De Simone and Supuran, 2007; 2009; Chegwidden and Spencer, 1996). Indeed, in agreement with these hypotheses, several other studies have demonstrated that often the use of CAIs is associated with weight loss (Supuran, 2008a).

Recently, a comparative structural study on the adducts that **TPM** forms with hCA VA and hCA II has been reported describing the atomic interactions that account for the high affinity of **TPM** for these two enzymes (Casini *et al.*, 2003; Lopez *et al.*, 2009; Vitale *et al.*, 2007).

These studies have suggested that **TPM** could be a promising lead molecule for the design of CAIs targeting isozymes involved in lipogenesis, allowing the development of a possible new approach for the treatment and prophylaxis of obesity. In this context the study of the interactions of **TPM** with all human CA isoforms represents an important step for the rational drug design of selective hCA VA/VB inhibitors to be used as anti-obesity drugs. For these reasons, part of this Ph.D thesis has been dedicated to the structural characterization of a complex which **TPM** forms with hCA I. The comparative analysis of such structure with that of the hCA II/**TPM** and hCA VA/**TPM** complexes allowed us to provide useful insights into the molecular bases responsible for recognition of the protein-inhibitor, thus providing important hints for the design of new isoform-specific CA inhibitors.

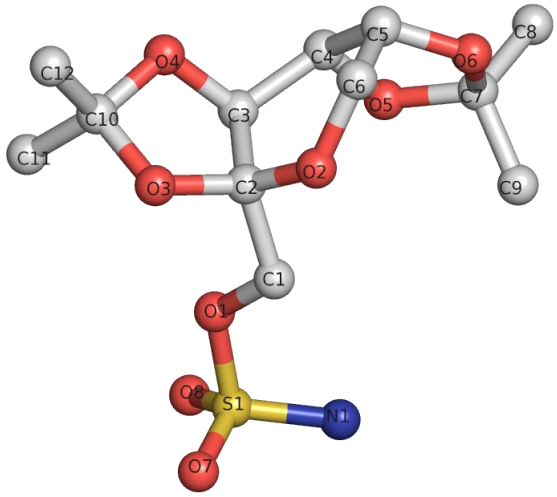

(K_I for CA I= 250 nM; K_I for CA II= 10 nM; K_I for CA VA= 63 nM)

Figure 4.1 *TPM chemical structure, crystallographic numbering and inhibitory activity against hCA I, II and VA are also reported.*

4.2 RESULTS AND DISCUSSION

4.2.1 Quality of the model

The hCA I/**TPM** complex was crystallized in the space group $P2_12_12_1$, with two molecules per asymmetric unit (called A and B). The structure was solved by molecular replacement using native hCA I (Kannan *et al.*, 1984) as starting model and refined to a crystallographic Rfactor of 19.9 % and Rfree of 22.8 % in the 20.00-1.90 Å resolution range (Table 4.1).

The final model includes 4016 protein atoms and 470 water molecules. The overall quality of the model was high, with 87.4 % of the nonglycine residues located in the most favored regions of the Ramachandran plot, whereas 12.6 % lies in additional allowed regions (Figure 4.2). The statistics of refinement are reported in Table 4.1. Poor electron density was observed for the first four N-terminal residues of both molecules in the asymmetric unit; thus such residues were not included in the final model. The refined structure presented a good geometry with RMSD from ideal bond lengths and angles of 0.007 Å and 1.4 °, respectively. The average temperature factor (B) for all atoms was 27.0 $Å^2$.

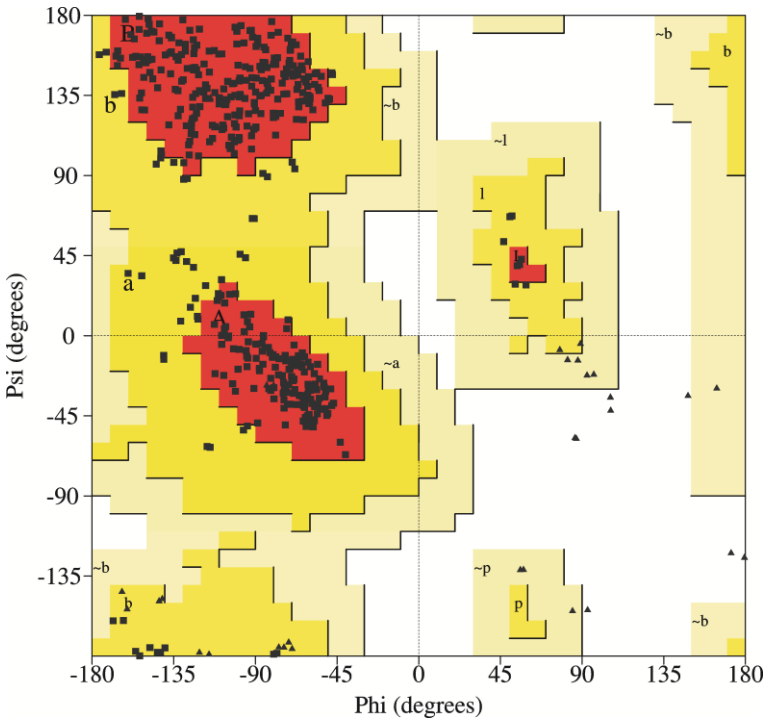

Figure 4.2 *Ramachandran plot of hCA I/**TPM** complex.*

Table 4.1 *Summary of refinement statistics*

Refinement Results	
Resolution limits (Å)	20.00-1.90
Number of reflections used in the refinement	39341
No. of reflections in working set	37385
No. of reflections in test set	1956
Rfactor/Rfree	0.200/0.228
No. of protein atoms	4016
No. of inhibitor atoms	44
No. of water molecules	470
RMSD from ideal values	
Bond lengths (Å)	0.007
Bond angles (°)	1.4
Average B-factors (Å^2)	
Protein, overall	27.0
Main chains	24.8
Side chains	27.1
Solvent and inhibitor atoms	36.2/27.1
Ramachandran plot statistics	
Residues in the most favored regions (%)	87.4
Residues in the additionally allowed regions (%)	12.6

[a] *Rfactor= $\Sigma_{hkl}\,\Sigma_i\,||F_0(hkl)|-|F_C(hkl)||/\Sigma_{hkl}\,|F_0(hkl)|$, Rfree calculated with 5% of data withheld from refinement.*

4.2.2 Overall structure

The two independent molecules in the asymmetric unit overlapped quite well; indeed, the superimposition carried out on the backbone positions of all 256 residues led to an RMSD of 0.2 Å. Furthermore, all residues delimiting the active site region adopted an identical conformation within the two molecules. Consequently, the following discussion will be conducted based on only one arbitrarily chosen molecule, unless otherwise stated.

Analysis of the structure of the hCA I/**TPM** complex shows that hCA I is a compact globular protein, whose roughly ovoid shape is approximately 47 x 35 x 42 Å^3 in size. Its structure is characterized by a central twisted antiparallel ten-stranded β-sheet surrounded by helical connections and additional β-strands (Figure 4.3)

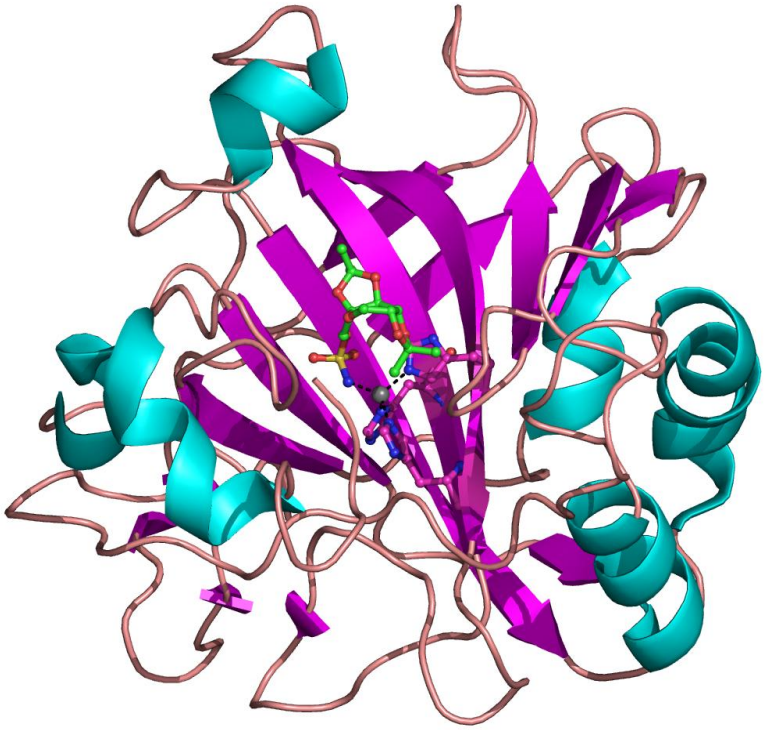

Figure 4.3 *hCA I/**TPM** complex overall fold.* β-Strands are reported in magenta and α-helices in cyan. Zinc ion, catalytic histidine and inhibitor molecule are also shown.

As observed in the structure of other α-CA isozymes, the hCA I active site is located in a large conical cavity, which spans from the surface to the center of the protein. The zinc ion is located at the bottom of this cavity. Within this cavity a clear electron density for the **TPM** molecule was observed (Figure 4.4).

The main interactions of the inhibitor with protein are shown in Figure 4.4. The ionized nitrogen atom of the sulfamate group of **TPM** is coordinated to the Zn^{2+} ion, displacing the hydroxyl ion/water molecule found in the native enzyme. The zinc coordination sphere is completed by the imidazolic nitrogens of His94, His96 and His119. The sulfamate nitrogen is also involved in a hydrogen bond with the hydroxyl group of Thr199, while one of the two sulfamate oxygens accepts a hydrogen bond from the backbone amide group of the same residue. Several other polar interactions are observable between the sugar moiety of the inhibitor and the enzyme active site. In particular, **TPM**O6 and **TPM**O4 atoms of the

inhibitor are hydrogen bonded to His64NE2 and Gln92NE2, respectively (Figure 4.4), while **TPM**O2 and **TPM**O3 atoms are engaged in a bifurcated hydrogen bond with a water molecule, which in turn interacts with the carboxyl group of Pro201. Several other strong van der Waals interactions involving residue at distance <4.5 Å (Val62, Ser65, His67, Phe91, Leu198, His200) contribute to the stabilization of the complex.

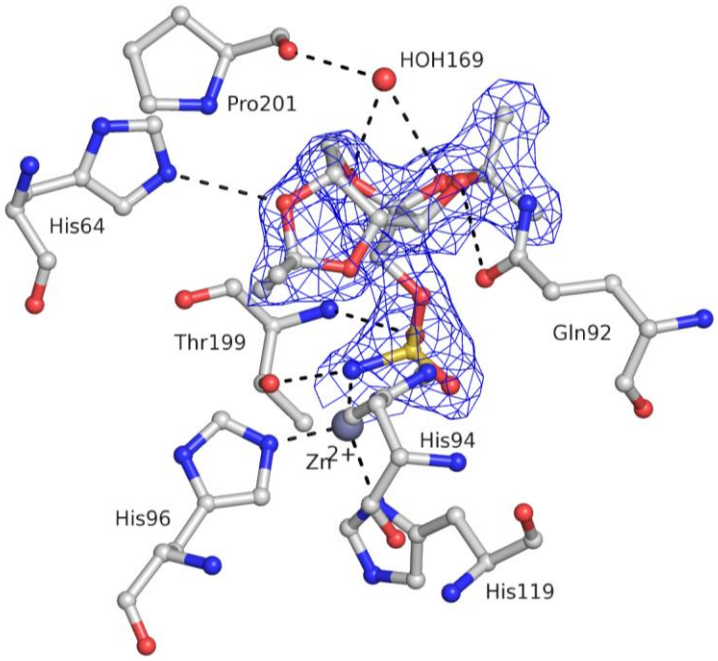

Figure 4.4 *Active site region of the hCAI/**TPM** complex*. The simulated annealing omit map, calculated with Fourier coefficients |2Fo-Fc|, relative to the inhibitor molecule is shown. Zn^{2+} coordination and hydrogen bonds are also shown as dotted lines.

4.2.3 Structural comparison with the native enzyme

A comparison of the hCA I structure in the complex under investigation with the native enzyme shows that a significant conformational rearrangement is necessary in the active site in order to allow the binding of the inhibitor (Figure 4.5A). Such a rearrangement has never before been evidenced in CA–inhibitor adducts, as the active site of this protein is a highly rigid one (Alterio *et al.*, 2009b). In particular, in hCA I the residue in position 200 is a bulky

histidine residue whereas in all other isoforms a threonine or a valine is present in this position (Figure 4.6). As a consequence, the bulky sugar moiety of the **TPM** molecule cannot enter the hCA I active site without a significant displacement of the His200 residue, which in turn causes a contemporary movement of residues Trp5 and His67. The movement of His200 also causes the lost of a hydrogen bond with Pro201 present in the native structure, and the consequent formation of a new hydrogen bond with Tyr7.

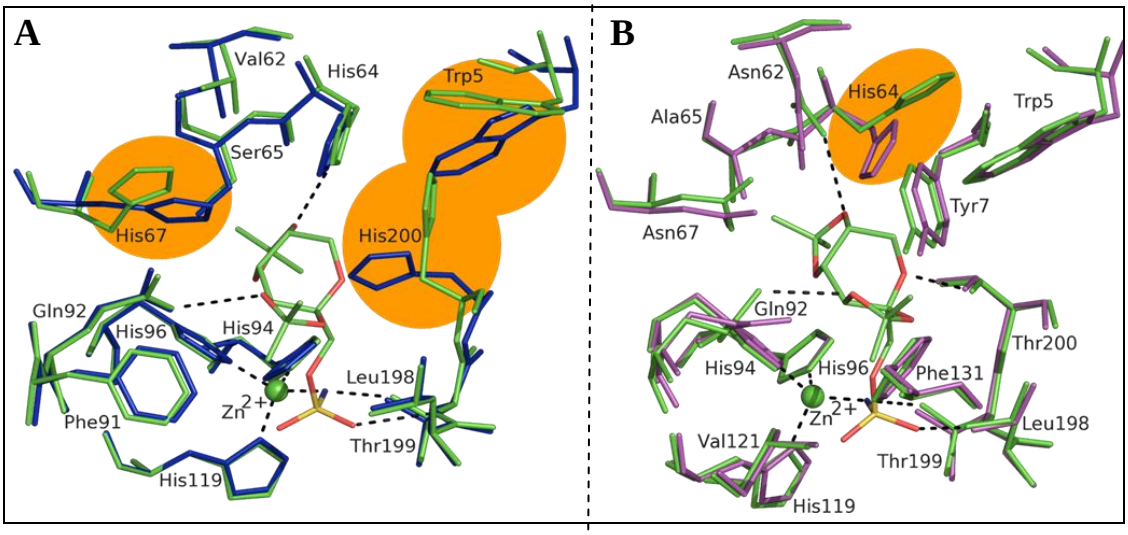

Figure 4.5 ***(A)*** *Superposition of the 3D structures of hCA I in the native state (blue) (PDB code 2CAB) (Kannan et al., 1984) with hCA I in complex with* ***TPM*** *(green).* ***(B)*** *Superposition of the structures of hCA II in the native state (magenta) (PDB code 1CA2) (Eriksson et al., 1988) with hCA II in complex with* ***TPM*** *(green) (PDB code 3HKU) (Casini et al., 2003; Lopez et al., 2009).*

```
hCA I     1  ASPDWGYDDKNGPEQWSKLYPIANGNNQSPVDIKTSETKHDTSLKPISVSYNPATAKEIINVGHSFHV
hCA II    2  -SHHWGYGKHNGPEHWHKDFPIAKGERQSPVDIDTHTAKYDPSLKPLSVSYDQATSLRILNNGHAFNV
hCA VA    3  --CAWQTSNNTLHPLWTVPVSVPGGTRQSPINIQWRDSVYDPQLKPLRVSYEAASCLYIWNTGYLFQV

hCA I    69  NFEDNDNRSVLKGGPFSDSYRLFQFHFHWGSTNEHGSEHTVDGVKYSAELHVAHWNSAKYSSLAEAAS
hCA II   69  EFDDSQDKAVLKGGPLDGTYRLIQFHFHWGSLDGQGSEHTVDKKKYAAELHLVHWNT-KYGDFGKAVQ
hCA VA   69  EFDDATEASGISGGPLENHYRLKQFHFHWGAVNEGGSEHTVDGHAYPAELHLVHWNSVKYQNYKEAVV
                                  * *     *       *

hCA I   137  KADGLAVIGVLMKVGEANPKLQKVLDALQAIKTKGKRAPFTNFDPSTLLPSSLDFWTYPGSLTHPPLY
hCA II  137  QPDGLAVLGIFLKVGSAKPGLQKVVDVLDSIKTKGKSADFTNFDPRGLLPESLDYWTYPGSLTTPPLL
hCA VA  137  GENGLAVIGVFLKLGAHHQTLQRLVDILPEIKHKDARAAMRPFDPSTLLPTCWDYWTYAGSLTTPPLT
                                                                        *

hCA I   205  ESVTWIICKESISVSSEQLAQFRSLLSNVEGDNAVPMQHNNRPTQPLKGRTVRASF---------
hCA II  205  ECVTWIVLKEPISVSSEQVLKFRKLNFNGEGEPEELMVDNWRPAQPLKNRQIKASFK--------
hCA VA  205  ESVTWIIQKEPVEVAPSQLSAFRTLLFSALGEEEKMMVNNYRPLQPLMNRKVWASFQATNEGTRS
```

Figure 4.6 *Sequence alignment of hCA I, hCA II and hCA VA*. Strictly conserved residues are highlighted in yellow; catalytic histidines, Thr199 and Glu106 are starred, while residues delimiting the active site cavity are boxed.

Since residues 5, 67 and 200 present a well conserved conformation within various CA–inhibitor complexes so far studied (Alterio *et al.*, 2009b; Temperini *et al.*, 2006; 2007; Jude *et al.*, 2006; Srivastava *et al.*, 2007; Chakravarty and Kannan, 1994; Kannan, 1981; Kumar *et al.*, 1994; Kumar and Kannan, 1994), it is reasonable to hypothesize that their movement requires a considerable energy cost. This finding is in agreement with the observation that, despite the presence of a large number of polar and hydrophobic interactions between the enzyme and the inhibitor, **TPM** does not show high affinity toward the enzyme with an inhibition constant of only 250 nM.

4.2.4 Structural comparison with hCA II/TPM and hCA VA/TPM

A detailed comparative analysis of the inhibition constants of **TPM** for the various CAs (Figure 4.1) revealed that this molecule binds human isozyme I with an efficiency 25 and 4 times lower than that measured for hCA II and hCA VA, respectively. To identify the molecular features that could be responsible for such behaviour, a detailed structural comparison between the adducts that **TPM** forms with these three isoforms (Casini *et al.*, 2003; Lopez *et al.*, 2009; Vitale *et al.*, 2007) has been performed. Since hCA I, hCA II and hCA VA share a high degree of sequence homology, several hCA I residues involved in **TPM** recognition are also conserved in hCA II and hCA VA (Figure 4.6). Accordingly the interactions which **TPM** established within the three active sites are rather similar (see Figure 4.7). However, amino acid substitutions at positions 62 and 200 determine important differences in inhibitor binding. The main interactions that **TPM** establishes with residues into the active sites of hCA I, hCA II and hCA VA are schematically depicted in Figure 4.7. In both cases, as observed for hCA I/**TPM** (Figures 4.4 and 4.7A) and other CA–sulfamate complexes (Alterio *et al.*, 2009b), the **TPM** sulfamate moiety is tetrahedrally coordinated to the zinc ion of the enzyme *via* its deprotonated nitrogen atom and hydrogen bonded to the

Thr199 residue. An extended network of polar interactions between the sugar scaffold of the inhibitor and active site protein residues contributes to the stabilization of the complex. It is interesting to note that the presence of an additional H-bond interaction in the case of the hCA II/**TPM** complex (Figure 4.7B) could be responsible for the higher affinity of **TPM** toward this isoform (Ki value = 10 nM) with respect to hCA VA (Ki value = 63 nM), even if it does not explain such a big difference with hCA I. However, the comparison of the hCA II structure in complex with **TPM** with that of native enzyme reveals that, differently from what observed in the case of hCA I, the binding of **TPM** to hCA II does not cause any significant movement of the active site residues (Figure 4.5B). This different behaviour can explain the difference in the affinity of **TPM** toward hCA II and hCA I and further confirms the role of the movement of the active site residues in determining the enzyme–inhibitor affinity. Since no native structure is available in the case of hCA VA it is not possible to clarify if in this case a movement of the active site residues is present or not.

Altoghter these data suggest that a different H-bond network together with the movement of some amino acid residues in order to accommodate the inhibitor are the main players in determining the difference of inhibition constants of **TPM** toward different CA isozymes. Thus these data may be helpful in the design of CAIs selective for various isozymes (e.g., hCA VA/VB, etc) with potential as anti-obesity drugs or other pharmaceutical applications.

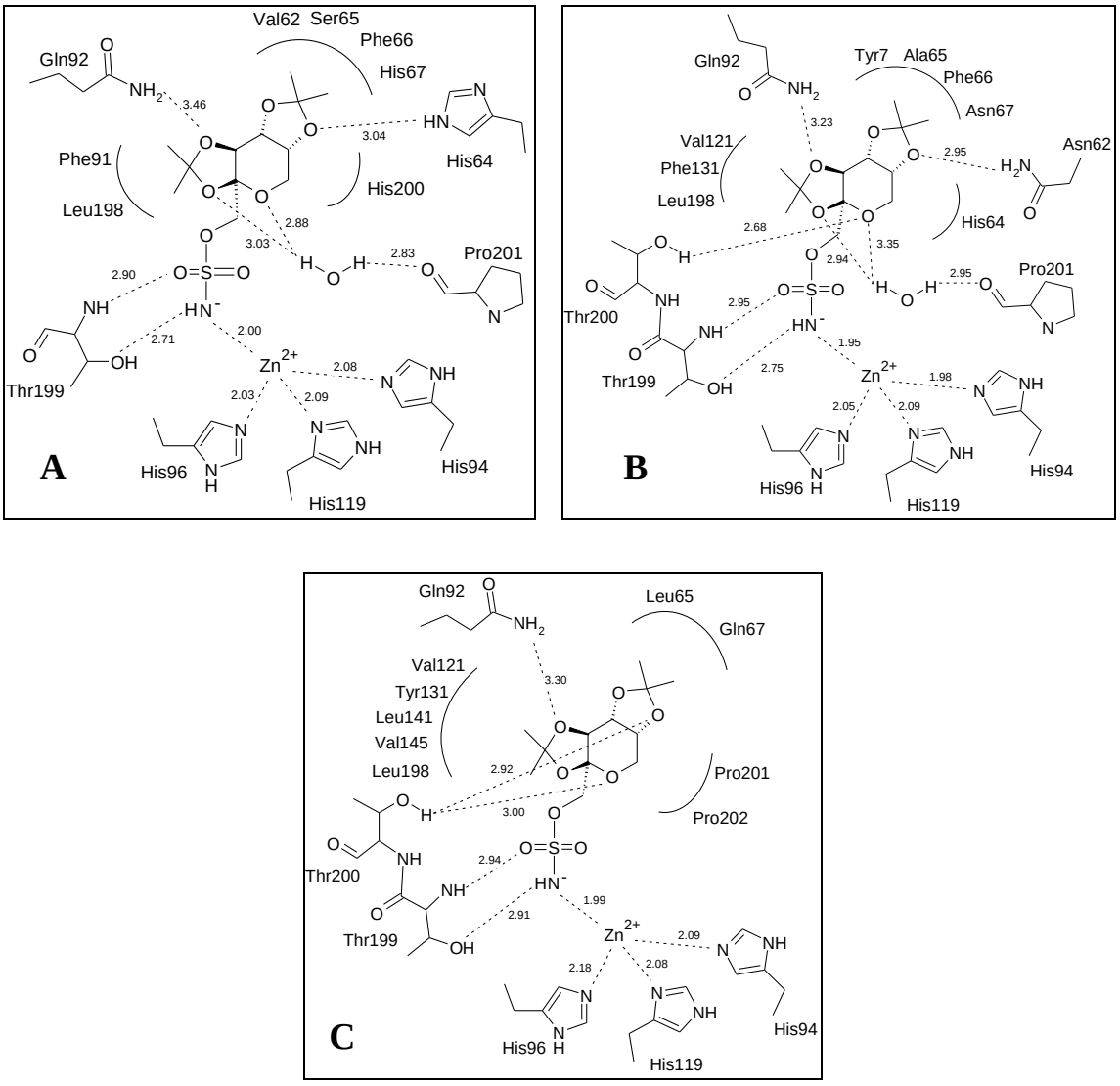

Figure 4.7 *Schematic representation of **TPM** binding within the hCA I (**A**), hCA II (**B**)* (Casini *et al.*, 2003; Lopez *et al.*, 2009) *and hCA VA (**C**)* (Vitale *et al., 2007) active sites*.

4.3 MATERIALS AND METHODS

4.3.1 hCA I/TPM crystallization and data collection

hCA I was purchased by Sigma and further purified, as described in paragraph 2.3.8, on NHS-activated Sepharose 4 FF resin (GE Healthcare) preactivated with pAMBS (Sigma). Eluted protein was concentrated to 10 mg ml^{-1} and used for crystallization experiments.

The hCA I/**TPM** complex was obtained by adding a 5-molar excess of the inhibitor to a 10 mg mL^{-1} protein solution in 50 mM Tris-SO_4, pH 8.5. Crystals of the complex were obtained by the hanging drop vapour diffusion technique at 20° C. Drops were prepared by mixing 1 μL of the hCA I/**TPM** adduct with 1 μL of precipitant solution (30% (w/v) PEG 4000, 0.2 M sodium acetate, 0.1 M Tris-HCl, pH 8.5), and equilibrated over a well containing 1 mL of precipitant solution. Crystals appeared in the drops after two days and grew in about one week to maximum dimensions of 0.2x0.3x0.3 mm^3 (Figure 4.8).

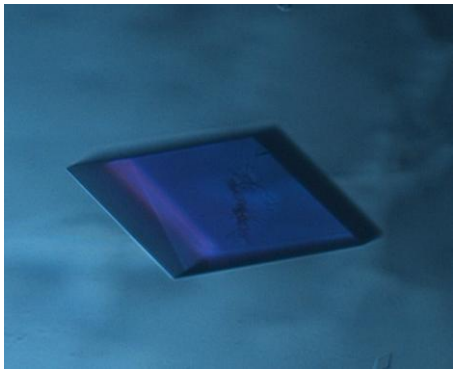

Figure 4.8 *Crystal of hCA I/**TPM** complex.*

X-ray diffraction data were collected at 100 K, at the Synchrotron source Elettra in Trieste, Italy, using a Mar CCD detector. Prior to cryogenic freezing, the crystals were transferred to the precipitant solution with the addition of 15% (v/v) glycerol. The data were processed using the HKL2000 package (Otwinowski and Minor, 1997). The crystals belonged to the

space group $P2_12_12_1$ with unit cell dimension of a = 63.32 Å, b = 71.07 Å, and c = 120.66 Å. The Matthews coefficient (V_M = 2.4 $Å^3$/Da) indicated that the crystallographic asymmetric unit contained two molecules according to a solvent content of 48%. Data collection statistics are reported in Table 4.2

Table 4.2. *X-Ray data collection statistics for hCA I/**TPM** complex.*

Space group	$P2_12_12_1$
Unit cell parameters	
a (Å)	63.32
b (Å)	71.07
c (Å)	120.66
Resolution limits (Å)	20.00-1.90
No. of observations	220776
No. of unique reflections	41817
Completeness (%)	95.7 (74.5)
I/σ(I)	21.2 (2.3)
Average multiplicity	5.3
R-sym (%)[a]	6.7 (33.4)
Mosaicity	0.24
V_M ($Å^3Da^{-1}$)	2.4
Solvent content (%)	47.8

[a]$Rsym=\Sigma_{hkl}\Sigma i\ |Ii(hkl)-<I(hkl)>|/\Sigma_{hkl}\Sigma i\ Ii\ (hkl)$, where Ii(hkl) is the ith measurement and <I(hkl)> is the weighted mean of all measurements of I(hkl). Values in parentheses refer to the highest resolution shell (1.97-1.90 Å).

4.3.2 Structure determination and refinement

The hCA I/**TPM** crystal structure was solved by molecular replacement using the program AMoRe (Navaza, 1994) and the crystallographic structure of native hCA I (PDB code 2CAB) (Kannan *et al.*, 1984) as starting model. The rotation and translation functions were calculated using data between 15.0 and 3.5 Å resolution. The one-body translation search, using the centred-overlap function (c-o), on the first 50 rotation solutions led to a single solution with a correlation coefficient of 37.3 % and an Rfactor of 46.9 %. The n-body translation search carried out with the phased-translation function (p-t), by including a PC refinement before each n-body translation search led to finding the second molecule contained into the

asymmetric unit. This improved the correlation coefficient and the Rfactor to 71.3 % and 33.0 %, respectively. Refinement of the structure was carried out using CNS (Brunger *et al.,* 1998) and manual model building was performed with O (Jones *et al.,* 1991). Clear electron density for one inhibitor molecule in each active site was observed in the |Fo| - |Fc| maps. Inhibitor molecules were gradually built into the model over several rounds of refinement. Restraints on inhibitor bond angles and distances were taken from similar structures in the Cambridge Structural Database and standard restraints were used on protein bond angles and distances throughout refinement. Various cycles of rebuilding and positional and temperature factor refinement were necessary to reduce the crystallographic Rfactor and Rfree values (in the 20.00-1.90 Å resolution range) to 20.0 % and 22.8 %, respectively. The correctness of stereochemistry was finally checked using PROCHECK (Laskowski *et al.,* 1993). Refinement statistics are summarized in Table 4.1. Coordinates and structure factors have been deposited in the Protein Data Bank (accession code 3LXE).

5. Conclusions and Perspectives

Carbonic anhydrases (CAs) are ubiquitous zinc enzymes present in prokaryotes and eukaryotes, all over the phylogenetic tree. These enzymes are efficient catalysts for the hydration of carbon dioxide to bicarbonate and protons, playing crucial physiological/pathological roles in acid-base homeostasis, secretion of electrolytes, transport of ions, biosynthetic reactions, and tumorigenesis. A consistent part of these enzymes are of clinical relevance and regarded as drug targets; for this reason, their inhibitors have been reported and developed as diuretics, antiglaucoma, anticancer, antiobesity, and antiepileptic agents (Supuran, 2007; 2008a). Among the 15 isoforms known in humans one of the least investigated when I started my Ph.D thesis was the hCA VII. For years hCA VII has been considered as a "brain enzyme" being mainly detected in most of the brain tissues, where it contributes to neuronal excitability by providing bicarbonate anion that can mediate current through channels coupled to $GABA_A$ receptor (Thiry *et al*., 2008b). Subsequently, hCA VII was proposed as acting a role in the control of neuropathic pain, suggesting that its inhibition could constitute a new pharmacological mechanism in designing drugs useful for the treatment of this pathological condition (Asiedu *et al*., 2010). Only recently, its presence has been detected, by immunohistochemistry, also in other tissues, such as stomach, duodenum, colon, liver and skeletal muscle (Bootorabi *et al.*, 2010), indicating that together with hCA VA and hCA XIV it represents the major isoform in hepatocytes, even though its function still has to be investigated. Apart the above mentioned biological studies, and some characterization of hCA VII with developed inhibitors carried out by Supuran's group (Güzel *et al.*, 2009; Carta *et al.*, 2009), few literature was present on this enzyme; thus, considering also that hCA VII is a highly catalytic CA enzyme, second only to hCA II, we started a deep biochemical and structural characterization on this enzyme.

For this purpose, *hCA 7* gene was cloned in pGex-4T-3 vector and hCA VII was expressed and purified following tag removal. The recombinant protein was obtained with a purity

greater than 98% and its analysis by circular dicroism showed a high percentage of α-helix and β-sheet secondary structure, as reported also for the other α–family hCAs. The analysis by LC-ESI-MS/MS highlighted the particular reactivity of two cysteine residues. In particular, among the four cysteines present in the aminoacidic sequence, Cys183 and Cys217 were involved in S-glutathionylation, which occurred during *in vitro* purification, whereas Cys54 and Cys178 were involved in the formation of an intramolecular disulfide bridge. Due to the high similarity of hCA VII to hCA III, for which S-glutathionylation was also reported *in vivo* (Supuran, 2008a; Hilvo *et al.*, 2008) and associated to protective response to oxidative stress (Zimmerman *et al.,* 2004), we investigated whether this modification observed *in vitro* for hCA VII could be present also *in vivo,* and if it could affect its catalytic efficiency. To this aim, we extensively investigated catalytic activity of this enzyme, looking at the canonical catalytic activity, *i.e.* CO_2 hydration, and also at the non-canonical ones, such as esterase, phosphatase and sulfatase activities. Obtained data were compared to those achieved with native enzyme and with a mutated form where reactive cysteines were mutated in serines (C183S/C217S). Results showed that S-glutathionylation does not affect any of the investigated catalytic activities of the various forms of the enzyme, which, unexpectedely, showed a high degree of phosphatase and esterase activity. Thus, it could be concluded that the observed S-glutathionylation, if present *in vivo*, is not involved in the regulation of the enzyme catalytic activity but rather, as already observed for hCA III, could help hCA VII to function as an oxygen radical scavenger to protect cells from oxidative damage. Work is still in progress to investigate *in vivo* the eventual hCA VII protective role towards oxidative stress. A possible role of hCA VII acting as an esterase and/or phosphatase enzyme is also currently investigated as well as eventual alternative substrates are to be determined.

In order to complete the structural characterization of human cytosolic α-CAs, during my Ph.D thesis the X-ray structure of isoform VII, which was the last undefined structure, was

solved. An important hint for the X-ray study was given by the production of a stable and homogenous preparation of the enzyme, achieved by using the C183S/C217S mutated form, this avoiding a covalent intermolecular cross-linking of reactive cysteines. As already observed for other α-CAs (Alterio *et al.*, 2009b), hCA VII structure consists of a central 10-stranded β-sheet surrounded by four α- and four 3_{10}-helices and five additional β-strands. The active site is located in a conical cavity about 15 Å wide and 15 Å deep, which extends from the surface of the protein to the centre of the molecule. The catalytic zinc ion is located at the bottom of this cavity, coordinated by three histidine residues; the fourth coordination position is occupied by the deprotonated sulfonamide NH^- group of the **AZM** inhibitor which co-crystallized with the enzyme. The obtained X-ray structure will be very helpful for the rational design of selective hCA VII inhibitors. Work is in progress to this aim.

Even though cytosolic hCAs share a high sequence identity, they are characterized by very different kinetic features; limiting the comparison to the active site regions, it is possible to observe that most of the residues which delimit the cavity are generally conserved either by nature or conformation. In order to clarify the contribution to the catalytic activity of each single residue within the enzyme active site, I performed a rational design on hCA VII and hCA XIII enzymes producing in total 10 mutants, where the amminoacid present into their catalitic surroundings were replaced by the corresponding aminoacid present in hCA II. Results showed that both for hCA VII and hCA XIII improvements were reached even if none of the substitution managed to achieve the same hCA II catalytic efficiency.

Finally, during my Ph.D project, I carried out also the structural characterization of a complex which hCA I forms with topiramate (**TPM**), a clinically used drug for the treatment of epilepsy. The analysis of the structure of such complex showed that, upon binding of the inhibitor, the active site of hCA I undergoes a profound reorganization, which has never been observed in any other CA/inhibitor complex and might therefore be useful in designing CAIs

which exploit it. Moreover, the comparison with hCA II/**TPM** and hCA VA/**TPM** complex structures, previously investigated (Casini *et al.*, 2003; Lopez *et al.*, 2009; Vitale *et al.*, 2007), showed that a different H-bond network together with the movement of some active site residues in order to accommodate the inhibitor may account for the diverse inhibition constants of **TPM** toward different CA isozymes. These data may be helpful in the design of CAIs selective for various isozymes.

6. References

Almstedt, K., Rafstedt, T., Supuran, C. T., Carlsson, U., Hammarström, P. *Biochemistry* **2009**, 48, 5358.

Alterio, V., Hilvo, M., Di Fiore, A., Supuran, C. T., Pan, P., Parkkila, S., Scaloni, A., Pastorek, J., Pastorekova, S., Pedone, C., Scozzafava, A., Monti, S. M., De Simone, G. *Proc. Natl. Acad. Sci. U.S.A.* **2009a**, 106, 16233.

Alterio, V., Di Fiore, A., D'Ambrosio, K., Supuran, C. T., De Simone, G. In *Drug Design of Zinc-Enzyme Inhibitors: Functional, Structural, and Disease Applications*; Supuran, C. T., Winum, J.-Y., Eds.; Wiley: Hoboken, New Jersey, **2009b**; p 73-138.

Asiedu, M., Ossipov, M. H., Kaila, K., Price, T. J. *Pain.* **2010**, 148, 302.

Aspatwar, A., Tolvanen, M. E., Ortutay, C., Parkkila, S. *Curr. Pharm. Des*. **2010**, 16, 3264.

Astrup, A., Toubro, S. *Obesity*, **2004**, 12, 167S.

Avenell, A., Broom, J., Brown, T. J., Poobalan, A., Aucott, L., Stearns, S. C., Smith, W. C., Jung, R. T., Campbell, M. K., Grant, A. M. *Health Technol Assess.* **2004**, 8, 1-182.

Barreiro, E., Hussain, S. N. A. *Antioxid. Redox Signal*. **2010**, 12, 417.

Basnyat, B., Gertsch, J. H., Johnson, E. W., Castro-Marin, F., Inoue, Y., Yeh, C. *High Alt. Med. Biol*. **2003**, 4, 45.

Battke, C., Kremmer, E., Mysliwietz, J., Gondi, G., Dumitru, C., Brandau, S., Lang, S., Vullo, D., Supuran ,C. T, Zeidler, R. *Cancer Immunol. Immunother*. **2011**, 60, 649.

Bendaly, E. A., Jordan, C. A., Staehler, S. S., Rushing, D. A. *Supportive Cancer Therapy* **2007**, 4, 241.

Berlin, H. A. *Current Psychiatry Reports* **2007**, 9, 291.

Bertini, I., Luchinat, C., and Scozzafava, A. *Structure and Bonding* **1982**, 48, 45.

Bialer, M., Johannessen, S. I., Kupferberg, H. J., Levy, R. H., Loiseau, P., Perucca, E. *Epilepsy Res.* **2001**, 43, 11.

Bootorabi, F., Jänis, J., Smith, E., Waheed, A., Kukkurainen, S., Hytönen, V., Valjakka, J., Supuran, C. T., Vullo, D., Sly, W. S., Parkkila, S. *Biochimie*. **2010**, 92, 1072.

Boriack-Sjodin, P. A., Heck, R. W., Laipis, P. J., Silverman, D. N., Christianson, D. W. *Proc. Natl. Acad. Sci. U.S.A.* **1995**, 92, 10949.

Bourgeois, B. F. D. *Journal of Child Neurology* **2000**, 15, S27–30.

Bradford, M.M. *Anal. Biochem*., **1976**, 72, 248.

Brancaccio, P., Lippi, G., Maffulli, N. *Clin. Chem. Lab. Med*. **2010**, 48, 757.

Briganti, F., Mangani, S., Orioli, P., Scozzafava, A., Vernaglione, G., Supuran, C. T. *Biochemistry* **1997**, 36, 10384.

Brunger, A. T, Adams, P. D., Clore, G. M., De Lano, W. L., Gros, P., Grosse-Kunstleve, R. W., Jiang, J. S., Kuszewski, J., Nilges, M., Pannu, N. S., Read, R. J., Rice, L. M., Simonson, T., Warren, G. L. *Acta Crystallogr., Sect. D: Biol. Crystallogr.* **1998**, 54, 905.

Campfield, L. A., Smith, F. J., Burn, P. *Science* **1998**, 280, 1383.

Carta, F., Temperini, C., Innocenti, A., Scozzafava, A., Kaila, K., Supuran, C. T. *J. Med. Chem*. **2010**, 53, 5511.

Casini, A., Antel, J., Abbate, F., Scozzafava, A., David, S., Waldeck, H.,Schäfer S., Supuran, C. T. *Bioorg. Med. Chem. Lett.* **2003**, 13, 841.

Celebisoy, N., Gökçay, F., Sirin, H., Akyürekli, O. *Acta Neurol. Scand.* **2007**, 116, 322.

Chai, Y. C., Jung, C. H., Lii, C. K., Ashraf, S. S., Hendrich, S., Wolf, B., Sies, H., Thomas, J. A. *Arch. Biochem. Biophys*. **1991**, 284, 270.

Chakravarty, S., Kannan, K. K. *J. Mol. Biol.* **1994**, 243, 298.

Chegwidden, W. R., Spencer, I. M. *Comp. Biochem. Physiol.* **1996**, 115B, 247.

Chirica, L. C., Elleby, B., Jonsson, B. H., Lindskog, S. *European Journal of Biochemistry* **1997**, 224, 755.

Christianson, D. W., Fierke, C. A. *Acc. Chem. Res.* **1996**, 29, 331.

Cooke, D., Bloom, S. *Nat. Rev. Drug Discov.* **2006**, 5, 919.

Cudney, R., Patel, S., Weisgraber, K., Newhouse, Y., McPherson, A. *Acta Crystallogr. D. Biol. Crystallogr.* **1994**, 50, 414.

Datta, R., Waheed, A., Bonapace, G., Shah, G. N., Sly, W. S. *Proc. Natl. Acad. Sci. U.S.A.* **2009**, 106, 3437.

Davis, R. A., Hofmann, A., Osman, A., Hall, R. A., Mühlschlegel, F. A., Vullo, D., Innocenti, A., Supuran, C. T., Poulsen, S. A. *J. Med. Chem*. **2011**, 54, 1682.

Del Vecchio, P., Graziano, G., Barone, G., Mandrich, L., Rossi, M., Manco, G. *Thermochimica Acta*. **2006**, 441, 144.

De Simone, G., Supuran, C. T. *Curr. Top. Med. Chem.* **2007**, 7, 879.

De Simone, G., Di Fiore, A., Supuran, C. T. *Curr. Pharm. Des.* **2008**, 14, 655.

De Simone, G., Scozzafava, A., Supuran, C. T. *Chem. Biol. Drug Des*. **2009**, 74, 317.

De Simone, G., Supuran, C. T. In *Drug Design of Zinc-Enzyme Inhibitors: Functional, Structural, and Disease Applications*; Supuran, C. T., Winum, J.-Y., Eds.; Wiley: Hoboken, New Jersey, **2009**; p 241-254.

De Simone, G., Supuran, C. T. *Biochim. Biophys. Acta* **2010**, 1804, 404.

Di Fiore, A., Monti, S. M., Hilvo, M., Parkkila, S., Romano, V., Scaloni, A., Pedone, C., Scozzafava, A., Supuran, C. T., De Simone, G. *Proteins* **2008**, 74, 164.

Di Fiore, A., Truppo, E., Supuran, C. T., Alterio, V., Dathan, N., Bootorabi, F., Parkkila, S., Monti, S. M., De Simone, G. *Bioorg. Med. Chem. Lett*. **2010**, 20, 5023.

Domsic, J. F., Avvaru, B. S., Kim, C. U., Gruner, S. M., Agbandje-McKenna, M., Silverman, D. N., McKenna, R. *J. Biol. Chem*. **2008**, 283, 30766.

Ducruix, A., Giegè, R. In *Crystallization of Nucleic Acids and Proteins: a practical approach*; Ducruix, A., Giegè, R., Eds.; Oxford University Press, **1999**; p 121-148.

Duda, D. M., Tu, C., Fisher, S. Z., An, H., Yoshioka, C., Govindasamy, L., Laipis, P. J., Agbandje-McKenna, M., Silverman, D. N., McKenna, R. *Biochemistry* **2005**, 44, 10046.

Edmonds, H. L., Jiang, Y. D., Zhang, P. Y, Shank, R. P. *Life Sci.*, **1996**, 59, PL127–131.

Elder, I., Han, S., Tu, C., Steele, H., Laipis, P. J., Viola, R. E., Silverman, D. N. *Arch. Biochem. Biophys.* **2004**, 421, 283.

Elleby, B., Sjöblom, B., Lindskog, S. *Eur. J. Biochem*. **1999**, 262, 516.

Eriksson, A. E.; Jones, T. A.; Liljas, A. *Proteins* **1988**, 4, 274.

Eriksson, A. E., Liljas, A. *Proteins* **1993**, 16, 29.

Fierke, C. A., Calderone, T. L., Krebs, J. F. *Biochemistry* **1991**, 30, 11054.

Filomeni, G., Rotilio, G., Ciriolo, M. R. *Cell Death Differ*. **2005**, 12, 1555.

Fisher, Z., Prada, J. A. H., Tu, C., Duda, D., Yoshioka, C., An, H. Q., Govindasamy, L., Silverman, D. N., McKenna, R. *Biochemistry* **2005**, 44, 1097.

Fisher, S. Z., Maupin, C. M., Budayova-Spano, M., Govindasamy, L., Tu, C. K., Agbandje-McKenna, M., Silverman, D. N., Voth, G. A., McKenna, R. *Biochemistry* **2007a**, 46, 2930.

Fisher, S. Z., Tu, C., Bhatt, D., Govindasamy, L., Agbandje-McKenna, M., McKenna, R., Silverman, D. N. *Biochemistry* **2007b**, 46, 3803.

Friedman, J.M. *Science* **2003**; 299, 856.

Gao, B. B., Clermont, A., Rook, S., Fonda, S. J., Srinivasan, V. J., Wojtkowski, M., Fujimoto, J. G., Avery, R. L., Arrigg, P. G., Bursell, S. E., Aiello, L. P., Feener, E. P. *Nat. Med*. **2007**, 13, 181.

Genis, C., Sippel, K. H., Case, N., Cao, W., Avvaru, B. S., Tartaglia, L. J., Govindasamy, L., Tu, C., Agbandje-McKenna, M., Silverman, D. N., Rosser, C. J., McKenna, R. *Biochemistry* **2009**, 48, 1322.

Guler, O. O., De Simone, G., Supuran, C. T. *Curr. Med. Chem*. **2010**, 17, 1516.

Güzel O, Innocenti A, Scozzafava A, Salman A, Supuran CT Biorg. Med. Chem. Lett. **2009**, 19, 3170.

Håkansson, K., Carlsson, M., Svensson, L. A., Liljas, A. *J. Mol. Biol*. **1992**, 227, 1192.

Hen, N., Bialer, M., Yagen, B., Maresca, A., Aggarwal, M., Robbins, A. H., McKenna, R., Scozzafava, A., Supuran, C. T. *J. Med. Chem*. **2011**, 54, 3977.

Hewett-Emmett, D., Tashian, R. E. *Mol. Phylogenet. Evol.* **1996**, 5, 50.

Hewett-Emmett, D. *Gene families* **2000**, 90, 29.

Hill, J. O., Wyatt, H. R., Reed, G. W., Peters, J. C. *Science*. **2003**, 299, 853.

Hilvo, M., Innocenti, A., Monti, S.M., De Simone, G., Supuran, C.T., Parkkila, S. *Curr. Pharm. Des*. **2008**; 14, 672.

Hollander, E., Dell'Osso, B. *International Clinical Psychopharmacology*, **2006**, 21, 189.

Hunt, J. A., Fierke, C. A. *J. Biol. Chem*. **1997**, 272, 20364.

Ioannides-Demos, L. L., Proietto, J., Tonkin, A. M., Mc Neil, J. J. *Drug Saf.* **2006**, 29, 277.

Jancarik, J., Scott, W. G., Milligan, D. L., Koshland, D. E. Jr, Kim, S. H. *J. Mol. Biol.* **1991**, 221, 31.

Johnson, W.C. *Methods Biochem Anal*. **1985**, 31, 61.

Jones, T. A., Zou, J. Y., Cowan, S. W., Kjeldgaard, M. *Acta Crystallogr., Sect. A: Found. Crystallogr.*, **1991**, 47, 110.

Jude, K. M., Banerjee, A. L., Haldar, M. K, Manokaran, S., Roy, B., Mallik, S., Srivastava, D. K., Christianson, D. W. *J. Am. Chem. Soc.*, **2006**, 128, 3011.

Kadokura, H., Katzen, F., Beckwith, J. *Annu. Rev. Biochem*. **2003**, 72, 111.

Kannan, K. K., Notstrand, B., Fridborg, K., Lövgren, S., Ohlsson, A., Petef, M. *Proc Natl Acad Sci U S A*. **1975**, 72, 51.

Kannan, K. K. In *Biomolecular Structure, Conformation, Function and Evolution vol 1*, Ed. R. Srinivasan, Pergamon, Oxford, **1981**, pp. 165-181.

Kannan, K. K., Ramanadham, M., Jones, T. A. *Ann. N.Y. Acad. Sci*. **1984**, 429, 49.

Khalifah, R.G. *J. Biol. Chem.* **1971**, 246, 2561.

Kivelä, J., Parkkila, S., Parkkila, A. K., Rajaniemi, H. *Caries Res*. **1999**, 33, 178.

Kivelä, A. J., Kivelä, J., Saarnio, J., Parkkila, S. *World J. Gastroenterol.* **2005**, 11, 155.

Kockar, F., Maresca A, Aydin M, Işik S, Turkoglu S, Sinan S, Arslan O, Güler OO, Turan Y, Supuran CT. *Bioorg Med Chem.* **2010**, 18, 5498.

Krungkrai, S.R., Suraveratum, N., Rochanakij, S., Krungkrai, J. *International Journal of Parasitology.* **2001**, 31, 661.

Kumar, V., Kannan, K. K. *J. Mol. Biol.* **1994**, 241, 226.

Kumar, V., Kannan, K. K., Sathyamurthi, P. *Acta Crystallogr., Sect. D: Biol. Crystallogr.*, **1994**, 50, 731.

Laemmli, U. K. *Nature* **1970**, 227, 680.

Lane, T.W, Saito, M. A., George, G. N., Pickering, I. J., Prince, R. C., Morel, F. M. M. *Nature*, **2005**, 435, 42.

Laskowski, R. A., MacArthur, M. W., Moss, M. D., Thorton, J. M. *J. Appl Crystallogr*. **1993**, 26, 283.

Lau, D. C. *CMAJ* **2007**, 176, 951.

Lehtonen, J., Shen, B., Vihinen, M., Casini, A., Scozzafava, A., Supuran, C. T., Parkkila, A. K., Saarnio, J., Kivelä, A. J., Waheed, A., Sly, W. S., Parkkila, S. *J. Biol. Chem.* **2004**, 279, 2719.

Leibel, R. L., Rosenbaum, M., Hirsch, J. *N. Engl. J. Med.* **1995**, 332, 621.

Liang, Z., Xue, Y., Behravan, G., Jonsson, B. H., Lindskog, S. *Eur. J. Biochem*. **1993**, 211, 821.

Liao, S. Y., Ivanov, S., Ivanova, A., Ghosh, S., Cote, M. A., Keefe, K., Coca-Prados, M., Stanbridge, E. J., Lerman, M. I. *J. Med. Genet*. **2003**, 40, 257.

Lii, C. K., Wang, S. T., Chen, H. W. *Toxicol. Lett.* **1996**, 84, 97.

Lindskog S, Behravan G, Engstrand C, Forsman C, Jonsson BH, Liang Z, Ren X, Xue Y. In: *Botre'*; F, Gros G, Storey BT, editors. Carbonic anhydrases from biochemistry and genetics to physiology and clinical medicine. Weinheim: Verlag Chemie; **1991**. pp 1–13

Lindskog, S. *Pharmacol. Ther*. **1997**, 74, 1.

Lindskog, S., Silverman, D. N. *EXS.* **2000**, 90, 175.

Lobley, A., Whitmore, L., Wallance, B. A. *Bioinformatics* **2002**, 18, 211.

Lopez, M., Paul, B., Hofmann, A., Morizzi, J., K.Wu, Q., Charman, S. A., Innocenti, A., Vullo, D., Supuran, C. T., Poulsen, S. A. *J. Med. Chem.* **2009**, 52, 6421.

Lyseng-Williamson, K. A., Yang, L. P. *Drugs* **2007**, 67, 2231.

Mallis, R. J., Poland, B. W., Chatterjee, T. K., Fisher, R. A., Darmawan, S., Honzatko, R. B., Thomas, J. A. *FEBS Lett*. **2000**, 482, 237.

Maren, T. H. *Physiol. Rev.* **1967**, 47, 595.

Maresca, A., Temperini, C., Vu, H., Pham, N. B., Poulsen, S. A., Scozzafava, A., Quinn, R. J., Supuran, C. T. *J. Am. Chem. Soc*. **2009**, 131, 3057.

Maresca, A., Temperini, C., Pochet, L., Masereel, B., Scozzafava, A., Supuran, C. T. *J. Med. Chem*. **2010**, 53, 335.

Marí, M., Morales, A., Colell, A., García-Ruiz, C., Fernández-Checa, J.C. *Antioxid Redox Signal.* **2009**, 11, 2685.

Marí, M., Colell, A., Morales, A., von Montfort, C., Garcia-Ruiz, C., Fernández-Checa, J.C. *Antioxid. Redox Signal.* **2010**, 12, 1295.

Matsui, H., Murakami, M., Wynns, G. C., Conroy, C. W., Mead, A., Maren, T. H., Sears, M. L. *Exp. Eye Res*. **1996**, 62, 409.

McElroy, S. L., Guerdjikova, A. I., Martens, B., JrKeck, P. E., Pope, H. G., Hudson, J. I. *CNS Drugs*, **2009**, 23, 139.

Meldrum, N. U., Roughton, F. J. W. *The Journal of Physiology* **1933**, 80, 113.

Merz, K. M. Jr. *J. Am. Chem. Soc*. **1991**, 113, 406.

Mikulski, RL, Silverman, DN. *Biochim Biophys Acta* **2010**, 1804, 422.

Mincione, F., Scozzafava, A., Supuran, C. T. *Curr. Pharm. Des*. **2008**, 14, 649.

Mirza, N., Marson, A. G., Pirmohamed, M. *Br. J. Clin. Pharmacol.*, **2009**, 68, 655.

Montgomery, J. C., Venta, P. J., Eddy, R. L., Fukushima, Y. S., Shows, T. B., Tashian, R. E. *Genomics.* **1991**, 11, 835.

Nair, S. K., Ludwig, P. A., Christianson, D. W. *J. Am. Chem. Soc*. **1994**, 116, 3659.

Navaza, J. *Acta Crystallogr., Sect. A.* **1994**, 50, 157.

Nishimori, I., Minakuchi, T., Onishi, S., Vullo, D., Scozzafava, A., Supuran, C. T. *J. Med. Chem*. **2007**, 50, 381.

Ochrietor, J. D., Clamp, M. F., Moroz, T. P., Grubb, J. H., Shah, G. N., Waheed, A., Sly, W. S., Linser, P. J. *Exp. Eye Res*. **2005**, 81, 492.

Ogilvie, J. M., Ohlemiller, K. K., Shah, G. N., Ulmasov, B., Becker, T. A., Waheed, A., Hennig, A. K., Lukasiewicz, P. D., Sly, W. S. *Proc. Natl. Acad. Sci. U.S.A.* **2007**, 104, 8514.

Otwinowski, Z., Minor, W. *Methods Enzymol*. **1997**, *276*, 307.

Papa, S., Monti, S. M., Vitale, R. M., Bubici, C., Jayawardena, S., Alvarez, K., De Smaele, E., Dathan, N., Pedone, C., Ruvo, M., Franzoso, G. *J. Biol. Chem*. **2007**, 282, 19029.

Parkkila, S., Parkkila, A. K. *Scand. J. Gastroenterol.* **1996**, 31, 305.

Parkkila, S., Kivela, A. J., Kaunisto, K., Parkkila, A. K., Hakkola, J., Rajaniemi, H., Waheed, A., Sly, W. S. *BMC Gastroenterol* **2002**, 2, 13.

Pastorekova, S., Parkkila, S., Pastorek, J., Supuran, C. T. *J. Enzyme Inhib. Med. Chem.* **2004**, 19, 199.

Pastorekova, S., Parkkila, S., Zavada, J. *Adv. Clin. Chem*. **2006**, 42, 167.

Räisänen, S. R., Lehenkari, P., Tasanen, M., Rahkila, P., Härkönen, P. L., Väänänen, H. K. *FASEB J*. **1999**, 13, 513.

Ramadan, N. M., Buchanan, T. M. *Pharmacol. Ther.* **2006**, 112, 199.

Richard, D., Picard, F., Lemieux, C., Lalonde, J., Samson, P., Deshaies, Y. *Int. J. Obes.* **2002**, 26, 344.

Rizzello, A., Ciardiello, M. A., Acierno, R., Carratore, V., Verri, T., di Prisco, G., Storelli, C., Maffia, M. *Protein J.* **2007**, 26, 335.

Roberts, S. B., Lane, T. W., Morel, F. M. M. *J Phycol*. **1997**, 33, 845.

Rokutan, K., Thomas, J. A., Sies, H. *Eur. J. Biochem.* **1989**, 179, 233.

Roy, A.; Taraphder, S. *J. Phys. Chem. Sect. B* **2007**, 111, 10563.

Ruusuvuori, E., Li, H., Huttu, K., Palva, J. M., Smirnov, S., Rivera, C., Kaila, K., Voipio, J. *J. Neurosci*. **2004**, 24, 2699.

Sabers, A., Gram, L. *Drugs*, **2000**, 60, 23.

Scolnick, L. R., Christianson, D. W. *Biochemistry*. **1996**, 35, 16429.

Shah, G. N., Hewett-Emmett, D., Grubb, J. H., Migas, M. C., Fleming, R. E., Waheed, A., Sly, W. S. *Proc. Natl. Acad. Sci. USA* **2000**, 97, 1677.

Shah, G. N., Ulmasov, B., Waheed, A., Becker, T., Makani, S., Svichar, N., Chesler, M., Sly, W. S. *Proc. Natl. Acad. Sci .U.S.A.* **2005**, 102, 16771.

Shank, R. P., Gardocki, J. F, Vaught, J. L., Davis, C. B., Schupsky, J. J., Raffa, R. B., Dodgson, S. J., Nortey, S.O., Maryanoff, B. E. *Epilepsia*, **1994**, 35, 450.

Silverman, D. N., McKenna, R. *Acc. Chem. Res* **2007**, 40, 669.

Smith, K.S., Ferry J.G. *FEMS Microbiol Rev.* **2000**, 24, 335.

Soto, A. R., Zheng, H., Shoemaker, D., Rodriguez, J., Read, B. A., Wahlund, T. M. *Appl Environ Microbiol.* **2006**, 72, 5500.

Srivastava, D. K., Jude, K. M., Banerjee, A. L., Haldar, M., Manokaran, S., Kooren, J., Mallik, S., Christianson, D. W. *J. Am. Chem. Soc.*, **2007**, 129, 5528.

Stams, T., Nair, S. K., Okuyama, T., Waheed, A., Sly, W. S., Christianson, D. W. *Proc. Natl. Acad. Sci. U.S.A.* **1996**, 93, 13589.

Stams, T., Christianson, D. W. In *The Carbonic Anhydrases. New Horizons*; Chegwidden, W. R., Carter, N. D., Edwards, Y. H., Eds.; Birkhäuser Verlag: Basel, Switzerland, **2000**; p 159–74.

Stringer, J. L. *Epilepsy Res.*, **2000**, 40, 147.

Supuran, C. T., Scozzafava, A. *Therapeutic Patents***. 2000**, 10, 575**.**

Supuran, C. T., Scozzafava, A. *Expert Opinion on Therapeutic Patents.* **2002**, 12, 217.

Supuran, C. T., Scozzafava, A., Casini, A. *Med. Res. Rev.* **2003**, 23, 146.

Supuran, C. T., Scozzafava, A., Conway, J., Eds.; *Carbonic Anhydrase: Its Inhibitors and Activators*; CRC Press: Boca Raton, FL, **2004**.

Supuran, C. T. *Curr Top Med Chem*. **2007**, 7, 825.

Supuran, C. T. *Nat. Rev. Drug Discov*. **2008a**, 7, 168.

Supuran, C. T. *Curr. Pharm. Des*. **2008b**, 14, 641.

Supuran, C. T., Di Fiore, A., De Simone, G. *Expert Opin. Emerg. Drugs* **2008**, 13, 383.

Swenson, E. R., Teppema, L. J. *J. Appl. Physiol*. **2007**, 102, 1305.

Tang, Y., Xu, H., Du, X., Lit, L., Walker, W., Lu, A., Ran, R., Gregg, J. P., Reilly, M., Pancioli, A., Khoury, J. C., Sauerbeck, L. R., Carrozzella, J. A., Spilker, J., Clark, J., Wagner, K. R., Jauch, E. C., Chang, D. J., Verro, P., Broderick, J. P., Sharp, F. R. *J. Cereb. Blood Flow Metab*. **2006**, 26, 1089.

Taoka, S., Chen, X., Tarnuzzer, R. W., Van Heeke, G., Tu, C., Silverman, D. N. *Biochim. Biophys. Acta* **1992**, 1159, 274.

Tashian, R. E., Venta, P. J., Nicewander, P. H., Hewett-Emmett, D. *Prog. Clin. Biol. Res.* **1990**, 344, 159.

Tashian, R. E., Hewett-Emmett, D., Carter, N., Bergenhem, N. C. *EXS*. **2000**, 90, 105.

Temperini, C., Scozzafava, A., Supuran, C. T. *Bioorg. Med. Chem. Lett.*, **2006**, 16, 5152.

Temperini, C., Innocenti, A., Guerri, A., Scozzafava, A., Rusconi, S., Supuran, C. T. *Bioorg. Med. Chem. Lett.*, **2007**, 17, 2210.

Thiry, A., Dogné, J. M., Supuran, C. T., Masereel, B. *Curr. Top. Med. Chem*. **2007a**, 7, 855.

Thiry, A., Masereel, B., Dogné, J. M., Supuran, C. T., Wouters, J., Michaux, C. *Chem. Med.Chem.* **2007b**, 2, 1273.

Thiry, A., Rolin, S., Vullo, D., Frankart, A., Scozzafava, A., Dogné, J. M., Wouters J., Supuran, C. T., Masereel, B. *Eur. J. Med. Chem*. **2008a**, 43, 2853.

Thiry, A.; Dogné, J. M.; Supuran, C. T.; Masereel, B. *Curr. Pharm. Des*. **2008b**, 14, 661.

Tornatore, L., Marasco, D., Dathan, N., Vitale, R. M., Benedetti, E., Papa, S., Franzoso, G., Ruvo, M., Monti, S. M. *J. Mol. Biol.* **2008**, 378, 97.

Tu, C. K., Silverman, D. N., Forsman, C., Jonsson, B. H., Lindskog, S. *Biochemistry* **1989**, 28, 7913.

Van Gaal, L., Mertens, I. In *Clinical obesity*; Kopelman, P. Stock, M.J., Eds; Oxford, Blackwell, **1998**; pp. 205-225.

Vasudev, K., Macritchie, K., Geddes, J., Watson, S., Young, A. *Cochrane Database of Systematic Reviews* **2006**, (Issue 1). Art. No.: CD003384.

Vitale, R. M., Pedone, C., Amodeo, P., Antel, J., Wurl, M., Scozzafava, A., Supuran, C. T., De Simone, G. *Bioorg. Med. Chem.* **2007**, 15, 4152.

Whittington, D. A., Waheed, A., Ulmasov, B., Shah, G. N., Grubb, J. H., Sly, W. S., Christianson, D. W. *Proc. Natl. Acad. Sci. U.S.A.* **2001,** 98, 9545.

Whittington, D. A., Grubb, J. H., Waheed, A., Shah, G. N., Sly, W. S., Christianson, D. W. *J. Biol. Chem*. **2004**, 279, 7223.

Winum, J.-Y., Rami, M., Scozzafava, A., Montero, J. L., Supuran, C. T. *Med. Res. Rev*. **2008**, 28, 445.

Xu, Y., Feng, L., Jeffrey, P. D., Shi, Y., Morel, F. M. *Nature.* **2008**, 452, 56.

Zimmerman, U. J., Wang, P., Zhang, X., Bogdanovich, S., Forster, R. *IUBMB Life*. **2004**, 56, 343.

Zou, L. P., Lin, Q., Qin, J., Cai, F. C., Liu, Z. S., Mix, E. *Clinical Neuropharmacology*, **2008**, 31, 86.

ABBREVIATION INDEX

4-VP: 4-vinyl-pyridine

APS: ammonium persulfate

AZM: acetazolamide

BSA: albumin from bovine serum

CA: carbonic anhydrase

CAI: carbonic anhydrase inhibitor

CCD: charge-coupled device

CD: circular dichroism

dNTP: deoxy nucleotide tri-phosphate

DTT: dithiothreitol

ECL: enhanced chemi-luminescence

EDTA: ethylene-diamino-tetraacetic acid

ESI: electron spray ionization source

FPLC: fast protein liquid chromatography

GSH: reduced glutathione

GST: Glutathione S-Transferase

Hepes: 4-(2-hydroxyethyl)-1-piperazineethanesulfonic acid

HPLC: high performance liquid chromatography

IPTG: isopropyl-beta-D-thiogalactopyranoside

LB: Luria-Bertani broth

LC-MS: liquid chromatography mass spectrometry

MCS: multi cloning site

NHS: N-hydroxysuccinimide

OD: Optical Density

pAMBS: 4-aminomethyl benzene-sulfonamide hydrochloride

PBS: phosphate buffer saline

PCR: polymerase chain reaction

PEG: polyethylene glycol

PMSF: Phenylmethylsulphonylfluoride (Inhibitor of Serine proteases)

R.T.: room temperature

SDS-PAGE: sodium dodecyl sulfate polyacrylamide gel electrophoresis

TBE: Tris Borate EDTA

TBST: Tris Buffer Salin Tween 20

Tris: Tris (hydroxy methyl)-amino-methane

TFA: Trifluoroacetic acid

Tm: melting temperature

TPM: topiramate

ZBG: zinc binding group

PUBLICATIONS

Di Fiore A,[*] **Truppo E**,[*] Supuran CT, Alterio V, Dathan N, Bootorabi F, Parkkila S, Monti SM, De Simone G.

Crystal structure of the C183S/C217S mutant of human CA VII in complex with acetazolamide.

Bioorg Med Chem Lett. 2010; 20(17): 5023-6.

Abstract

Human carbonic anhydrase VII (hCA VII) is a cytosolic member of the alpha-CA family. This enzyme is mainly localized in a number of brain tissues such as the cortex, hippocampus and thalamus and has been noted for its contribution in generating neuronal excitation and seizures. Recently, it has been also proposed that hCA VII may be involved in the control of neuropathic pain, thus its inhibition may offer a new approach in designing pain killers useful for combating neuropathic pain. We report here the X-ray crystallographic structure of a mutated form of human CA VII in complex with acetazolamide, a classical sulfonamide inhibitor. These crystallographic studies provide important implications for the rational drug design of selective CA inhibitors with clinical applications.

* *These authors equally contributed to the paper.*

Alterio V, Monti SM, **Truppo E**, Pedone C, Supuran CT, De Simone G.

The first example of a significant active site conformational rearrangement in a carbonic anhydrase-inhibitor adduct: the carbonic anhydrase I-topiramate complex.

Org Biomol Chem. 2010; 8(15): 3528-33.

Abstract

Topiramate is a widely used antiepileptic drug, which has been demonstrated to act as an efficient weight loss agent. Since several studies have pointed out that is a potent in vitro inhibitor of several Carbonic anhydrase (CA) isozymes, it has been hypothesized that its anti-obesity properties could be ascribed to the inhibition of the CAs involved in de novo lipogenesis. Consequently, the study of the interactions of with all human CA isoforms represents an important step for the rational drug design of selective CA inhibitors to be used as anti-obesity drugs. In this paper we report the crystallographic structure of the adduct that forms with hCA I, showing for the first time a profound reorganization of the CA active site upon binding of the inhibitor. Moreover, a structural comparison with hCA II- and hCA VA-adducts, previously investigated, has been performed showing that a different H-bond network together with the movement of some amino acid residues in the active site may account for the different inhibition constants of toward these three CA isozymes.

Truppo E, Supuran, CT, Sandomenico A, Vullo D, Innocenti A, Di Fiore A, Alterio V, De Simone G and Monti SM

Carbonic anhydrase VII is S-glutathionylated without loss of catalytic activity and affinity for sulfonamide inhibitors

Bioorg Med Chem Lett. *submitted.*

Abstract

Human carbonic anhydrase (CA, EC 4.2.1.1) VII is a cytosolic enzyme with high carbon dioxide hydration activity. Here we report an unexpected S-glutathionylation of hCA VII which has also been observed earlier, *in vivo* for hCA III, another cytosolic isoform. Cys183 and Cys217 were found to be the residues involved in reaction with glutathione for hCA VII. The two reactive cysteines were then mutated and the corresponding variant (C183S/C217S) expressed. The native enzyme, the variant and the S-glutathionylated adduct (sgCA VII) as well as hCA III were fully characterized for their CO_2 hydration, esterase/phosphatase activities, and inhibition with sulfonamides. Our findings suggest that hCA VII could use the *in vivo* S-glutathionylation to function as an oxygen radical scavenger for protecting cells from oxidative damage, as the activity and affinity for inhibitors of the modified enzyme are similar to those of the wild type one.